I am submitting herewith a thesis written by Robert John Geierman entitled "Design of an Aluminum Powder Combustor for Simulating the Combustion Conditions in Solid Rocket Motors". I have examined the final copy of this thesis for form and content and recommend that it be accepted in partial fulfillment of the requirements for the degree of Master of Science, with a major in Mechanical Engineering.

Roger Crawford

Dr. Roger A. Crawford, Major Professor

We have read this thesis
and recommend its acceptance

Accepted for the Council

Associate Vice Chancellor
and Dean of The Graduate School

## STATEMENT OF PERMISSION TO USE

In presenting this thesis in partial fulfillment of the requirements for Masters degree at The University of Tennessee, Knoxville, I agree that the Library shall make it available to borrowers under the rules of the Library. Brief quotations from this thesis are allowable without special permission, provided that accurate acknowledgment of the source is made.

Permission for extensive quotation from or reproduction of this thesis may be granted by major professor, or in his absence, by the Head of Interlibrary Services when, in the opinion of either, the proposed use of the material is for scholarly purposes. Any copying or use of the material in this thesis for financial gain shall not be allowed without my written permission.

Signature Robert J Sherman

Date 8-17-67

# Design of an Aluminum Powder Combustor for Simulating the Combustion Conditions in Solid Rocket Motors

A Thesis

Presented for the

Master of Science

Degree

University of Tennessee, Knoxville

Robert John Geierman

December, 1993

DEDICATION

This thesis is dedicated to my wife

Mary Louise Geierman

who has given me invaluable support and encouragement.

ACKNOWLEDGMENTS

I would like to thank my major professor, Dr. Roger Crawford, for his educational guidance and advice. I would also like to thank the other committee members, Dr. Roy Schulz and Dr. Gary Flandro, for their additional comments and instruction over the past two years. Additionally, I would like to thank Dr. Robert Reed and the Air Force Office of Summer Research Programs for the excellent learning experience (and suggestions) which I received as a result of my summer employment terms (1992 and 1993) at Arnold Engineering Development Center. I would especially like to thank my wonderful wife, Mary, whose continuous understanding and support made this thesis possible. Her words of encouragement and love kept me going through the difficult times. I would also like to thank my parents, Daniel and Eleanor Geierman, for their love and financial support throughout my college career. Last, but not least, I would like to thank my fellow office residents and friends, Allen, Mike, Jonathan, Brian, and Rob, for their additional assistance and for all of the fun times which we had during my stay at UTSI.

## ABSTRACT

This research presents the design of a combustion device which will simulate the aspects of aluminum particle combustion inside a solid rocket motor. At the same time this combustor will allow optical data to be collected during the combustion process.

The first step in this combustor design was to examine past experiments and methods which have been used to examine the combustion of aluminum particles. Next, the fuels and oxidizers, which will be used in the first planned combustion experiments, were selected. The flame temperatures and transport properties of these fuels and oxidizers were calculated using a version of a NASA chemical equilibrium code. The third step in this combustor design was to define the physical dimensions and maximum operating times which would be allowed. These parameters were defined through simplified stress analysis and heat transfer calculations, respectively. The final steps in this combustor design process were to define the procedures and instrumentation to be used during the operation of this combustor.

TABLE OF CONTENTS

LIST OF FIGURES

## LIST OF VARIABLES AND ACRONYMS

| Variable | Definition |
|---|---|
| A | Area of subscripted region |
| Al | Aluminum |
| $AlO_2H$ or AlO(OH) | Aluminum Hydroxide |
| $Al_2O_3$ | Aluminum Oxide |
| a, b | Dummy variable related to Aluminum mass fraction |
| $cm^2$ | square centimeters |
| CETPC | Chemical Equilibrium and Transport (Properties) for the Personal Computer |
| $CH_4$ | Methane |
| CMDB | Composite modified double base |
| C | Carbon |
| $C_1$ | Packing fraction |
| $C_p$ | Specific heat at constant pressure |
| D | Particle diameter |
| $D_h$ | Hydraulic diameter |
| $d_i$ | Inner tube diameter |
| $d_o$ | Fuel injector diameter |
| g | Gas, acceleration due to gravity |
| $H_2$ | Hydrogen |
| $H_2O$ | Water, water vapor |

| | |
|---|---|
| $h_g$ | Gaseous convective heat transfer coefficient |
| $h_\ell$ | Liquid convective heat transfer coefficient |
| k | Burn rate constant, conductivity |
| L | Latent heat of fusion |
| $\ell$ | Liquid |
| $\ell_c$ | Axial length of convergent nozzle section |
| M | Molecular weight of subscripted species |
| MPa | megapascals |
| m | Mass flow rate of subscripted species |
| $m_{max}$ | Maximum mass flow rate |
| m/s | meters per second |
| $N_2$ | Nitrogen |
| NASA | National Aeronautics and Space Administration |
| n | Burn rate exponent |
| $\frac{O}{F}$ | Oxidizer to fuel mass ratio |
| $O_2$ | Oxygen |
| P | Pressure |
| $P_i$ | Inside pressure |
| $P_o$ | Outside pressure |
| Pr | Prandtl number |
| psia | pounds per square inch absolute |
| $q_{ft}$ | Heat transfer rate from flame to nozzle throat |

| | |
|---|---|
| $q_{qs(rad)}$ | Radiation heat transfer from quartz to the surroundings |
| $\bar{R}$ | Universal gas constant |
| R | Gas Constant |
| $R_i$ or $r_i$ | Inner radius |
| $R_o$ or $r_o$ | Outer radius |
| r | Radius |
| $r_{ci}$ | Inside radius of nozzle convergent section |
| $r_{co}$ | Outside radius of nozzle convergent section |
| $r_{di}$ | Inside radius of nozzle divergent section |
| $r_{do}$ | Outside radius of nozzle divergent section |
| $r_{ti}$ | Inside radius of nozzle throat |
| $r_{to}$ | Outside radius of nozzle throat |
| SRMACS | Solid Rocket Motor Aluminum Combustion Simulator |
| s | Solid |
| stoich. | stoichiometric |
| T | Temperature |
| $T_i$ | Apparent ignition temperature |
| $T_{mm}$ | Aluminum melting temperature |
| $T_o$ | Initial Temperature |
| $T_\infty$ | Temperature of surroundings |
| t | Time, thickness |
| $t_b$ | Burn time |

| | |
|---|---|
| $t_i$ | Ignition time |
| $t_{op}$ | Operational time limit |
| $t_{tot}$ | Total combustion time of particle |
| V, v | Average velocity or volume |
| $W_{Al}$ | Weight of Aluminum particles |
| $X_p$ | Core length |
| Y | Mole fraction of subscripted species |
| $\eta$ | Number of moles of subscripted species |
| $\gamma$ | Specific heat ratio |
| $\mu$ | Viscosity |
| $\mu_{am}$ | Arithmetic mean viscosity |
| $\mu_o$ | Viscosity at combustion or stagnation temperature |
| $\rho$ | Density |
| $\rho_\infty$ | Density of combustion gases |
| $\sigma_{t,max}$ | Maximum tangential stress |
| $\sigma_y$ | Yield strength |
| $\theta$ | Convergent or divergent nozzle angle |

# CHAPTER I. - Introduction

For many years, metals have been used as additives in solid rocket motor propellants. The reasons for the use of these additives include their ability to help eliminate combustion instabilities and their ability to increase specific impulse. By far, the most popular metal additive is aluminum. The popularity of aluminum usage is due to its high heat of formation (of its oxides) and its relatively low cost.

Although aluminum is widely used as a propellant additive, much of its combustion characteristics and optical properties, especially during solid propellant burning, have not been quantified. By obtaining a better understanding of aluminum combustion, one could possibly increase the specific impulse of solid rocket motors without degrading combustion stability. The increase in specific impulse could be accomplished by either increasing the aluminum content to near its stoichiometric limit, while maintaining a high combustion efficiency, or by minimizing the two-phase flow losses. Similarly, an adequate understanding of the optical properties of aluminum is important to predict the radiation heat transfer to the propellant surface and the spacecraft itself, from the exhaust gases. In order to gain a better understanding of the combustion of aluminum and its properties, it becomes necessary to observe the

process in the environment which is found inside a solid rocket motor. Since it is nearly impossible to observe the phenomena inside an actual solid rocket motor, a device is necessary which closely simulates these conditions while at the same time allows for observations of exhaust or combustion process to be made. This thesis contains a detailed design and pertinent information to construct and test a Solid Rocket Motor Aluminum Combustion Simulator (SRMACS).

Although much remains to be learned about aluminum combustion, there have been many previous experimental and analytical methods which have resulted in the collection of valuable data for the design of this combustor. The organization of this thesis is that it is divided into seven chapters. The first chapter consists of an introduction. The second chapter presents relevant background information. The third chapter consists of a detailed chemical analysis. This chemical analysis discusses the fuels and oxidizers to be used as well as their corresponding equilibrium reactions. From these reactions it becomes possible to predict flame temperatures and flame boundaries for the various fuel/oxidizer combinations. The fourth chapter uses the temperature calculations for the specific design requirements. These design requirements include the physical size of the combustor, the materials to be used, and a detailed stress analysis. The fifth chapter consists of all of the safety and operational requirements. The sixth chapter details

all of the necessary instrumentation design requirements and selections. The final, or seventh chapter provides the summary, conclusions, and recommendations of this study.

# CHAPTER II - Discussion of Previous Work

This chapter discusses the numerous experiments which were previously performed by other investigators and useful data which was obtained. The pertinent data from these previous experiments will be discussed further in this chapter and applied in later chapters. The previous experiments will be divide into three groups. These groups consist of a) Burning of Propellant Samples, b) Particle/Flame Burners, and c) Exotic Methods.

## 2.1. Burning of Propellant Samples

Probably the most common method which has been employed to investigate aluminum combustion phenomena is the burning of actual aluminized propellant samples. Two methods which are based on burning propellant samples are discussed below.

One method consists of burning propellant samples in some sort of combustion bomb [1-7]. This method is usually performed by placing a small strand of propellant within a combustion bomb which is usually pressurized with an inert or non reacting gas. The sample is ignited and the combustion process is observed with a high speed

camera (Figure 1). From these experiments it is possible to determine the size of the aluminum or aluminum oxide particles and agglomerates which leave the propellant surface, and the approximate burning times for some particles.

From many experiments, the size of the aluminum oxide particles were determined to consist of a bimodal size distribution. Approximately eighty percent of this bimodal distribution consisted of small "smoke" particles [5]. The small aluminum oxide "smoke" particles were typically less than 2 $\mu$m. The other portion of this distribution consisted of larger burning aluminum/aluminum oxide particles. Generally, as pressure is increased in the combustion chamber the size of the agglomerates decreases. Figure 2 shows the mass weighted agglomerate size verses pressure for various average Ammonium Perchlorate sizes. Although the size of the agglomerates may be up to 1000 times the size of the initial aluminum particles, the typical aluminum oxide particles produced ranged from 5 $\mu$m to 100 $\mu$m for the pressures at which this SRMACS will operate (500 psia (3.45 MPa) to 1000 psia (6.89 MPa)). It should also be noted that these size ranges are representative of the composite propellants (Aluminum / Ammonium Perchlorate / Hydrocarbon Binder) which were tested. Considering the fact that complete combustion of aluminum causes a 20% increase in particle diameter,

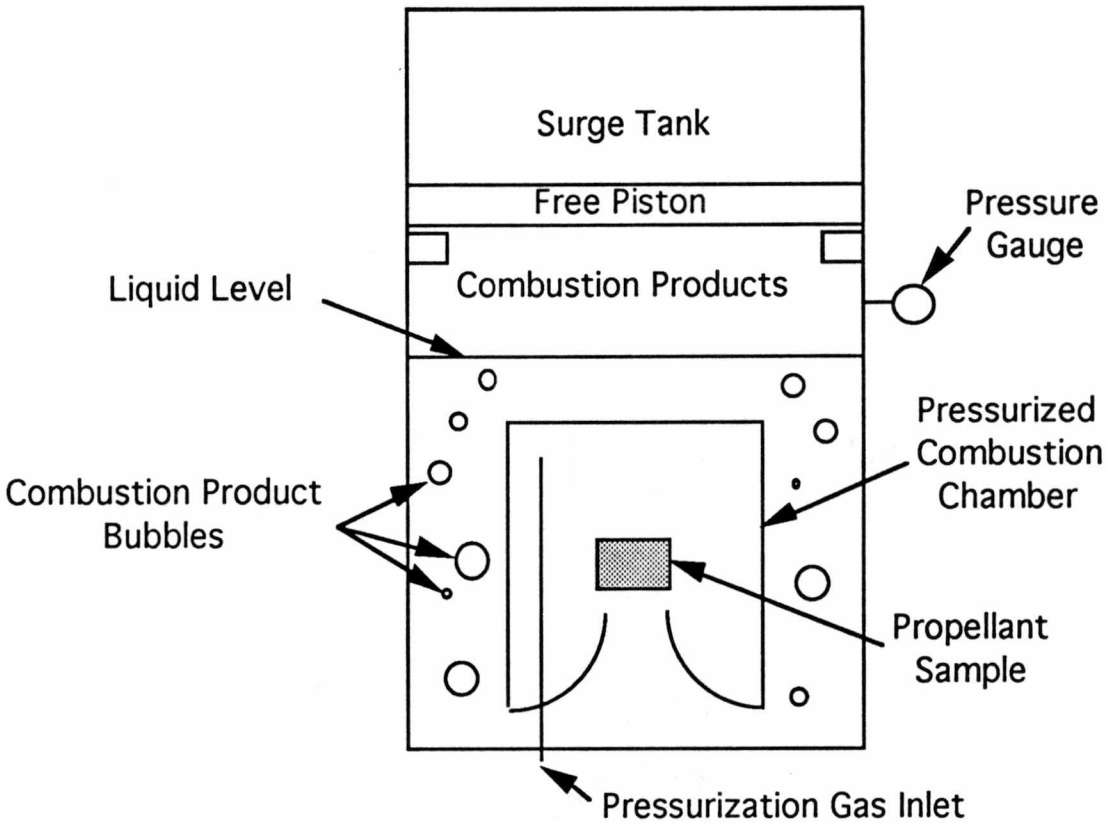


**Figure 1: Combustion Bomb Apparatus**

[Adapted from: 1. Mitani, T. and Izumikawa, M., "Combustion Efficiencies of Aluminum and Boron in Solid Propellants", Journal of Spacecraft and Rockets, Vol. 28, No. 1, 1991, pp. 79-84.]

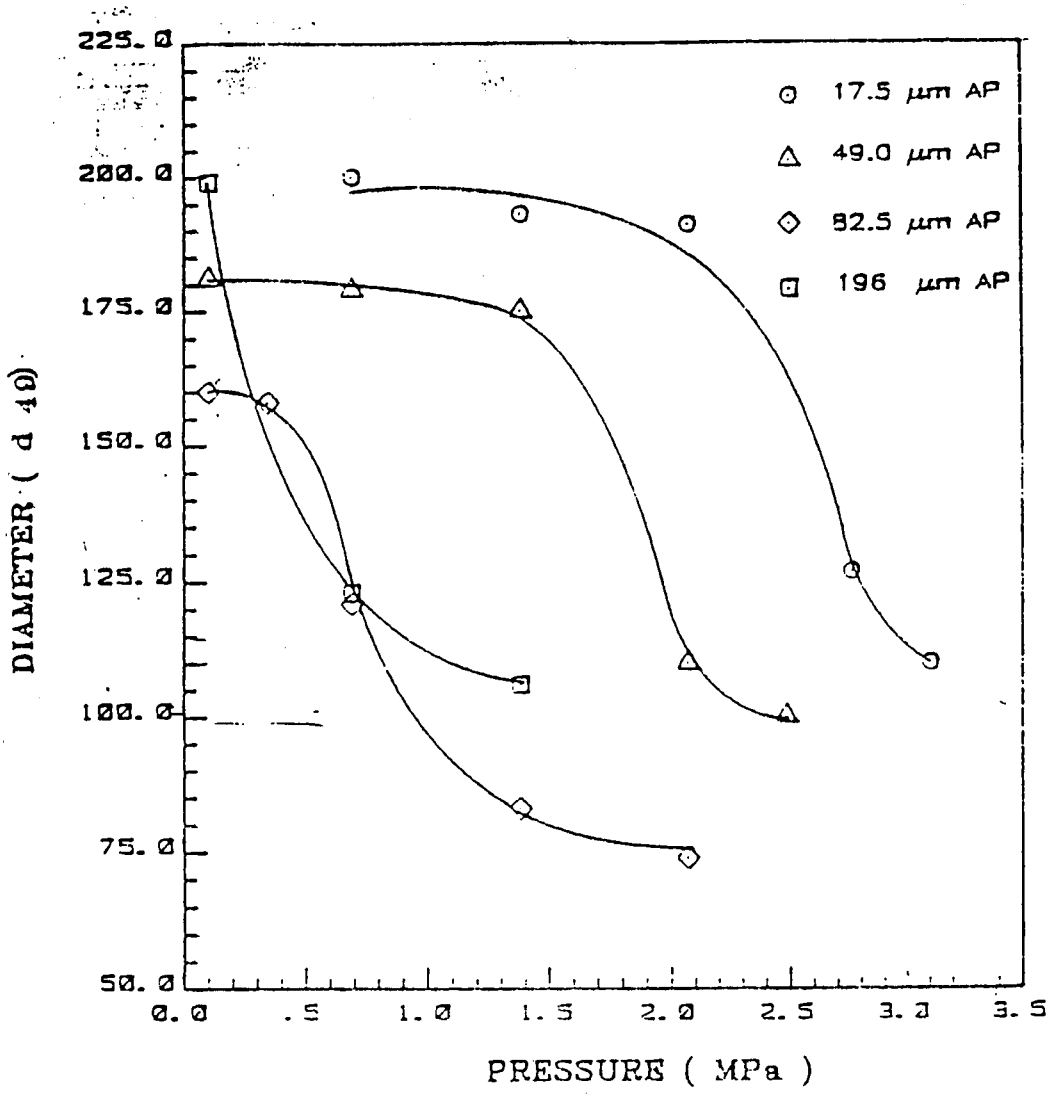


**Figure 2: Pressure Effects on Mass Average Agglomerate Size**
[Copied from: 2. Sauerwein, H. P., Lampert, A. and Schmucker, R. H., "Erosive and Transient Burning Effects on Performance Prediction Accuracy of Tactical Rockets", AGARD Propulsion and Energetics Symposium on Solid Rocket Motor Technology, 1979.]

the initial aluminum agglomerate (Agglomerates are composed of many small aluminum particles.) sizes must have been between 4 $\mu$m and 85 $\mu$m [7].

The burning time of the aluminum droplets was found to follow a droplet burning rate law of the form:

$$t_b = kD^n \qquad (1)$$

where k is a constant found to be equal to 0.5E-5 sec/($\mu$m)$^n$, D is the initial aluminum agglomerate diameter in $\mu$m and n is the burning rate exponent found to be between 1.5 and 2.0 [5].

It was also found in these experiments that aluminum particles less than 5 $\mu$m usually ignite on the propellant surface, while larger aluminum agglomerates ignite in the gas stream. One of the advantages of this process is the ability to test a variety of propellants at various ambient pressures. On the other hand, some of the drawbacks of this type of experiment are the lack of representative rocket motor internal cross flow conditions, and the lack of any optical data acquisition methodologies.

The second propellant sample method used in the investigation of aluminum particle combustion is the use of two-dimensional windowed motors [8-10]. This method consists of bonding a propellant sample between two pieces of glass and using a high

speed camera to observe the combustion process (Figure 3). In order to observe the aluminum combustion more efficiently, the aluminized propellant sample is usually placed between two non-aluminized propellant samples. The apparatus can also be used with a two-dimensional nozzle in order to see its effect on particle breakup.

This process has the advantage of incorporating cross flow conditions while at the same time allowing for the observation of the size and combustion times of the aluminum agglomerates. These experiments also revealed a bimodal size distribution of aluminum oxide particles. For the combustion of double-base propellants with cross flow it was found that the distribution again consisted of small "smoke" particles and larger burning agglomerates. The small "smoke" particles were approximately the same size for both composite and composite modified double-base (CMDB) propellants. CMDB propellants are typically composed of Nitrocellulose, Nitroglycerine, Ammonium Perchlorate, and Aluminum. However, the CMDB propellants were found to produce much larger burning agglomerates than the composite propellants. The size of these CMDB agglomerates ranged from approximately 300 $\mu$m at 1000 psia (6.89 MPa) to 700 $\mu$m at 500 psia (3.45 MPa) [8]. Also, the majority of the aluminum mass was found to be incorporated into these large agglomerates for CMDB propellants. On the other hand, when composite propellants were burned under cross flow conditions, they

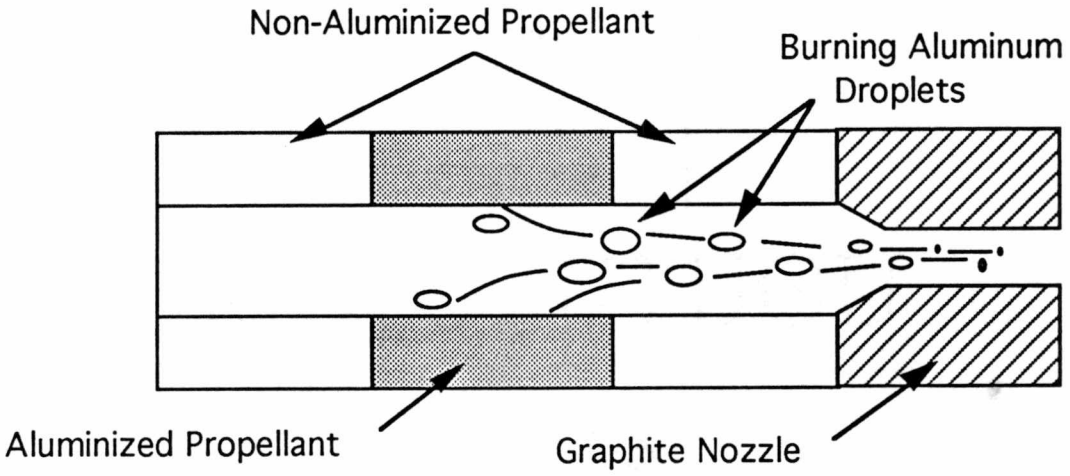


**Figure 3: Two-Dimensional Windowed Rocket Motor**
[Adapted from: 9. Caveny, L. H. and Gany, A., "Aluminum Combustion Under Rocket Motor Conditions", AGARD Propulsion and Energetics Symposium on Solid Rocket Motor Technology, 1979.]

produced agglomerates which were approximately the same size as the experiments which were performed without cross flow conditions [10]. Some disadvantages to these experiments, however, are the lack of optical information of the aluminum/aluminum oxide particles and the lack of knowledge as to which species react with the aluminum particles.

## 2.2. Particle/Flame Burners

A second method for aluminum particle combustion experiments is the use of a flame with aluminum particle injection [11-15]. This method consists of either a premixed flame or a diffusion flame with aluminum particles injected through the center of the flame. The aluminum particles are usually injected at a rate which allows them to be observed individually. As the particle traverses the flame, it can be observed by high speed cameras (Figure 4).

One of the main advantages of this process is the fact that by carefully controlling the species use to produce the flame one can control the type and the relative amounts of oxidizer available to react with the aluminum. Fuels used in these experiments included hydrogen, propane, natural gas and carbon monoxide. Oxygen was then used to create the flame. The flame temperature was controlled by either varying the fuel/oxidizer ratio or by the addition of nitrogen into the gas stream. When the aluminum is

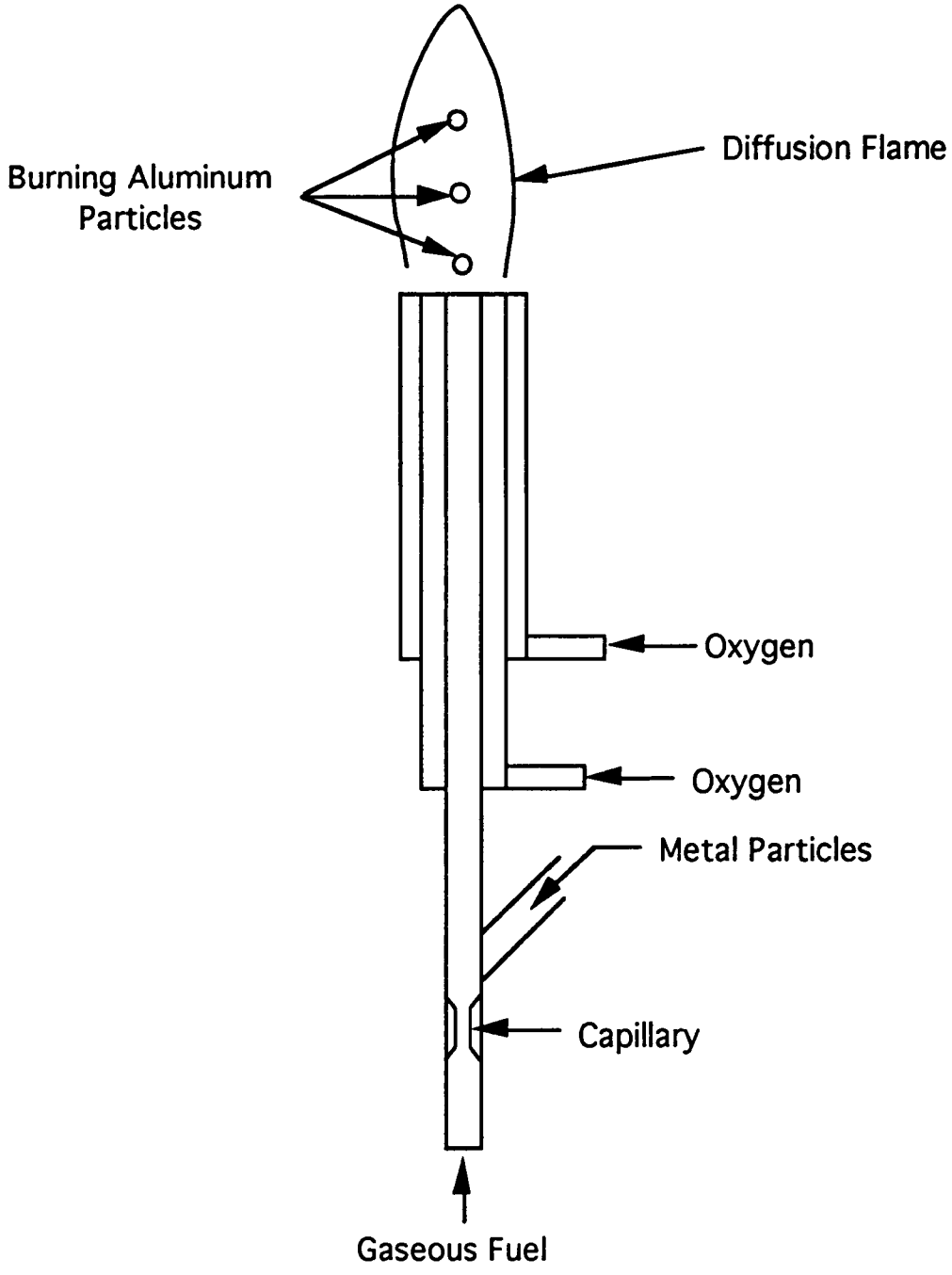


**Figure 4: Axisymmetric Particle/Flame Burner**

[Adapted from: 12. Fassell, W. M., et. al., "The Experimental Nature of the Combustion of Metallic Powders", Solid Propellant Rocket Research, Progress in Astronautics and Rocketry, Vol. 1, 1960, pp. 259-269.]

injected into the flame it is exposed to various species (oxidizers) including water vapor, carbon dioxide, carbon monoxide, and oxygen. It should be noted, however, that hydrochloric acid (HCl), a major product in the combustion of composite propellants, was not used in these experiments.

Another advantage to this type of process is the fact that individual particles are easier to observe. These two factors make it simpler to develop theoretical models from this method as opposed to the burning propellant processes. These experiments seem to verify that aluminum combustion occurs by a vapor phase diffusion process. In this type of process the rate at which oxygen diffuses through the aluminum oxide layer to react with the aluminum is considered to be the controlling process. Also, the flame temperature for aluminum combustion was found to equal the boiling temperature of the aluminum oxide. Thus, as pressure increases, the flame temperature for aluminum combustion increases. Since these flame burner experiments were carried out at atmospheric pressure, it is necessary to convert the data from these experiments to the operating pressures of the combustor. This is discussed in more detail in chapters 3 and 4.

Another aspect of these experiments which is relevant to the design of this combustor is the delay in ignition for the injected aluminum particles. This ignition delay is due to the fact that it

takes a finite amount of time to heat the aluminum particles from their injected temperature (usually room temperature) to their ignition temperature (found to be the melting temperature of aluminum oxide). Thus the ignition delay time was found to be:

$$t_i = \frac{\rho D^2}{12\lambda}\left\{C_p\left[\ln\left(\frac{T_\infty - T_o}{T_\infty - T_i}\right)\right] + \frac{L}{T_\infty - T_{mm}}\right\} \qquad (2)$$

where $\rho$ is the density of aluminum, D is the particle diameter, $\lambda$ is the thermal conductivity of the gas, $C_p$is the heat capacity for aluminum, $T_\infty$ is the gas temperature, $T_o$ is the initial temperature of the particle, $T_i$ is the apparent ignition temperature (the melting point of aluminum oxide which is approximately 2300 K at 1 atm.), L is the heat of fusion of aluminum and $T_{mm}$ is the melting temperature of aluminum (933 K) [14]. The variables in equation 2 are calculated by using the NASA SP273 or CETPC code in chapter 3 [16].

From the sum of equations 1 and 2 the total time required for the particle combustion can be calculated.

$$t_{tot} = t_i + t_b \qquad (3)$$

By using this equation and the velocity/thermal lag equations in chapter 3, the length of the tube required for complete combustion of the particle can be calculated.

## 2.3. Exotic Methods

Other methods which have been used for aluminum combustion studies shall be called, for lack of a better term, exotic methods. These methods are not often used, but do still provide some useful information. Three of these methods are briefly discussed below.

The first exotic method uses aluminum wires to investigate aluminum combustion [17-18]. This method consists of heating the aluminum wires by electrical resistance in a pressurized combustion chamber of known composition and observing the combustion process through a window (Figure 5). This process has the advantage of being very simplistic while still obtaining some useful information about aluminum combustion phenomena. From these experiments, spectroscopic observations were taken of aluminum/oxygen flames (Figure 6). It was also found in these experiments that the "smoke" particles formed in aluminum combustion (at up to 450 psia) were a "mixture of $\kappa$ - aluminum oxide, high temperature $\gamma$ - aluminum oxide and $\theta$ - aluminum oxide. No strong lines of $\alpha$ - aluminum oxide were detected in this product." [17]. The disadvantages to this process are that aluminum is not found in this state (a long wire strand) in a solid rocket motor and that the ignition process, in this case, is caused by internal heating instead of the external heating method observed in a solid rocket motor.

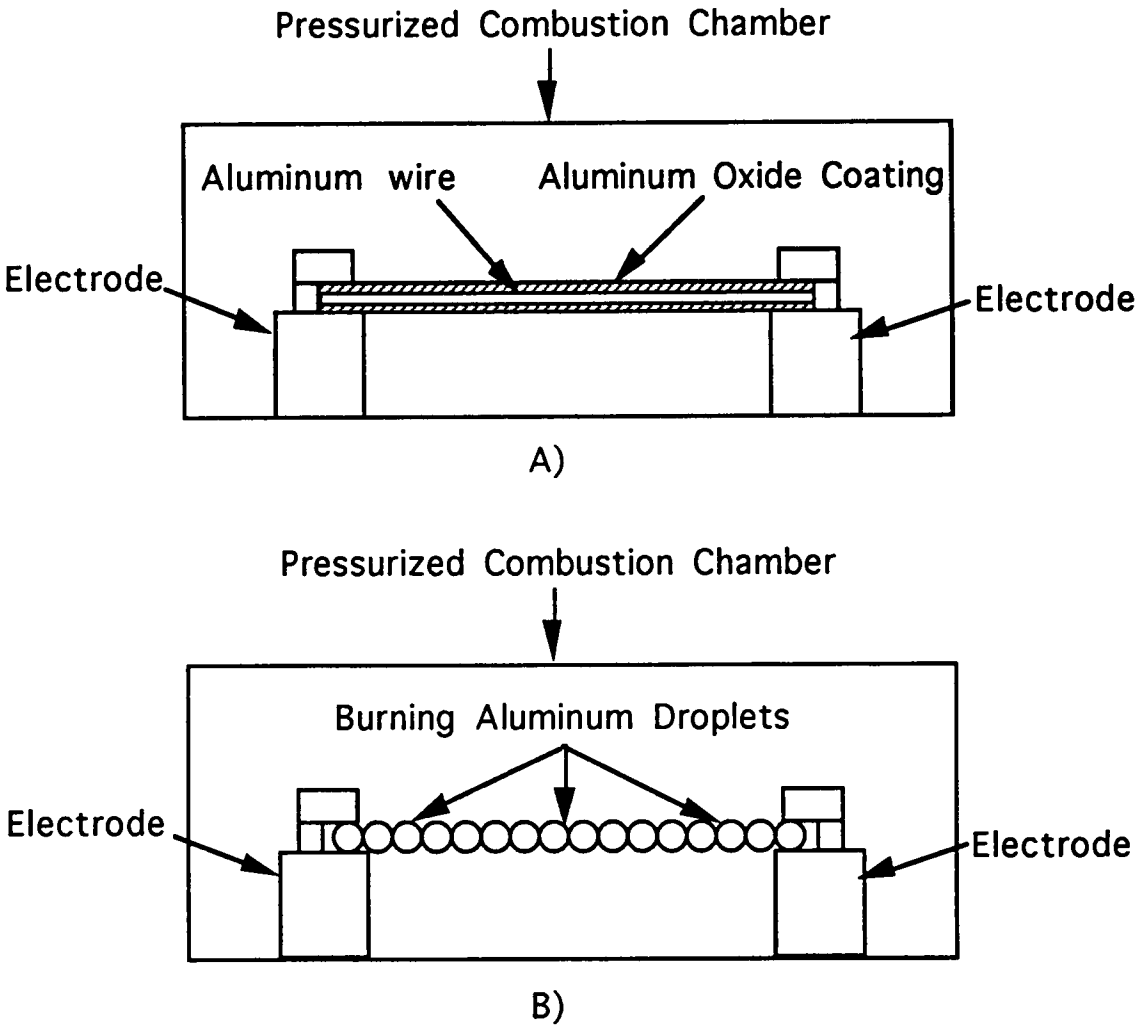


**Figure 5: Electrical Resistance Ignition**

A) Prior to Ignition(Before Oxide Melts)

B) At Ignition(When Oxide Begins to Melt)

[Adapted from: 17. Brzustowski, T. A. and Glassman, I., "Vapor-Phase Diffusion Flames in the Combustion of Magnesium and Aluminum: II. Experimental Observations in Oxygen Atmospheres", Heterogeneous Combustion, Progress in Astronautics and Aeronautics, Vol. 15, 1964, pp. 117-158.]

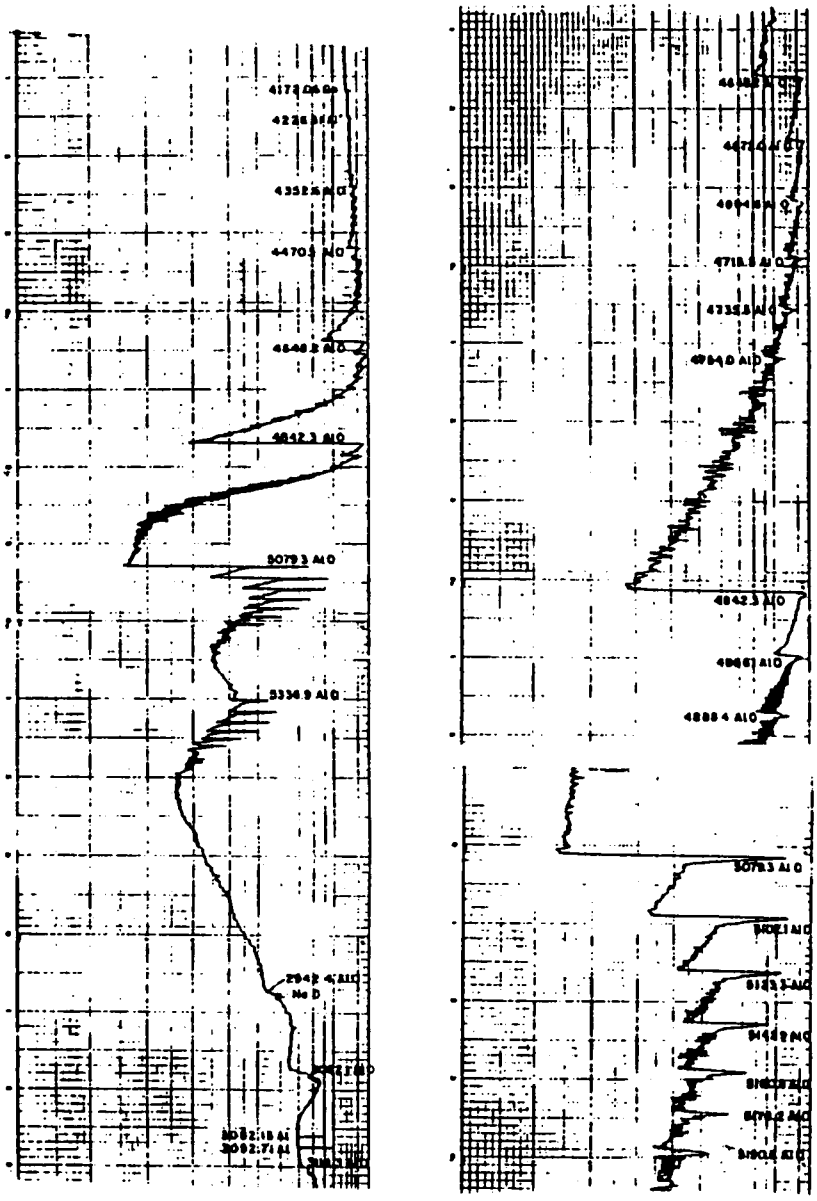

**Figure 6: Principal Features of Aluminum/Oxygen Flame Spectrum**

[Copied from: 18. Mellor, A. M. and Glassman, I., "Vapor-Phase Diffusion Flames in the Combustion of Magnesium and Aluminum: II. Experimental Observations in Carbon Dioxide Atmospheres", Heterogeneous Combustion, Progress in Astronautics and Aeronautics, Vol. 15, 1964, pp. 159-175.]

The second exotic method uses a laser to ignite single aluminum particles [19]. This experiment used an individual aluminum particle which was placed on the end of a quartz needle within a chamber of known composition. The particle was ignited with a laser and the combustion process was observed with a high speed camera (Figure 7). The benefits of this procedure were that the individual particles were easier to observe and the fact that the ambient atmosphere was of known composition. Researchers in this experiment used 400 $\mu$m particles which were comparable in size to the agglomerates found in CMDB propellants. This experiment determined that a radiation flux of 250 W/cm$^2$ was necessary to ignite these particles. However, one problem which was encountered with this experiment was the lack of any optical data acquisition.

The third, and final, type of exotic experiment used a reflected shock wave to investigate aluminum combustion [20]. In this method, a heated aluminum sample was mounted on the end wall of a single-pulse shock tube (Figure 8). The temperature (up to 5000 K) and pressures (up to 40 atm.) of the gas surrounding the sample were generated by a reflected shock wave. The driven gas used was either oxygen or a mixture with the same composition as ammonium perchlorate. The combustion process was recorded by its spectral emissions. One of the main advantages of this technique was the fact that the spectral bands of each species were easily identified (Figure 9). Another advantage was the fact that the ambient gas was

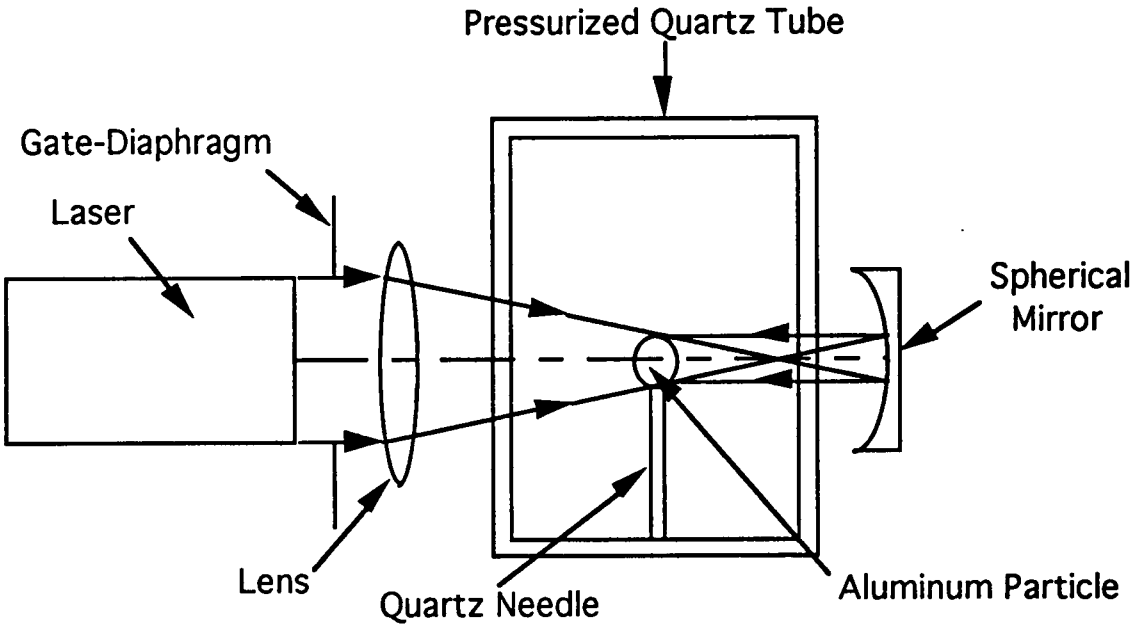


**Figure 7: Laser Ignition Technique**

[Adapted from: 19. Razdobreev, A. A., Skorik, A. I. and Frolov, Yu. V., "Ignition and Combustion Mechanism in Aluminum Particles", Tomsk State University, Translated from Fizika Goreniya i Vzryva, 1976, Vol. 12, No. 2, pp. 203-208. ]

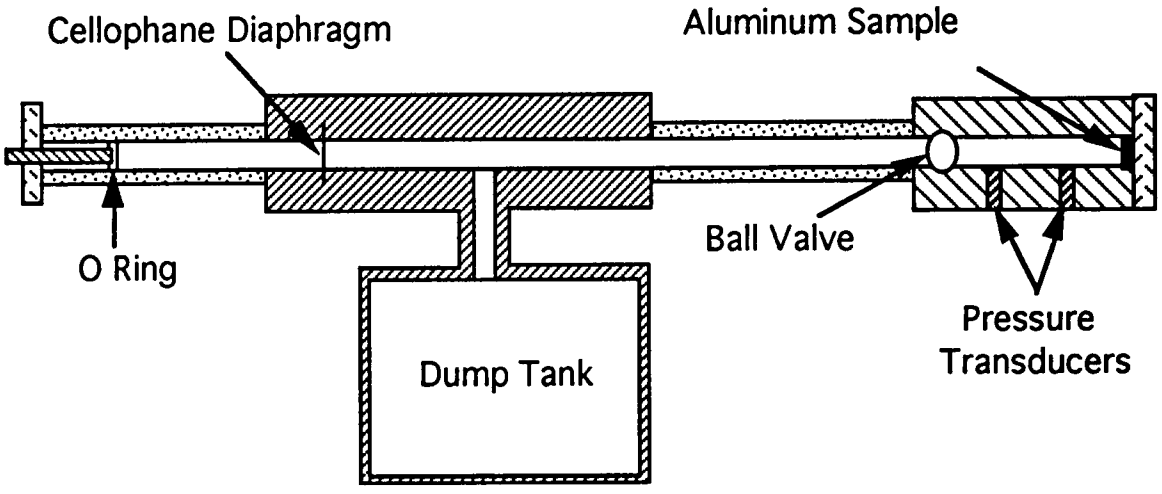


**Figure 8: Reflected Shock Wave Apparatus**

[Adapted from: 20. Lifschitz, A. and Bouer, S. H., "Studies with a Single Pulse Shock Tube", Journal of Chemical Physics, Vol. 38, No. 9, 1963, pp. 2056-2060.]

| Species | Wavelength (Angstrom) |
|---|---|
| Al | 3944, 3961 |
| Al+ | 5861 |
| AlO | 4648, 4842, 5079, 5337 |
| H | 4340, 4861, 6563 |
| O | 5350 |
| O+ | 4880 |
| N | 4103, 5666, 5679 |
| AlH | 4241, 4259 |

**Figure 9: Species Identified in the Emission Spectrum of Aluminum and Simulated Ammonium Perchlorate**
[Adapted from: 21. Driscoll, J. F., et. al., "Aluminum Combustion at 40 Atmospheres Using a Reflected Shock Wave", AIAA Journal, Vol. 24, No. 5, 1986, pp. 856-858.]

of known composition and could easily be varied. One of the problems with this type of experiment, however, is the fact that the aluminum is not found in such large samples within a solid rocket motor.

## 2.4. Improved Combustor Concept

In order to obtain a better understanding of aluminum combustion, it becomes necessary to improve on experiments which have been performed in the past. This is exactly what the combustor of this thesis is designed to accomplish. This combustor concept will have the versatility to observe aluminum combustion under a variety of oxidizing environments. This will be accomplished by varying the fuels and oxidizers used to produce the flame. Figure 10 shows a simplified schematic of the original conceptual design for this combustor. The original design concept is modified and improved in later chapters. Both optical and high speed camera data will be recorded during this combustor's operation. In addition, for a nominal cost, it will be possible to either vary the size of the injected particles (by changing the injector plate, if necessary) or to change the operating pressure at which the combustor operates (by changing the area of the exit nozzle throat).

This thesis presents, in detail, the simplest design in which the most useful data for aluminum combustion can be obtained. Since

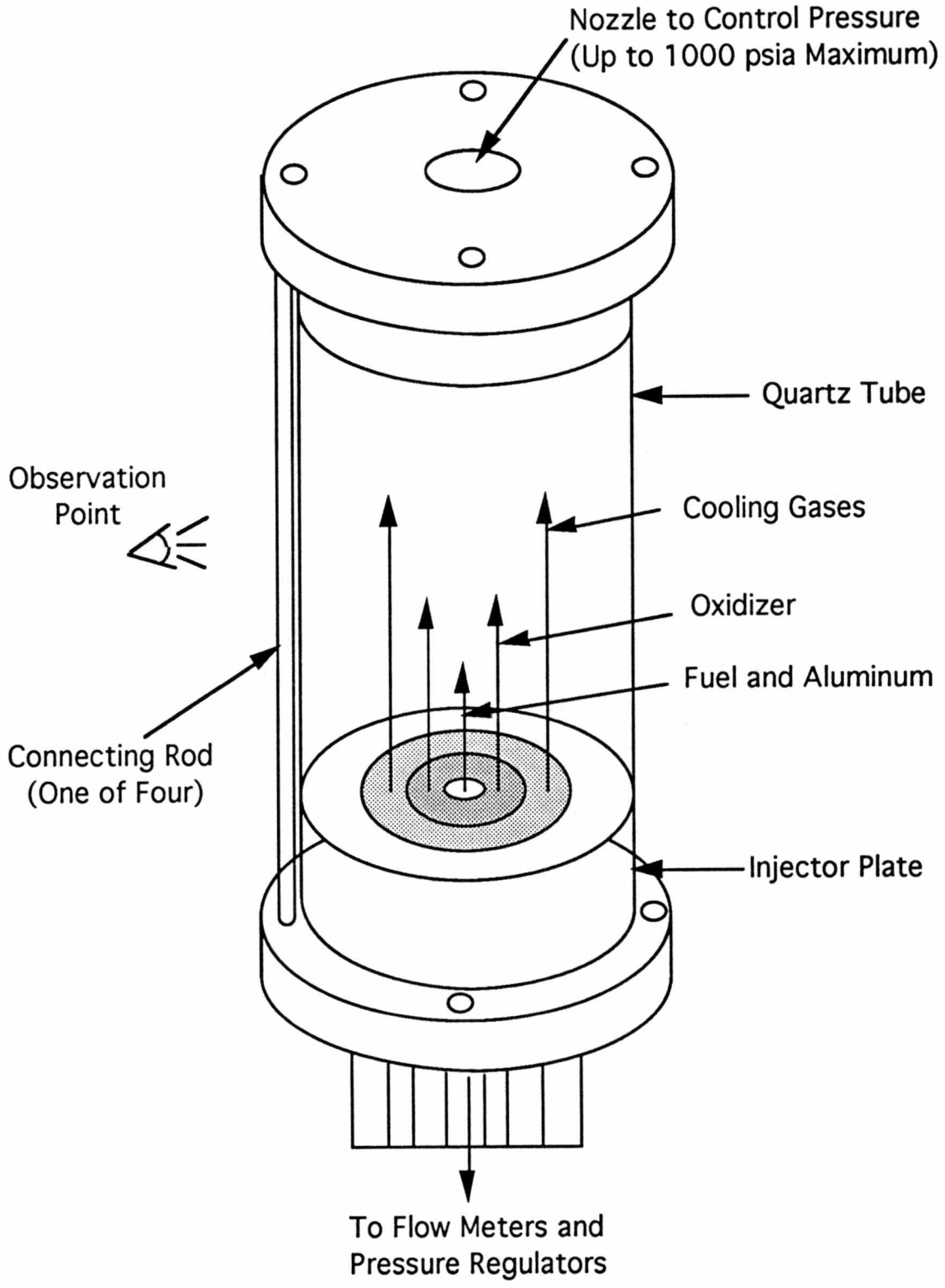


**Figure 10: Solid Rocket Motor Aluminum Combustor Simulator**
(Simplified Schematic)

the majority of heavy-lift launch vehicle in use today contain aluminized composite propellants, These composite propellants will be the first to be simulated by this combustor. In addition, this thesis discusses, in limited detail, methods which will be used in the future to vary the combustor to its fullest potential. Although these additional methods may only be discussed briefly, they will provide enough information to make modifications on the initial combustor design.

# CHAPTER III. - Combustion Analysis

Before any of the specific design characteristics of this combustor can be discussed, a detailed combustion analysis must be performed. This chapter discusses, in detail, the specific fuels and oxidizer which will be used during the first operational test of this combustor. This chapter also suggests and discusses, in less detail, alternative fuels and oxidizers which may be used for later combustor experiments. This chapter briefly describes the equilibrium chemistry of the combustion process. The equilibrium chemistry is used to determine, via a computer program, the flame temperature and physical constants of the mixture. These properties are then used to determine the flame boundaries. These boundaries and temperatures will play a key role in the physical dimensions and heat transfer analysis discussed in chapter 4. In addition, the chemical reactions determine the molar flow rates for the chemical species, which, in turn, determine the mass flow rates for the system.

## 3.1. Oxidizer Selection

Since the goal of this thesis is to present the simplest combustor design, the initial operation of this combustor will use gaseous

oxygen as the oxidizer species. The use of gaseous oxygen simplifies the design(as opposed to using liquid oxygen) by eliminating the need for cryogenics. Although gaseous oxygen may simplify the combustor design, the high pressures involved for this combustor lead to some additional safety considerations which are discussed in chapter 5. It should also be noted that although gaseous oxygen will be the first oxidizing specie to be used, other oxidizers will be introduced later in order to more accurately simulate the solid rocket motor environment. Most noteworthy of the later oxidizers to be tested is a mixture of nitrogen, hydrogen, chlorine, and oxygen combined at the proper mass fractions in order to accurately simulate ammonium perchlorate.

## 3.2. Fuel Selection

This section describes the two fuels which will be used during the initial tests of this combustor. Since the initial goal of this combustor is to accurately observe the aluminum combustion phenomena, this combustor will start by using low aluminum concentrations (mass fractions less than 5%). This low mass fraction should make it possible to observe individual burning aluminum particles. Due to the low aluminum content, it is possible to inject the aluminum particles using a gaseous carrier fuel (To avoid the problem of auto ignition of the small aluminum particles, it was decided to use the fuel as the carrier gas instead of the

oxidizer.) [22]. This simplifies the injection design (compared to using a liquid fuel) due to the fact that fuel droplet spray patterns and evaporation rates do not need to be considered. The gaseous fuels to be used are -a) gaseous hydrogen with solid aluminum particles; and -b) gaseous methane with solid aluminum particles. Each of these fuels and their assumed chemical reactions are discussed in detail in the following sections.

### 3.2.1. Gaseous Hydrogen with Solid Aluminum Particles

Gaseous hydrogen is an attractive fuel for this combustor due to its availability, high flame temperature and "clean" combustion (its main combustion product is water vapor). In addition, since water vapor is one of the combustion products in solid rocket motors, it is important to understand aluminum combustion in a water vapor environment. Its "clean" flame also allows for easy recognition of product species within the flame. It is for these reasons that the initial combustor operation will use gaseous hydrogen with solid aluminum as the fuel. Although hydrogen will be used as the initial fuel, it is important to note that some additional safety problems concerning its detonation must be considered. These safety considerations are discussed in more detail in chapters 4 and 5.

When the hydrogen and aluminum react with the gaseous oxygen, the assumed single step, stoichiometric reaction is:

$$4H_2(g) + 4aAl(s) + (3a+2)O_2(g) \rightarrow 2aAl_2O_3(\ell) + 4H_2O(g) \qquad (4)$$

where 'a' is a dummy variable which changes as the mass fraction of aluminum changes and $(g)$, $(\ell)$, and $(s)$ represent gaseous, liquid, and solid phases, respectively. Although this equation is very simplified (due to the fact that many more product species are actually produced) it is extremely useful in estimating the O/F ratio required for stoichiometry and other parameters which are used in the NASA CETPC program [16]. For example, the mass fraction of aluminum in equation 4 is:

$$X_{Al} = \frac{\eta_{Al} M_{Al}}{\eta_{H_2} M_{H_2} + \eta_{O_2} M_{O_2} + \eta_{Al} M_{Al}} \qquad (5)$$

where $\eta$ is the number of moles and M is the molecular weight of the subscripted species. Substituting the proper values one can solve equation 5 for the value of a:

$$a = \frac{72.064 X_{Al}}{107.92 - 203.92 X_{Al}} \qquad (6)$$

where $X_{Al}$ will be the specified mass fraction of aluminum.

Once 'a' has been calculated the assumed stoichiometric O/F ratio can be found by using:

$$\frac{O}{F} = \frac{\eta_{O_2} M_{O_2}}{\eta_{H_2} M_{H_2} + \eta_{Al} M_{Al}} = \frac{96a + 64}{107.92a + 8.064} \tag{7}$$

Due to the input procedure used for the CETPC program the fuel must be described in weight percent of the total fuel. In other words, the mass fraction of the hydrogen is:

$$X_{fuel_{H_2}} = \frac{\eta_{H_2} M_{H_2}}{\eta_{H_2} M_{H_2} + \eta_{Al} M_{Al}} = \frac{8.064}{107.92a + 8.064} \tag{8}$$

and the mass fraction of the aluminum is simply:

$$X_{fuel_{Al}} = 1 - X_{fuel_{H_2}} \tag{9}$$

From the single step reaction (equation 4) it is also possible to predict the mole ratio of aluminum oxide produced. The mole ratio from this equation will be the maximum amount of aluminum oxide which can be produced for a given mass fraction of aluminum. This is due to the fact that the single step reaction assumes that all of the aluminum is converted to aluminum oxide. Therefore, the

maximum mole ratio of aluminum oxide produced is given by:

$$\left(Y_{Al_2O_3}\right)_{max} = \frac{\eta_{Al_2O_3}}{\eta_{Al_2O_3} + \eta_{H_2O}} = \frac{a}{a+2} \qquad (10)$$

The parameters calculated in equations 6 - 10 are tabulated in Figure 11 for various mass fractions of aluminum.

### 3.2.2. Gaseous Methane with Solid Aluminum Particles

The second fuel which will be used in this combustor is gaseous methane. This fuel will provide the influence of carbon and its oxides, as well as water vapor, on aluminum combustion. This is important because carbon is used in the hydrocarbon binders of many solid rocket motors. Since carbon soot by itself is a very strong emitter in the same range as aluminum oxide it is important to run these experiments at high (above stoichiometry) O/F ratios [23-25]. Otherwise, the carbon may not form into its oxides causing optical data which may be difficult to decipher.

When methane and aluminum react with oxygen, the assumed single step stoichiometric reaction is:

$$2CH_4(g) + (3b+4)O_2(g) + 4bAl(s) \rightarrow 2CO_2(g) + 4H_2O(g) + 2bAl_2O_3(\ell) \qquad (11)$$

| Aluminum Mass Fraction $X_{Al}$ | Dummy Variable a | O/F Ratio | Hydrogen Fuel Mass Fraction $X_{fuel_{H_2}}$ | Aluminum Fuel Mass Fraction $X_{fuel_{Al}}$ | Aluminum Oxide Maximum Mole Fraction $(Y_{Al_2O_3})_{max}$ |
|---|---|---|---|---|---|
| 0.0005 | 3.342 E-4 | 7.905 | 0.9955 | 0.0045 | 1.671 E-4 |
| 0.0010 | 6.690 E-4 | 7.873 | 0.9911 | 0.0089 | 3.344 E-4 |
| 0.0015 | 1.004 E-3 | 7.843 | 0.9867 | 0.0133 | 5.017 E-4 |
| 0.0020 | 1.341 E-3 | 7.812 | 0.9824 | 0.0176 | 6.701 E-4 |
| 0.0050 | 3.371 E-3 | 7.632 | 0.9568 | 0.0432 | 1.682 E-3 |
| 0.0100 | 6.806 E-3 | 7.349 | 0.9165 | 0.0835 | 3.391 E-3 |
| 0.0500 | 3.687 E-2 | 5.608 | 0.6696 | 0.3304 | 1.810 E-2 |
| 0.1000 | 8.233 E-2 | 4.242 | 0.4758 | 0.5242 | 3.950 E-2 |

**Figure 11: Theoretical Parameters For H2 - O2 - Al Flame**

where b is a dummy variable which is related to the initial mass fraction of aluminum. As with the hydrogen single step reaction, this reaction is simplified due to the omission of the additional product species which would be produced. In addition, the actual reaction would not occur in a single step, but would require a series of many reactions to reach completion.

From equation 11, the mass fraction of aluminum is given by:

$$X_{Al} = \frac{\eta_{Al} M_{Al}}{\eta_{CH_4} M_{CH_4} + \eta_{O_2} M_{O_2} + \eta_{Al} M_{Al}} \tag{12}$$

Substituting and solving for b:

$$b = \frac{160.084 X_{Al}}{107.92 - 203.92 X_{Al}} \tag{13}$$

Similarly, the stoichiometric O/F ratio can be calculated using:

$$\frac{O}{F} = \frac{\eta_{O_2} M_{O_2}}{\eta_{CH_4} M_{CH_4} + \eta_{Al} M_{Al}} = \frac{96b + 128}{107.92b + 32.084} \tag{14}$$

As with the hydrogen case, the fuels must be expressed in percent of total fuel. Therefore, the relative amount of methane is given by:

$$X_{fuel_{CH_4}} = \frac{\eta_{CH_4} M_{CH_4}}{\eta_{CH_4} M_{CH_4} + \eta_{Al} M_{Al}} = \frac{32.084}{107.92b + 32.084} \tag{15}$$

Also, the relative weight of aluminum is given by:

$$X_{fuel_{Al}} = 1 - X_{fuel_{CH_4}} \tag{16}$$

Similar to the hydrogen case, the maximum amount of aluminum oxide for this reaction can be predicted. The maximum mole fraction of aluminum oxide produced is given by:

$$\left(Y_{Al_2O_3}\right)_{max} = \frac{\eta_{Al_2O_3}}{\eta_{Al_2O_3} + \eta_{H_2O} + \eta_{CO_2}} = \frac{b}{b+3} \tag{17}$$

The parameters calculated in equations 13 - 17 are listed in figure 12 for various aluminum mass fractions.

### 3.3. Chemical Equilibrium Calculations

Flame temperature, combustion products and transport were calculated using a version of NASA SP-273 [16] called CETPC. The CETPC version of this computer program is a version which is capable of running on most IBM compatible personal computers while maintaining equal accuracy. This versatile computer program is capable of calculating: -1) equilibrium compositions for assigned thermodynamic states; -2) theoretical rocket performance, -3) Chapman-Jouquet detonations; and -4) shock tube parameter calculations.

| Aluminum Mass Fraction $X_{Al}$ | Dummy Variable a | O/F Ratio | Hydrogen Fuel Mass Fraction $X_{fuel_{H_2}}$ | Aluminum Fuel Mass Fraction $X_{fuel_{Al}}$ | Aluminum Oxide Maximum Mole Fraction $(Y_{Al_2O_3})_{max}$ |
|---|---|---|---|---|---|
| 0.0005 | 7.424 E-4 | 3.982 | 0.9975 | 0.0025 | 2.474 E-4 |
| 0.0010 | 1.486 E-3 | 3.974 | 0.9950 | 0.0050 | 4.951E-4 |
| 0.0015 | 2.231 E-3 | 3.966 | 0.9926 | 0.0074 | 7.431 E-4 |
| 0.0020 | 2.978 E-3 | 3.959 | 0.9901 | 0.0099 | 9.917 E-4 |
| 0.0050 | 7.487 E-3 | 3.913 | 0.9754 | 0.0246 | 2.489 E-3 |
| 0.0100 | 1.510 E-2 | 3.839 | 0.9516 | 0.0484 | 5.008 E-3 |
| 0.0500 | 8.190 E-2 | 3.319 | 0.7840 | 0.7840 | 2.657 E-2 |
| 0.1000 | 1.829 E-1 | 2.809 | 0.6191 | 0.6191 | 5.746 E-2 |

**Figure 12: Theoretical Parameters For CH4 - O2 - Al Flame**

Since this project is interested in obtaining the properties of aluminum combustion, this thesis will use the equilibrium calculations portion of the CETPC program to calculate the necessary properties for this combustor. These equilibrium properties are calculated using the minimization of free-energy. Depending upon the thermodynamic properties which are specified, the minimization of free-energy can be found by using Gibbs free-energy, Helmholz free-energy, or the maximization of entropy. Since the initial temperature (and therefore heat of formation) and pressure of the reactants are known for this combustor, the minimization of Gibbs free-energy is used in the computer code equilibrium calculations. When making these calculations, this computer program assumes that all gases are ideal and all condensed phases are pure. The main interest in these calculations for this combustor is to determine the -a) products of combustion, -b) flame temperature and -c) transport properties. The above parameters are discussed further in the following sections.

### 3.3.1. Products of Combustion

Since the initial goal of this combustor is to observe the combustion phenomena of aluminum and the optical properties of aluminum and its oxides, it is important to verify that most of the aluminum is being converted into aluminum oxide. The CETPC program was use to find the species present in the equilibrium

combustion of the Hydrogen - Oxygen - Aluminum and the Methane - Oxygen - Aluminum systems. Samples of the mole fractions of the product species (for an aluminum mass fraction of 0.01) are listed in Appendix 1 (Hydrogen) and Appendix 2 (Methane). The chemical products were calculated using pressures ranging from 500 psia to 1000 psia, O/F ratios ranging from 1 to 25, and aluminum mass fractions ranging from 0.0005 to 0.10. One of the surprises which came from this array of data points was the formation of a type of aluminum hydroxide ($AlO_2H$ or AlO(OH)) instead of aluminum oxide ($Al_2O_3$) at low mass fractions of aluminum. Not surprising, however, was the fact that for a given O/F ratio and aluminum mass fraction, the mole fractions of these products were nearly constant with changing pressure. The mole fractions of these two products vs. the mass fraction of aluminum are plotted for the hydrogen fuel (Figures 13-17) and for the methane fuel (Figures 18-23) at 500 psia. As can be seen from these plots, at low mass fractions and low to stoichiometric O/F ratios the mole fraction of $AlO_2H$ is greater than the mole fraction of aluminum oxide. Since solid rocket propellants produce large quantities of aluminum oxide and little or no $AlO_2H$ it is necessary to operate this combustor at points where the amount of aluminum oxide is far greater than the amount of $AlO_2H$ produced. This occurs at high mass fractions of aluminum (5-10%) and high O/F ratios. Since erosion of the nozzle throat is a concern for high temperature, oxygen rich flows and since high O/F ratios may reduce the flame temperature so much that aluminum ignition becomes

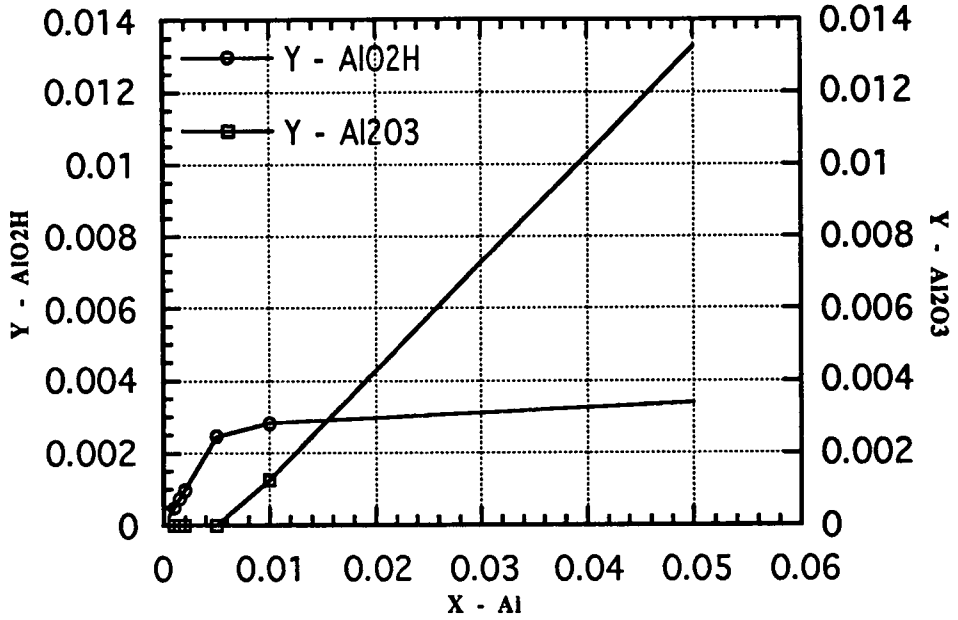


Figure 13: Mole Fractions of Species Vs. Mass Fraction of Aluminum
(Fuel = Hydrogen, O/F = Stoich., P = 500 psia)

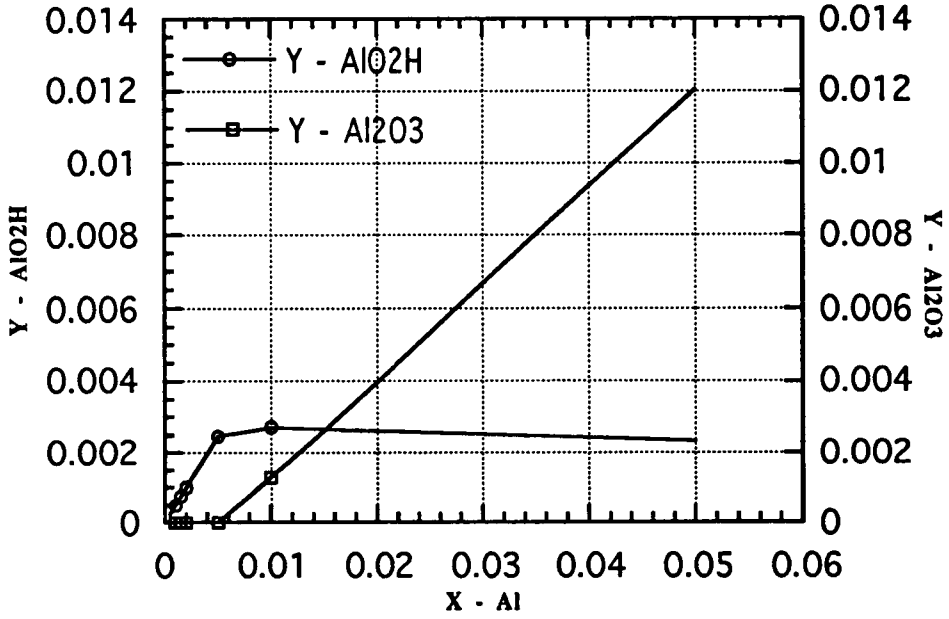


Figure 14: Mole Fractions of Species Vs. Mass Fraction of Aluminum
(Fuel = Hydrogen, O/F = 8.0, P = 500 psia)

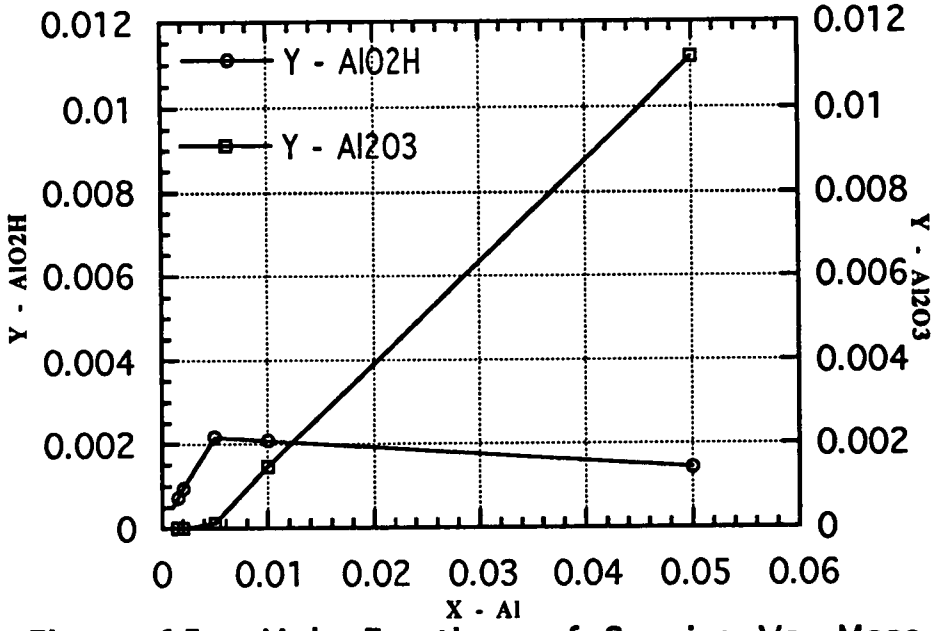


Figure 15: Mole Fractions of Species Vs. Mass Fraction of Aluminum
(Fuel = Hydrogen, O/F = 10.0, P = 500 psia)

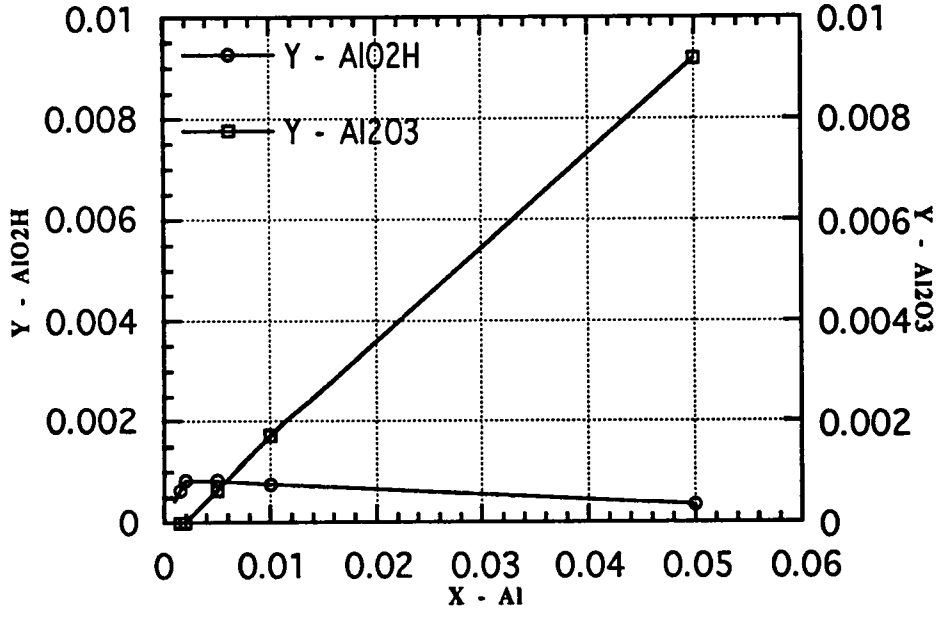


Figure 16: Mole Fractions of Species Vs. Mass Fraction of Aluminum
(Fuel = Hydrogen, O/F = 15, P = 500 psia)

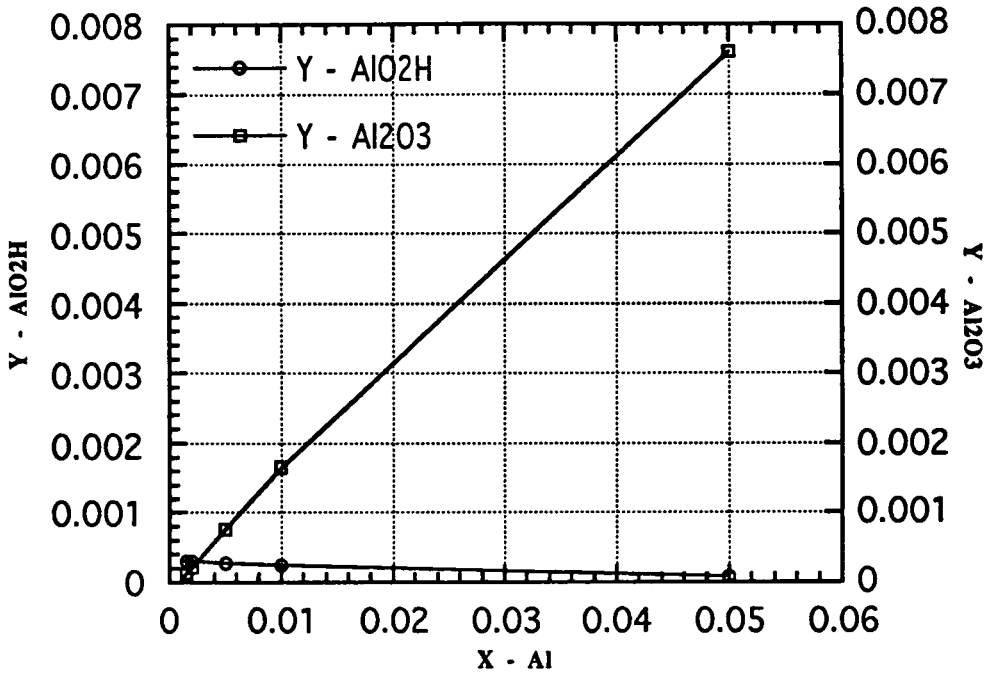


Figure 17: Mole Fractions of Species Vs. Mass Fraction of Aluminum
(Fuel = Hydrogen, O/F = 20.0, P = 500 psia)

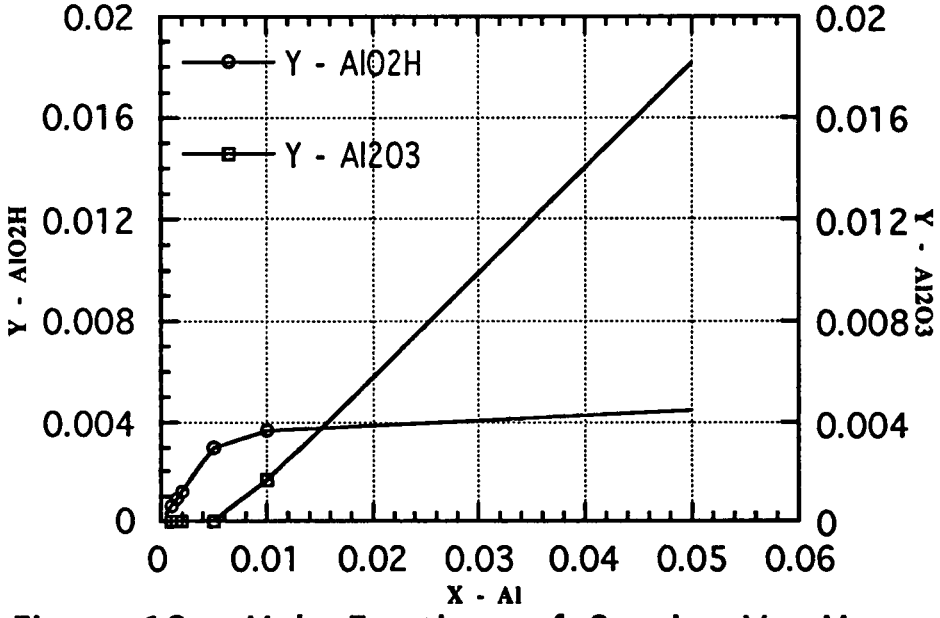


Figure 18: Mole Fractions of Species Vs. Mass Fraction of Aluminum
(Fuel = Methane, O/F = 3.0, P = 500 psia)

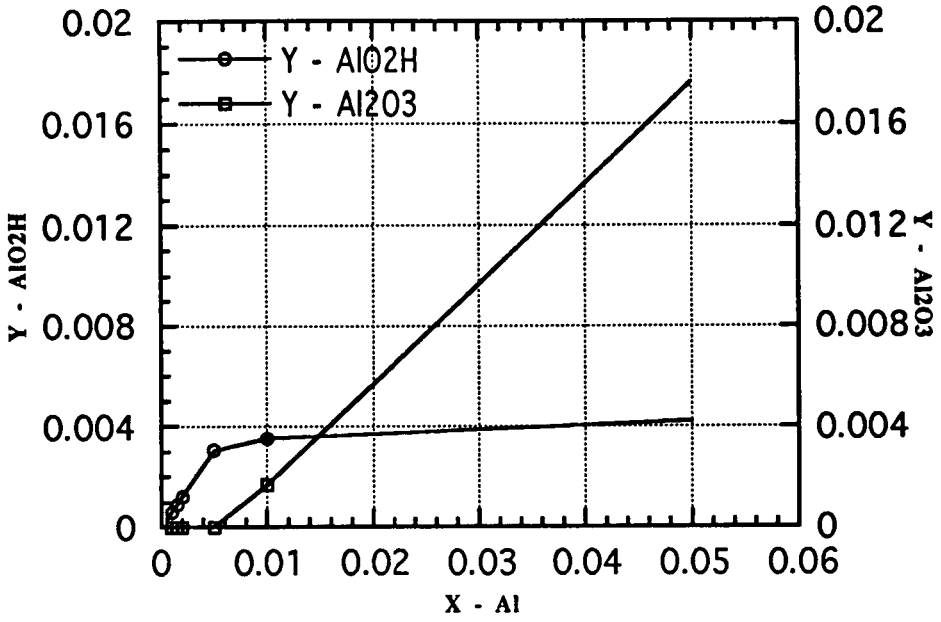


Figure 19: Mole Fractions of Species Vs. Mass Fraction of Aluminum
(Fuel = Methane, O/F = Stoich, P = 500 psia)

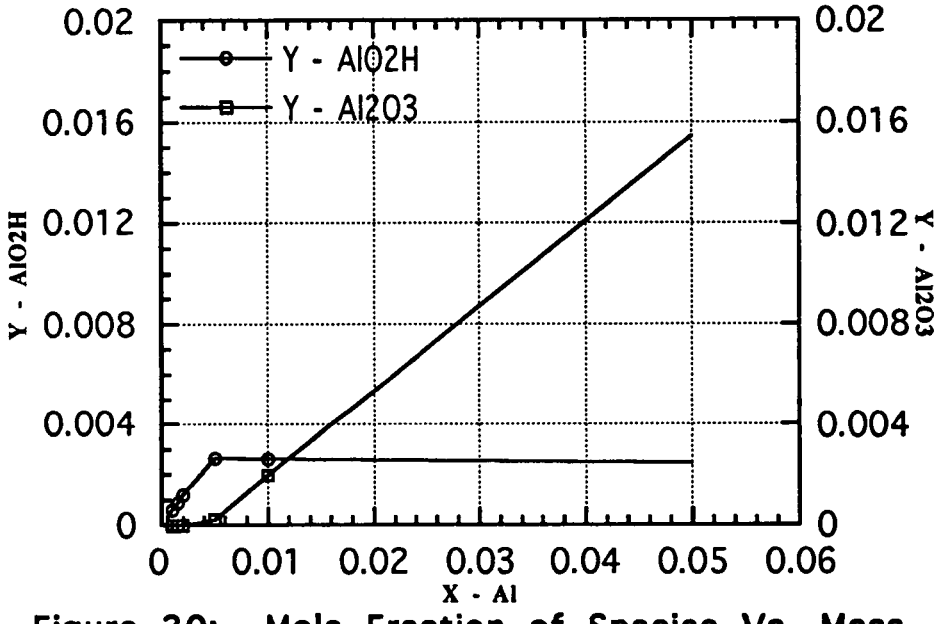


Figure 20: Mole Fraction of Species Vs. Mass Fraction of Aluminum
(Fuel = Methane, O/F = 5.0, P = 500 psia)

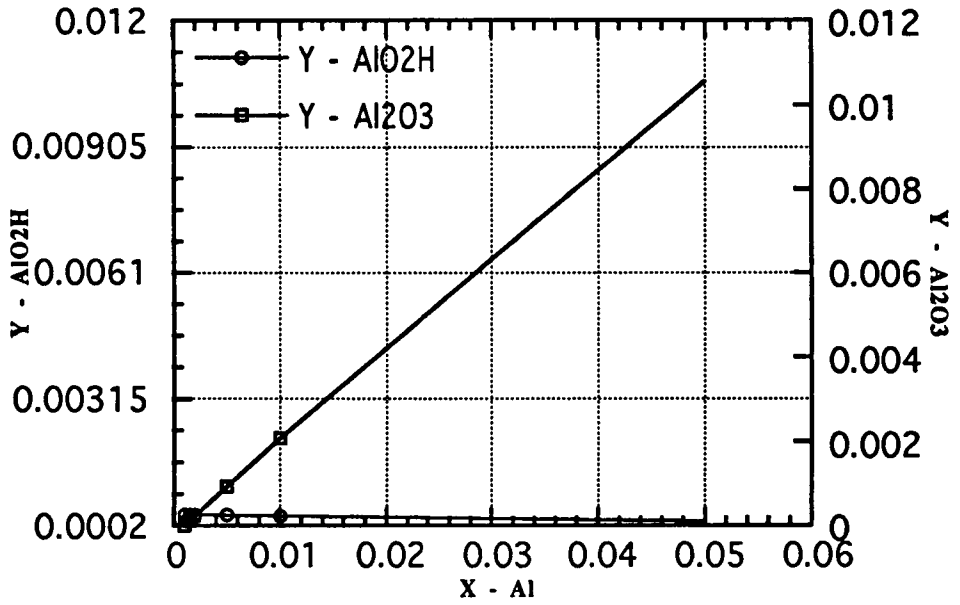


Figure 21: Mole Fractions of Species Vs. Mass Fraction of Aluminum
(Fuel = Methane, O/F = 10.0, P = 500 psia)

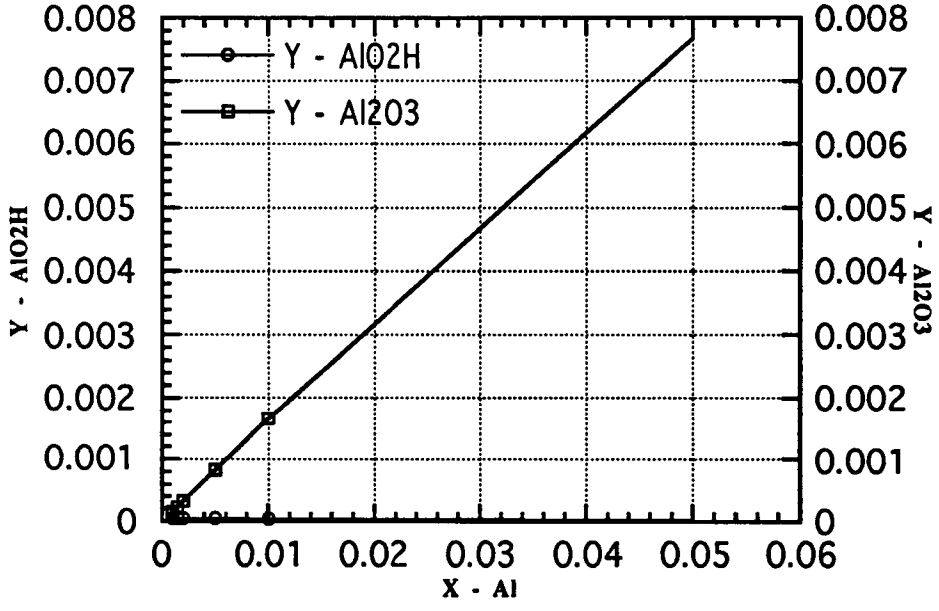


Figure 22: Mole Fractions of Species Vs. Mass Fraction of Aluminum
(Fuel = Methane, O/F = 15, P = 500 psia)

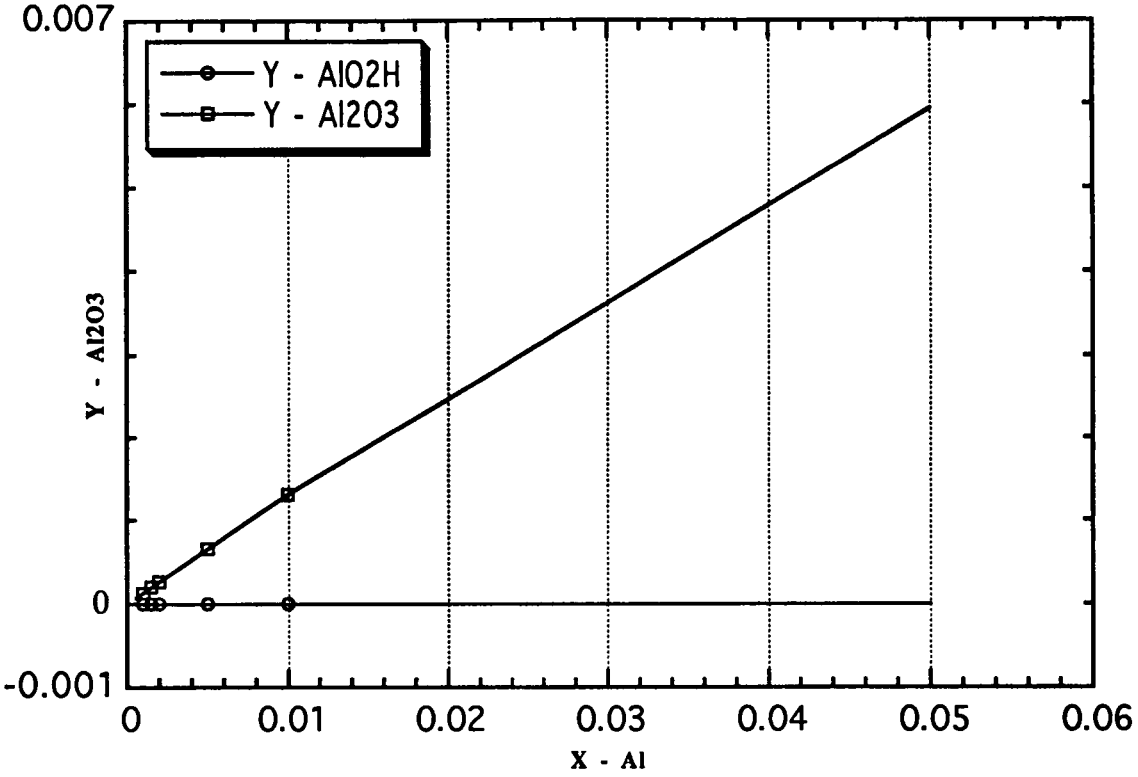


Figure 23: Mole Fractions of Species Vs. Mass Fraction of Aluminum (Fuel = Methane, O/F = 20, P = 500 psia)

difficult, it is necessary to limit the O/F ratio to as close to stoichiometric (fuel rich would be better) as possible. However, since it is difficult to obtain a large mass flow rate of aluminum particles while maintaining observational quality, it is necessary to also limit the mass fraction of aluminum injected. Therefore, it is necessary to make a trade off between high mass fraction of aluminum and high O/F ratios. In other words, the initial combustor will run at moderate mass fractions of aluminum (0.5-5%) and moderate O/F ratios (stoichiometric to 10 for hydrogen and stoichiometric to 5 for methane). It should also be noted that as aluminum content increases, stoichiometric O/F ratio decreases from the stoichiometric O/F ratio of the fuel alone (O/F = 8.0 for hydrogen and O/F = 4.0 for methane) at zero aluminum content to a minimum at the stoichiometric O/F ratio of the aluminum alone (O/F = 1.78) at zero fuel content. Obviously, the best combination of these two parameters will need to be experimentally determined.

### 3.3.2. Flame Temperature

The flame temperature calculations of the mixture were also performed using CETPC at a variety of pressures, O/F ratios and aluminum mass fractions. Since varying the aluminum content of the mixture only had a slight influence on temperature (less than 10% total change), the average temperature (between aluminum mass fractions of 0.001 and 0.05) vs. the O/F ratio were plotted and

are shown in Figure 24 for hydrogen and Figure 25 for methane. As can be seen from these figures the highest temperature for the hydrogen fuel mixture is near 3680 K and the methane fuel mixture maximum temperature is approximately 3900 K. Taking the largest of these and adding a 15% margin of error, the design temperature of 4485 K is obtained. This is the absolute maximum temperature which the combustor will ever see for either of these two fuels.

### 2.3.3. Transport Properties

The third, and final, parameters found using the CETPC code were the transport properties. These transport properties of the combustion products included: density ($\rho$), molecular weight (M), ratio of specific heats ($\gamma$), sonic velocity (c), viscosity ($\mu$), specific heat at constant pressure ($C_p$), conductivity (k), and Prandtl number (Pr). Most of these parameters remained fairly constant with changing aluminum mass fraction. However, some of these properties differed by up to 20% with varying aluminum mass fractions. Never the less, all of these transport properties were averaged from an aluminum mass fraction of 0.001 to an aluminum mass fraction of 0.05. These values were then plotted at pressures of 500 and 1000 psia at various O/F ratios (Figures 26-41). It should be noted that the values found for $C_p$, k, and Pr were found by using equilibrium reactions instead of frozen reactions. (By equilibrium reactions it is meant that the reaction is assumed to

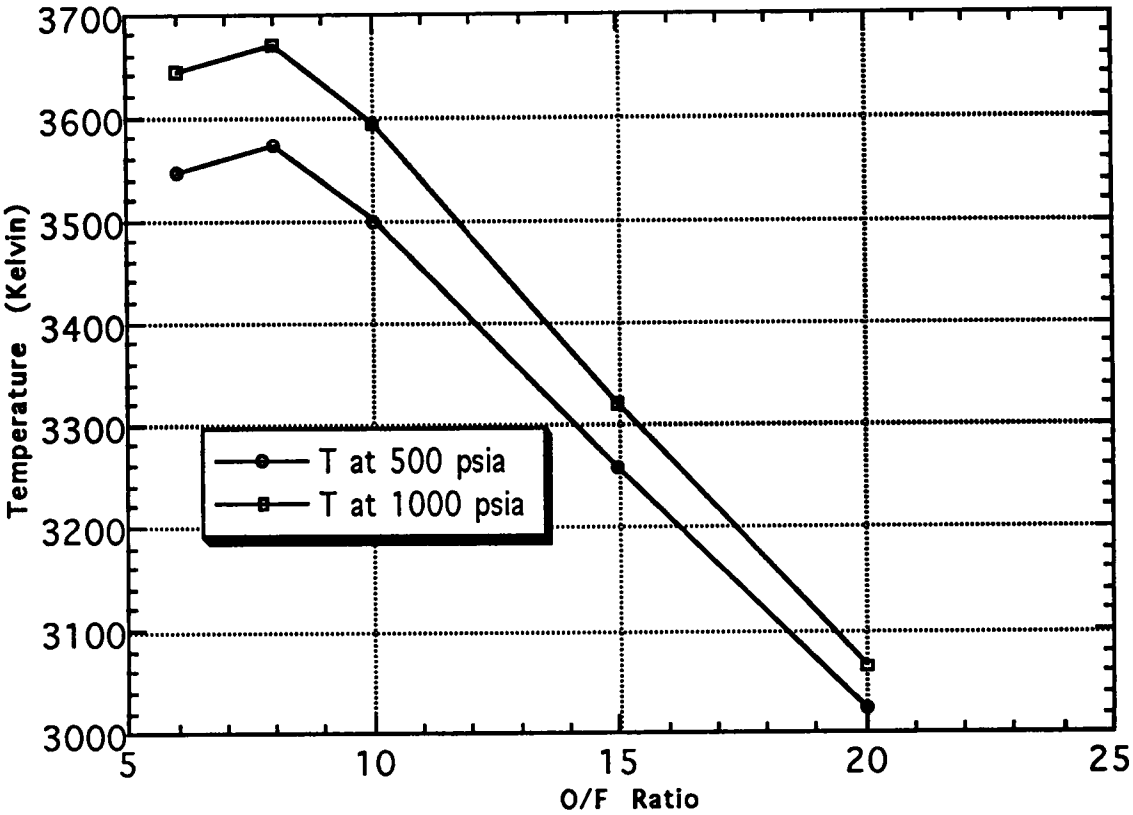


Figure 24: Mean Temperature vs. O/F Ratio
(Hydrogen - Oxygen - Aluminum Flame)

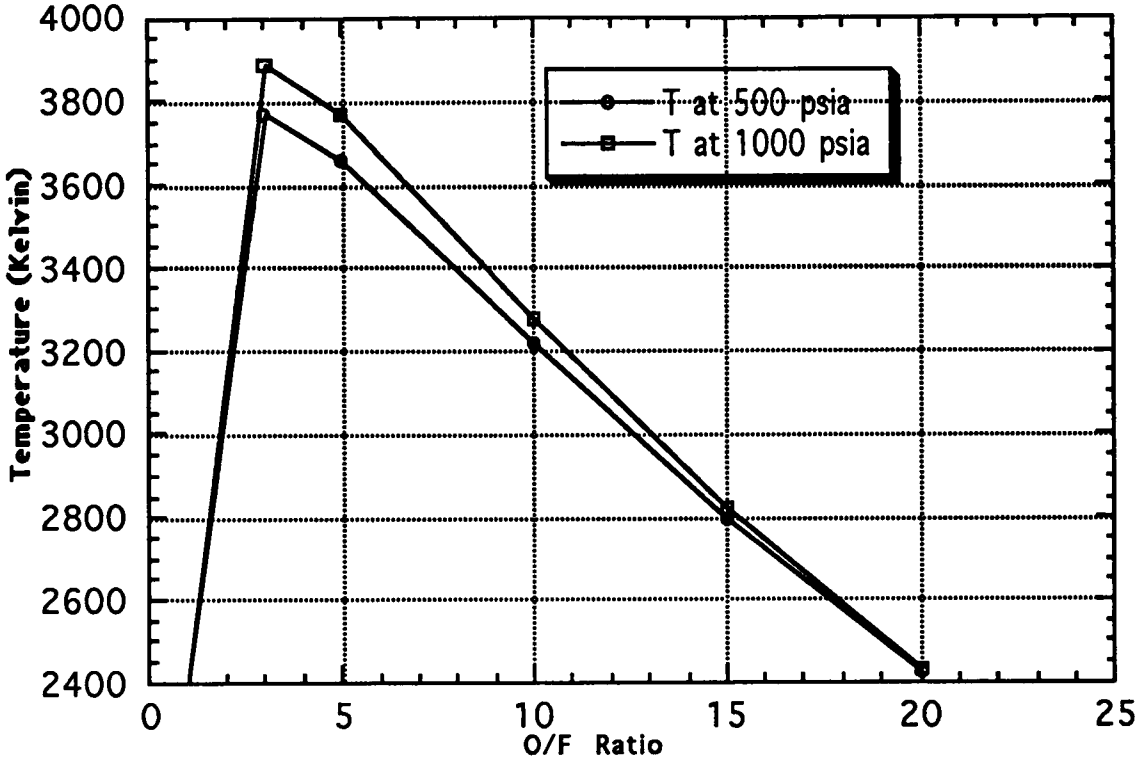


Figure 25: Mean Temperature Vs. O/F Ratio
(Methane - Oxygen - Aluminum Flame)

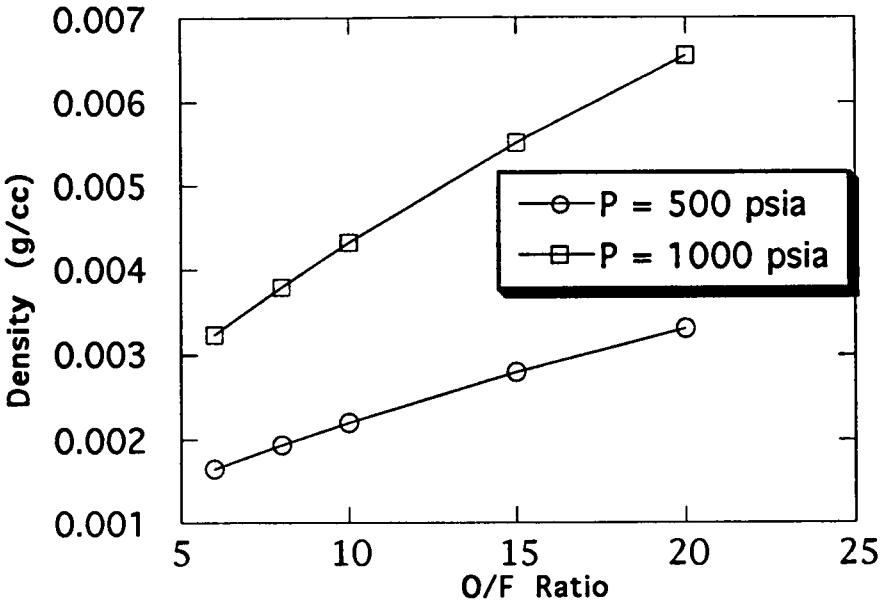


Figure 26: Density Vs. O/F Ratio
Fuel=Hydrogen, 0.001<Aluminum Mass Fraction<0.05

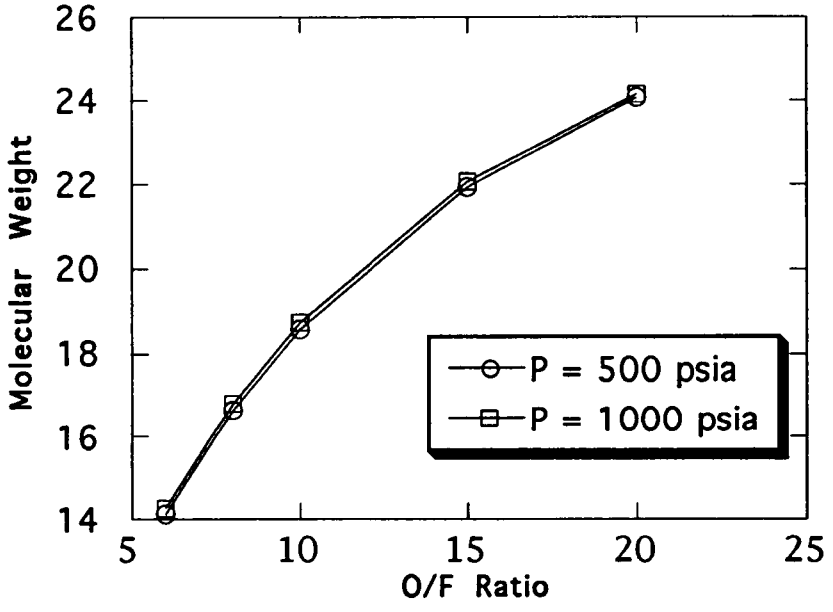


Figure 27: Molecular Weight Vs. O/F Ratio
Fuel=Hydrogen, 0.001<Aluminum Mass Fraction<0.05

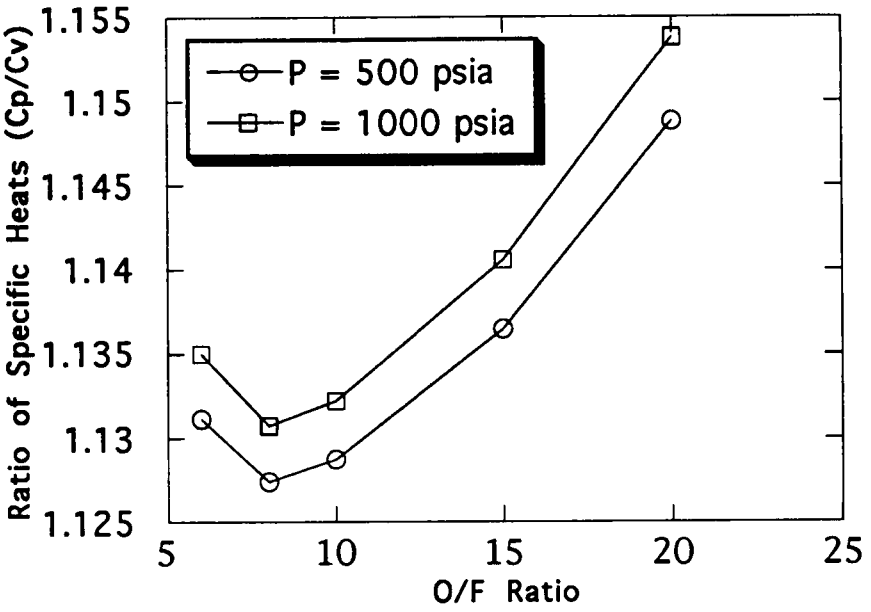


Figure 28: Specific Heat Ratio Vs. O/F Ratio
Fuel=Hydrogen, 0.001<Aluminum Mass Fraction<0.05

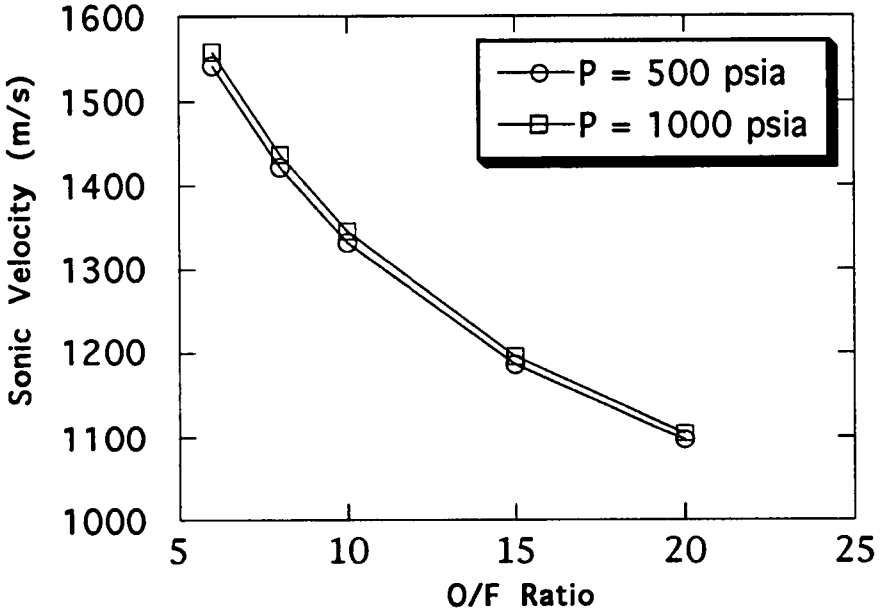


Figure 29: Average Sonic Velocity Vs. O/F Ratio
Fuel=Hydrogen, 0.001<Aluminum Mass Fraction<0.05

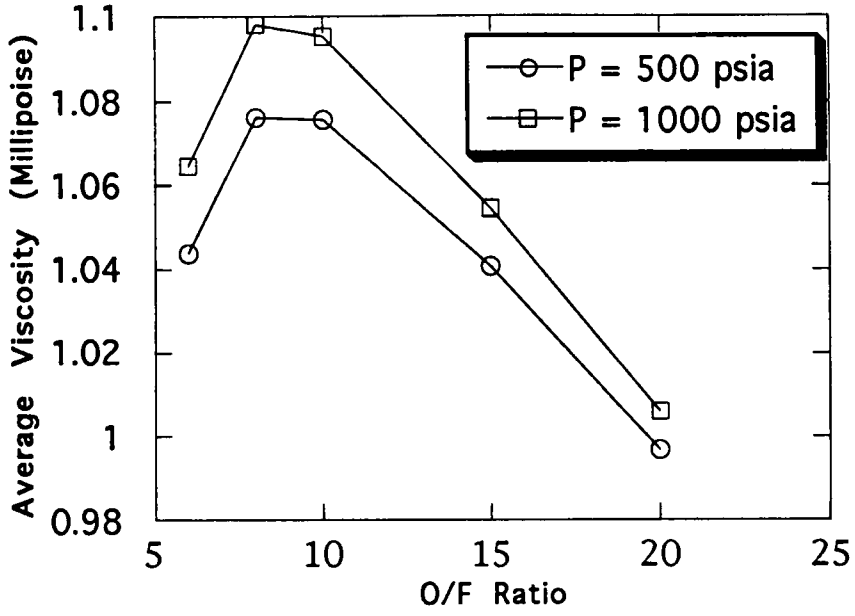


**Figure 30: Average Viscosity Vs. O/F Ratio Fuel=Hydrogen, 0.001<Aluminum Mass Fraction<0.05**

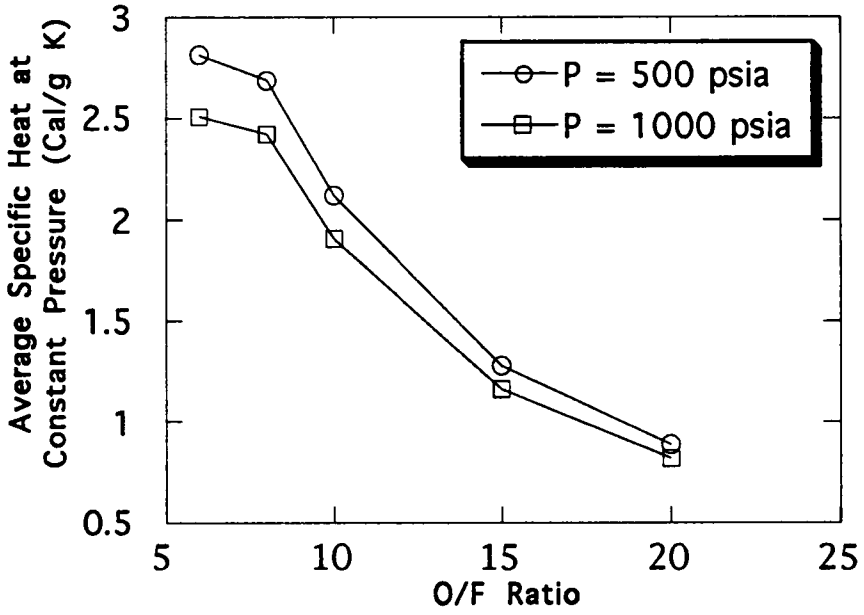


**Figure 31: Average Specific Heat Vs. O/F Ratio Fuel=Hydrogen, 0.001<Aluminum Mass Fraction<0.05**

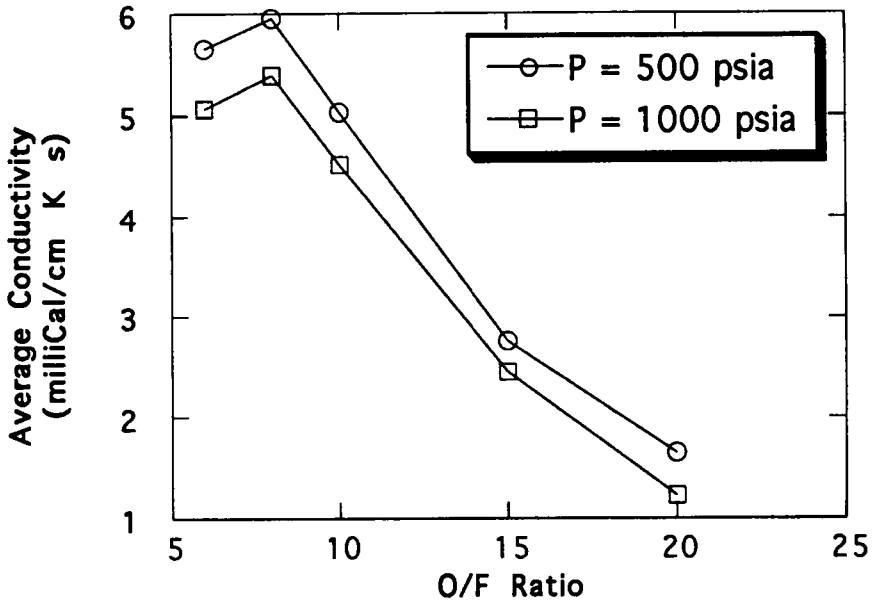


Figure 32: Average Conductivity Vs. O/F Ratio
Fuel=Hydrogen, 0.001<Aluminum Mass Fraction<0.05

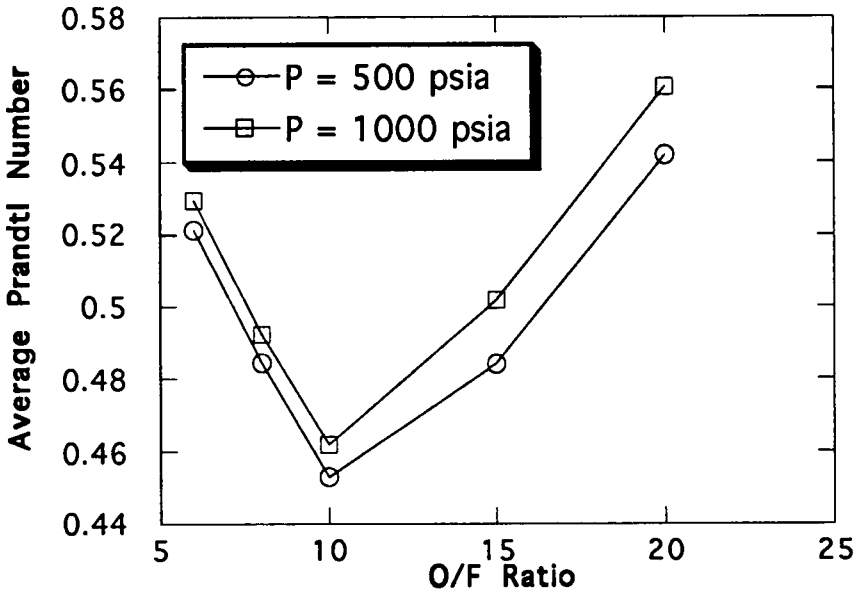


Figure 33: Average Prandtl Number Vs. O/F Ratio
Fuel=Hydrogen, 0.001<Aluminum Mass Fraction<0.05

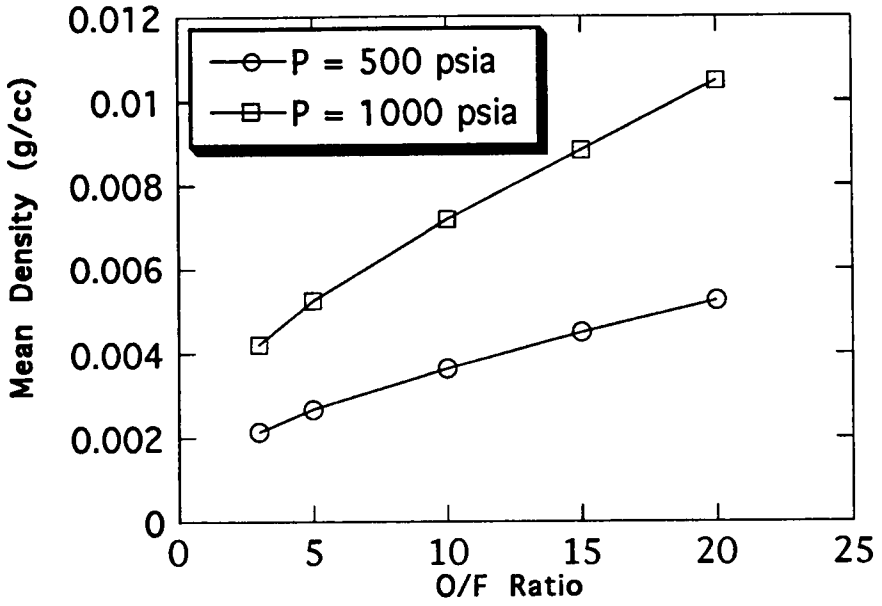


**Figure 34: Mean Density Vs. O/F Ratio**
**Fuel = Methane, 0.001<Aluminum Mass Fraction<0.05**

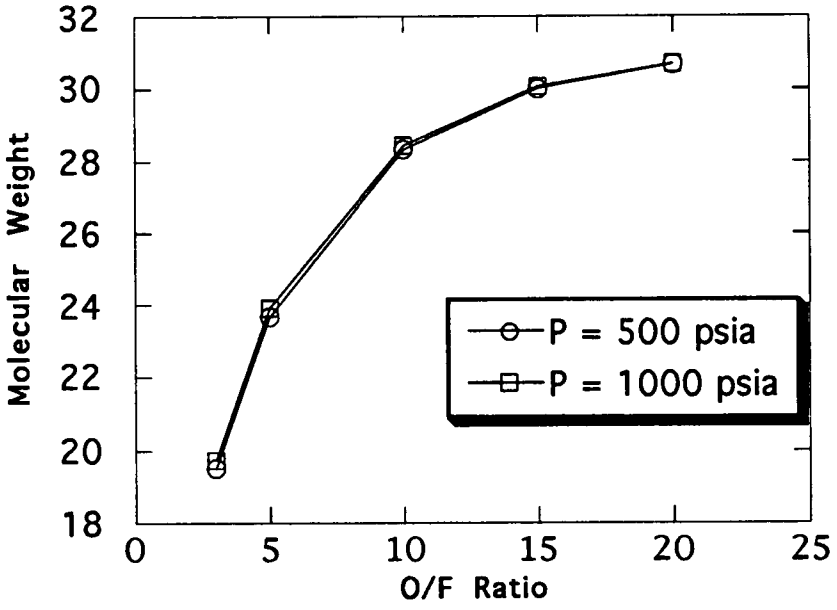


**Figure 35: Mean Molecular Weight Vs. O/F Ratio**
**Fuel = Methane, 0.001<Aluminum Mass Fraction<0.05**

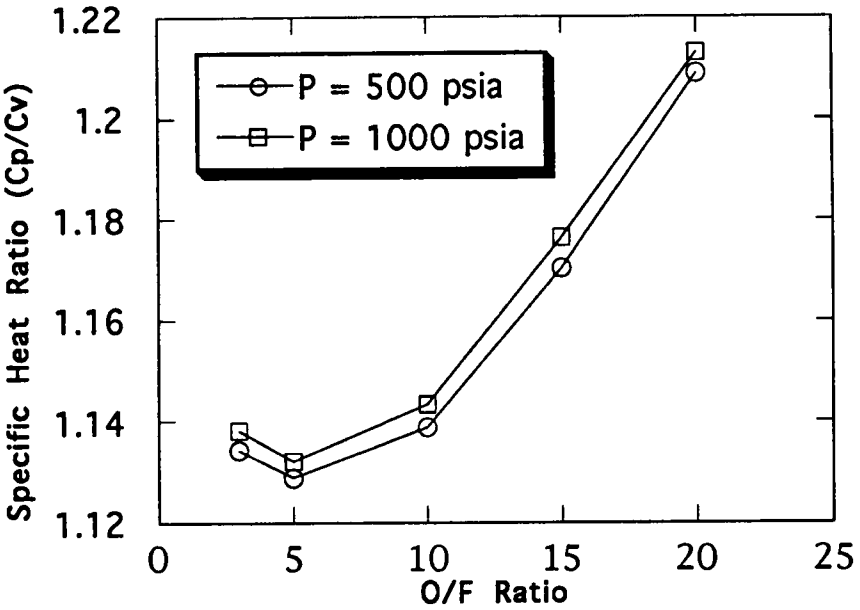


Figure 36: Specific Heat Ratio Vs. O/F Ratio
Fuel = Methane, 0.001<Aluminum Mass Fraction<0.05

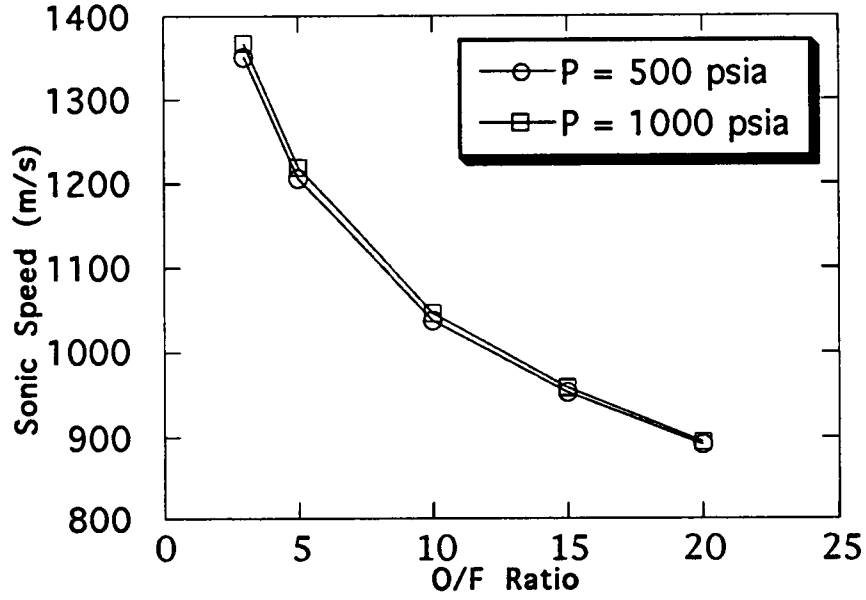


Figure 37: Sonic Speed Vs. O/F Ratio
Fuel = Methane, 0.001<Aluminum Mass Fraction<0.05

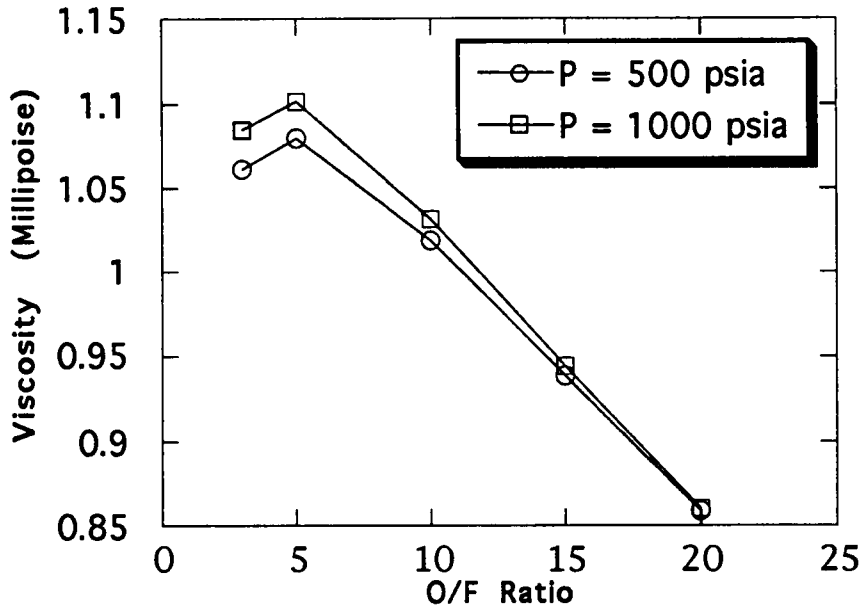


Figure 38: Viscosity Vs. O/F Ratio
Fuel = Methane, 0.001<Aluminum Mass Fraction<0.05

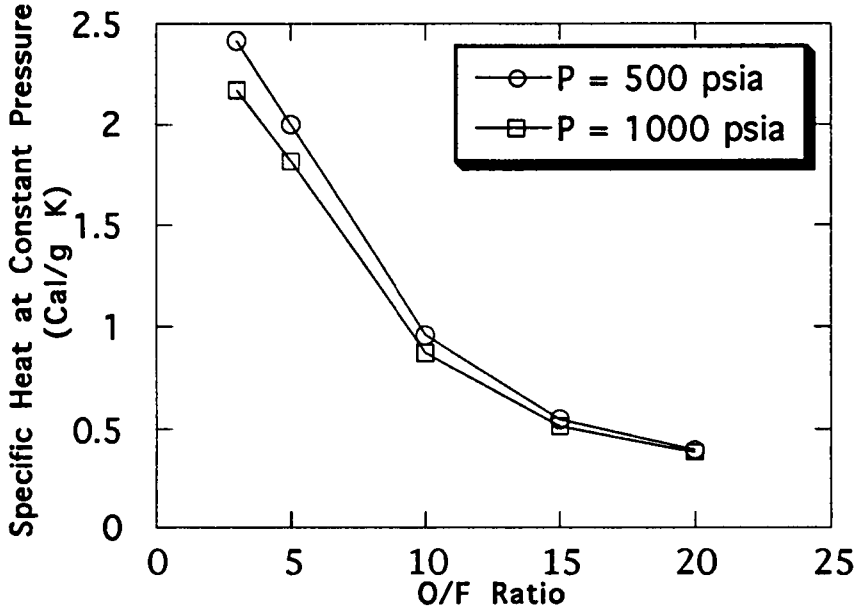


Figure 39: Specific Heat Vs. O/F Ratio
Fuel = Methane, 0.001<Aluminum Mass Fraction<0.05

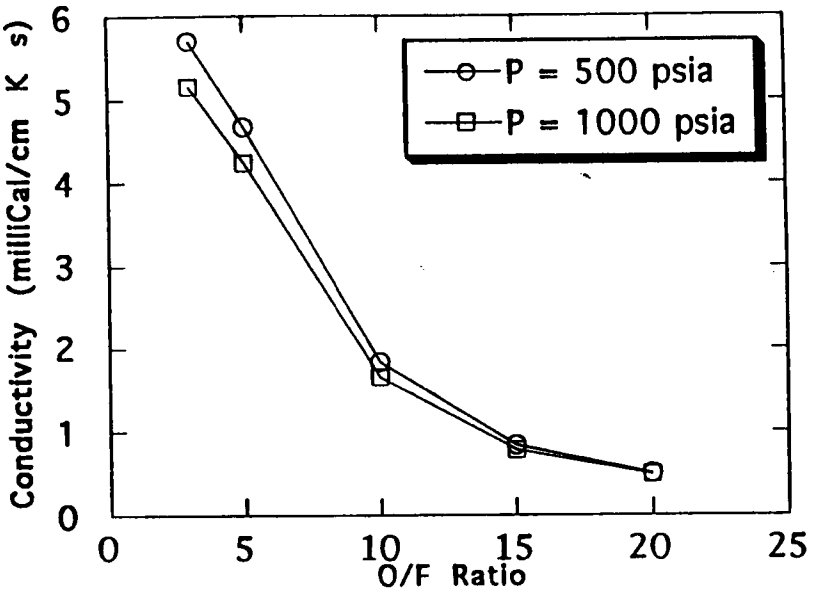


Figure 40: Conductivity Vs. O/F Ratio
Fuel = Methane, 0.001<Aluminum Mass Fraction<0.05

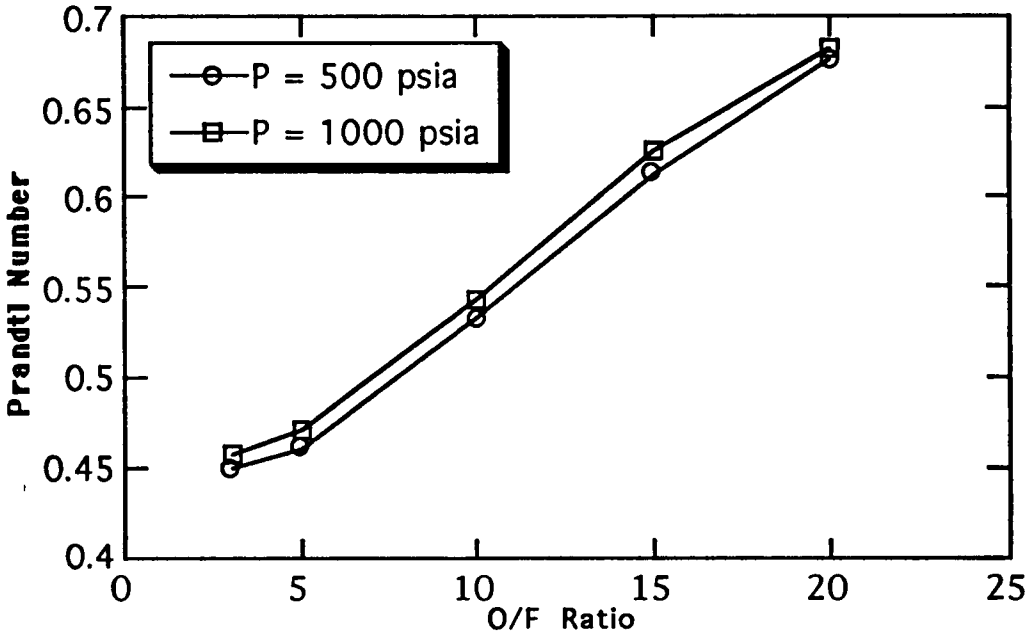


Figure 41: Prandtl Number Vs. O/F Ratio
Fuel = Methane, 0.001<Aluminum Mass Fraction<0.05

reach its equilibrium composition instantaneously. Conversely, frozen reactions assume that the reaction times are infinitely slow causing the chemical composition to remain fixed.)

As would be expected from the ideal gas equation, the density of the combustion mixture nearly doubles when the pressure is doubled. The density also increases as the O/F ratio increases. From the other figures it can be seen that the other transport properties do not vary significantly when the pressure is changed from 500 psia to 1000 psia. However, these properties do change substantially as the O/F ratio is changed. Therefore, it is necessary to use the correct value for these transport properties during the design portion in chapter 4.

# CHAPTER IV - Design Analysis

This chapter uses the information found in the previous chapters to determine the physical size and operating conditions to be used for this combustor. The first section of this chapter describes how the physical dimensions and materials of the combustor were determined. The next section presents a simplified heat transfer analysis in order to predict the temperatures and allowable operational times of this combustor.

## 4.1. Physical Dimension Calculations

The first step in the design process of this combustor is to determine the physical size of the combustor. Since this combustor is designed to operate at high pressures and high temperatures, the interior dimensions of the combustor must be limited in order to reduce the required thickness (and therefore cost) for the materials used in this combustor. This section presents the methods used to determine the dimensions of the injector, the necessary dimensions for the nozzle throat, and the length and thickness of the glass tube required.

### 4.1.1. Injector Dimensions

Since the dimensions of the combustor must be minimized, it is imperative that the overall injector diameter also is minimized. It would also be more cost effective if the same injector could be used for multiple fuel requirements. The first step in this injector design was to establish the maximum operating conditions for this combustor. Since the length of the combustor must also be kept to a minimum, the injection velocities of the aluminum particles must be slow enough to ensure complete combustion. Therefore, it was decided to limit the absolute maximum injection velocity to 10 m/s [26]. Using this assumption, design curves were generated for hydrogen, methane, and oxygen. These design curves show the mass flow rates possible for various pressures (Figures 42-56) and for various injection velocities (Figures 57-71). These figures were generated by using the equation:

$$m = \rho A V \tag{18}$$

where m is the mass flow rate, $\rho$ is the gas density, A is the area of the injector, and V is the average injection velocity.

Since the aluminum particle concentration is small, the two phase flow effects were neglected in these calculations. However,

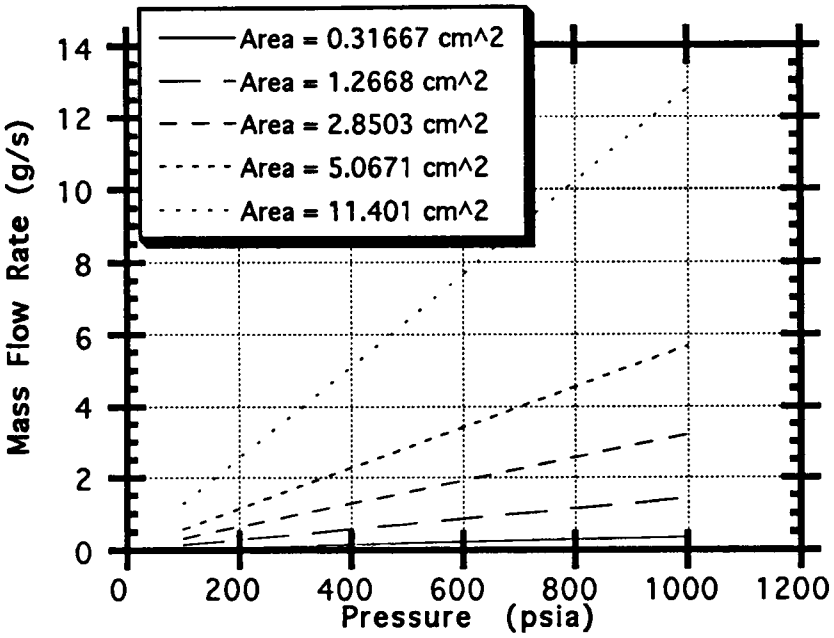


Figure 42: Mass Flow Vs. Pressure
(Gas = Hydrogen, Velocity = 2.0 m/s)

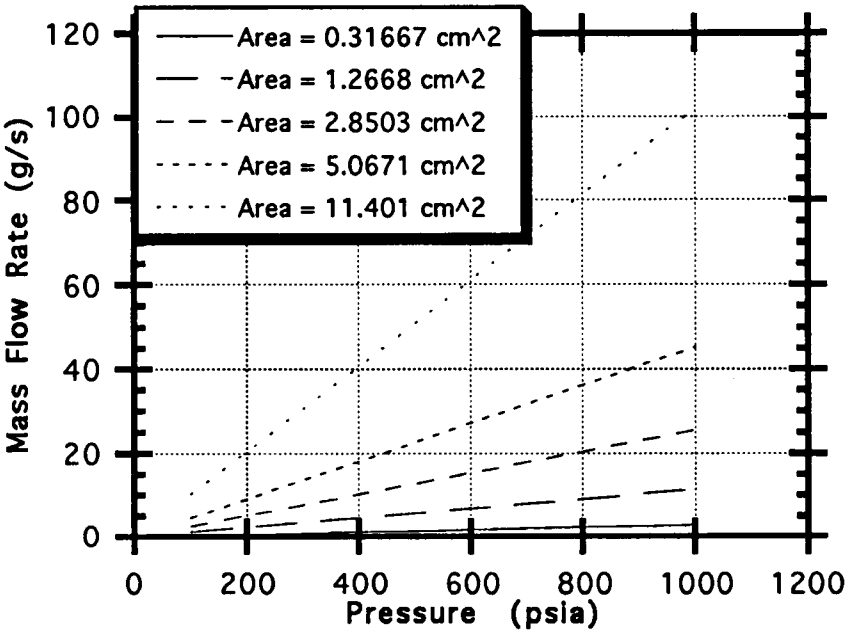


Figure 43: Mass Flow Vs. Pressure
(Gas = Methane, Velocity = 2.0 m/s)

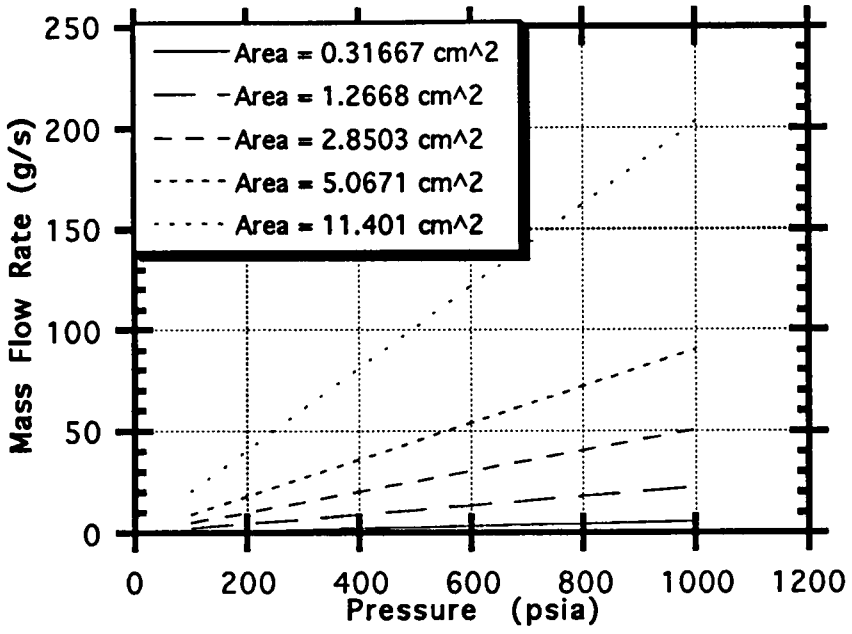


Figure 44: Mass Flow Vs. Pressure
(Gas = Oxygen, Velocity = 2.0 m/s)

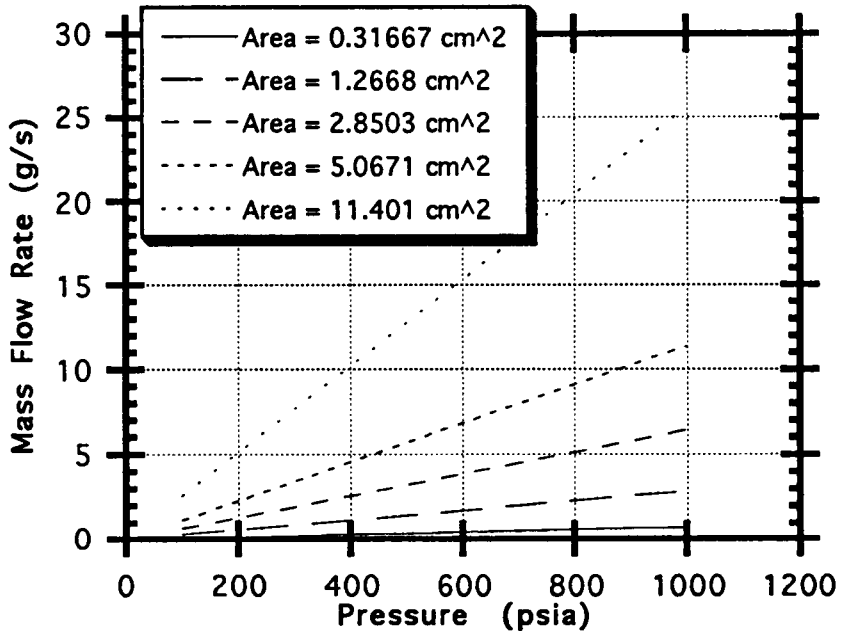


Figure 45: Mass Flow Vs. Pressure
(Gas = Hydrogen, Velocity = 4.0 m/s)

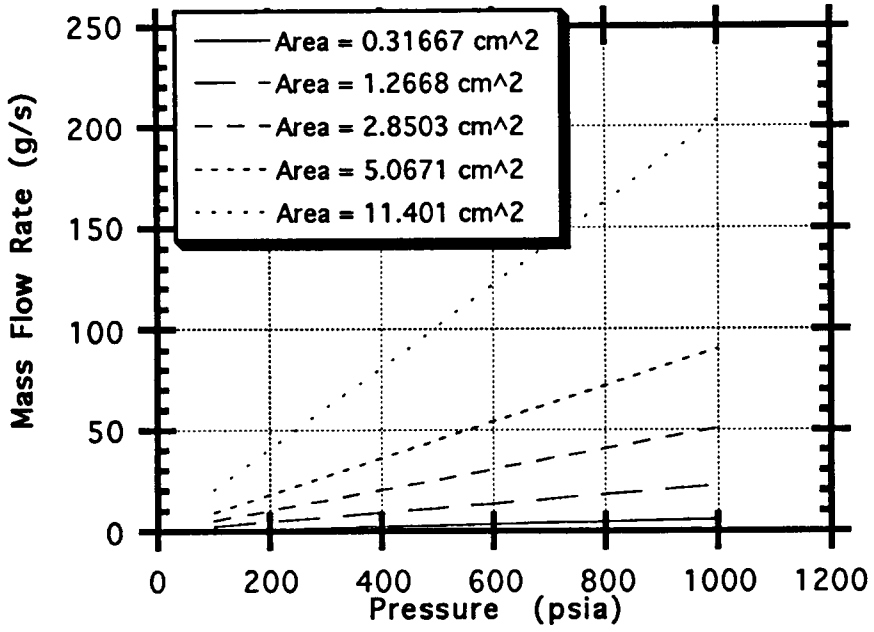


Figure 46: Mass Flow Vs. Pressure
(Gas = Methane, Velocity = 4.0 m/s)

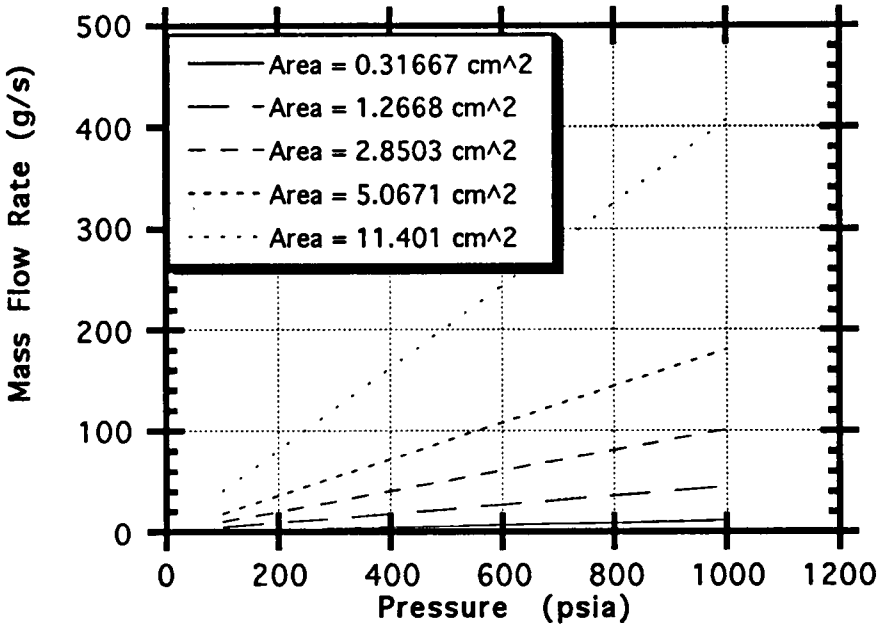


Figure 47: Mass Flow Vs. Pressure
(Gas = Oxygen, Velocity = 4.0 m/s)

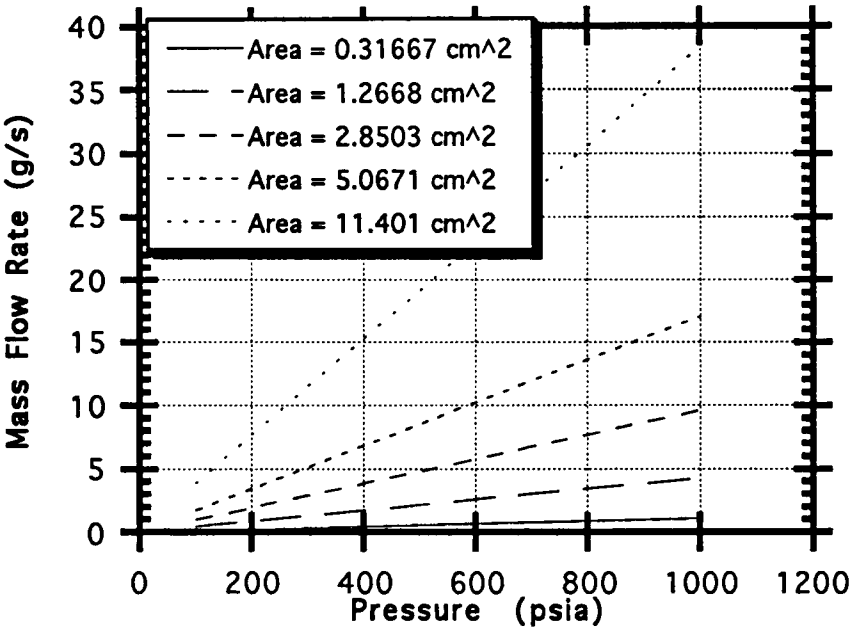


Figure 48: Mass Flow Vs. Pressure
(Gas = Hydrogen, Velocity = 6.0 m/s)

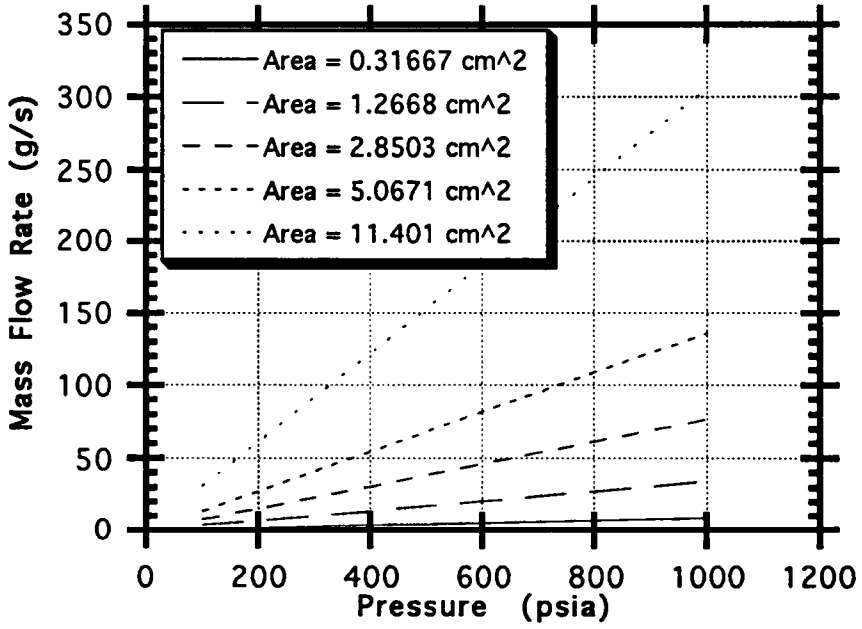


Figure 49: Mass Flow Vs. Pressure
(Gas = Methane, Velocity = 6.0 m/s)

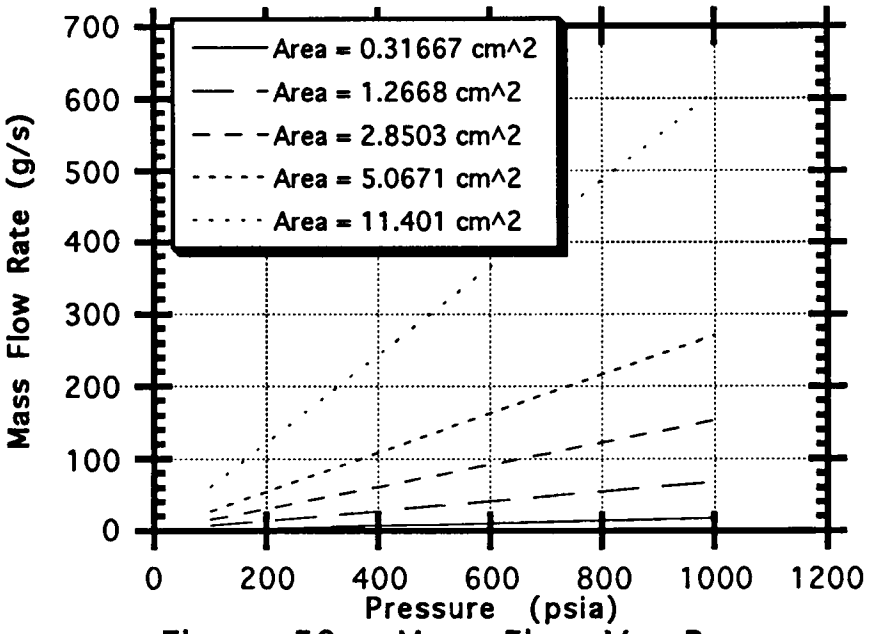


Figure 50: Mass Flow Vs. Pressure
(Gas = Oxygen, Velocity = 6.0 m/s)

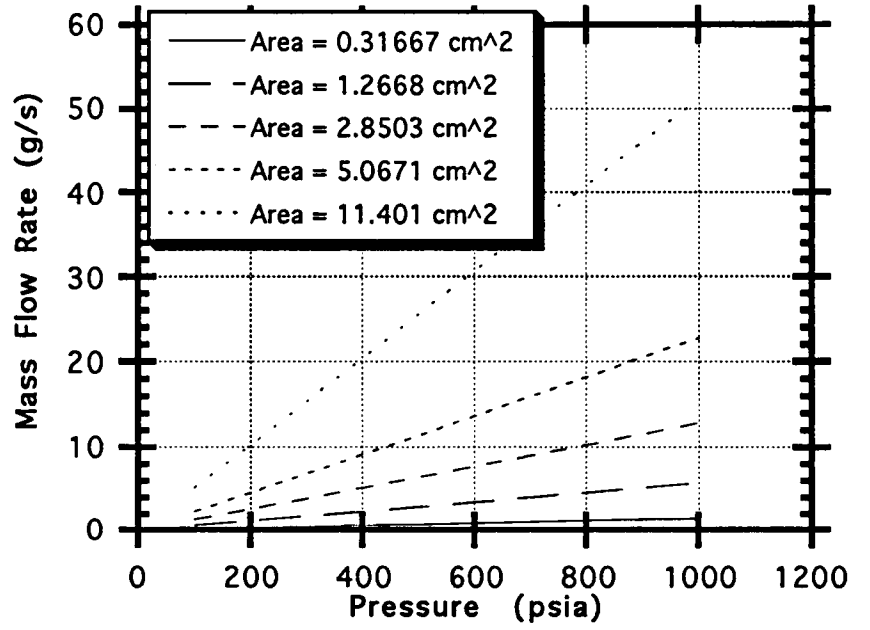


Figure 51: Mass Flow Vs. Pressure
(Gas = Hydrogen, Velocity = 8.0 m/s)

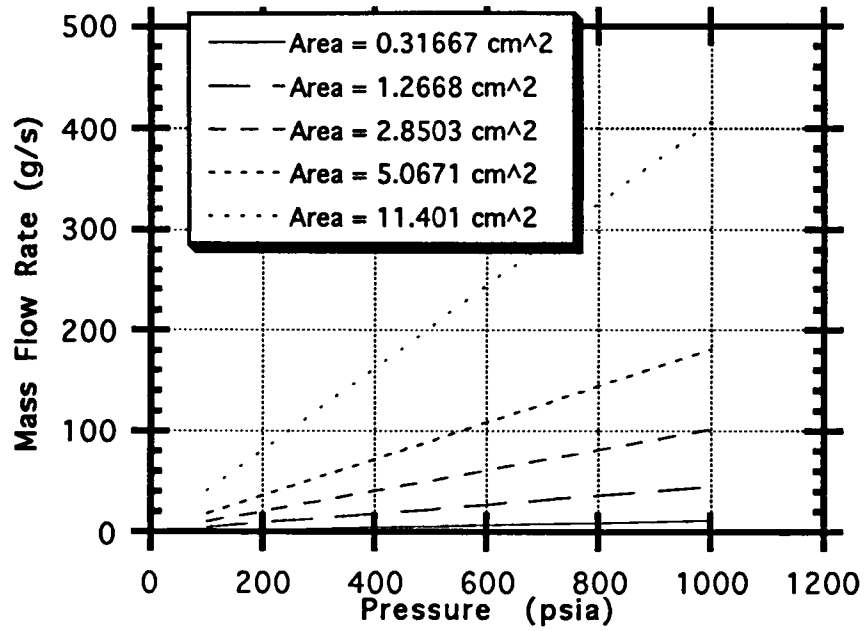


Figure 52: Mass Flow Vs. Pressure
(Gas = Methane, Velocity = 8.0 m/s)

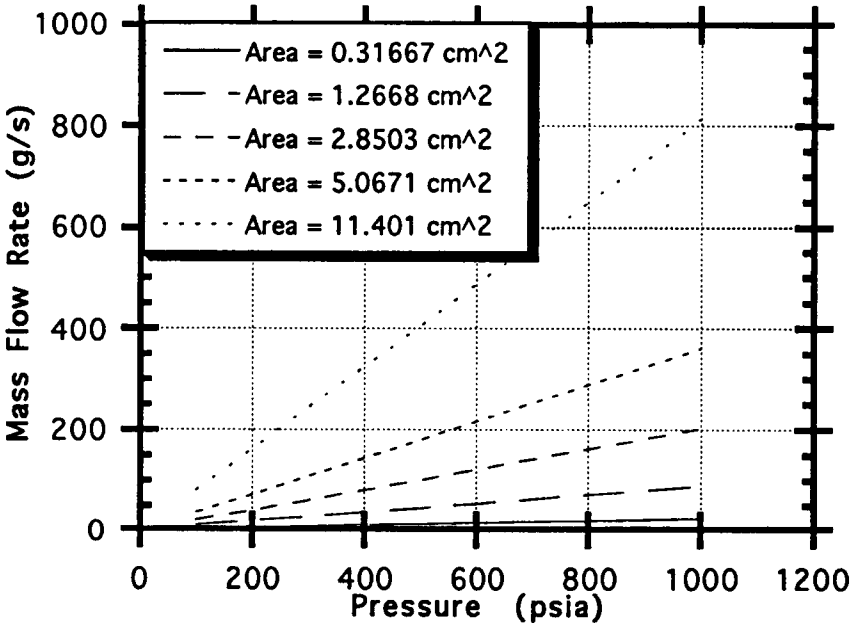


Figure 53: Mass Flow Vs. Pressure
(Gas = Oxygen, Velocity = 8.0 m/s)

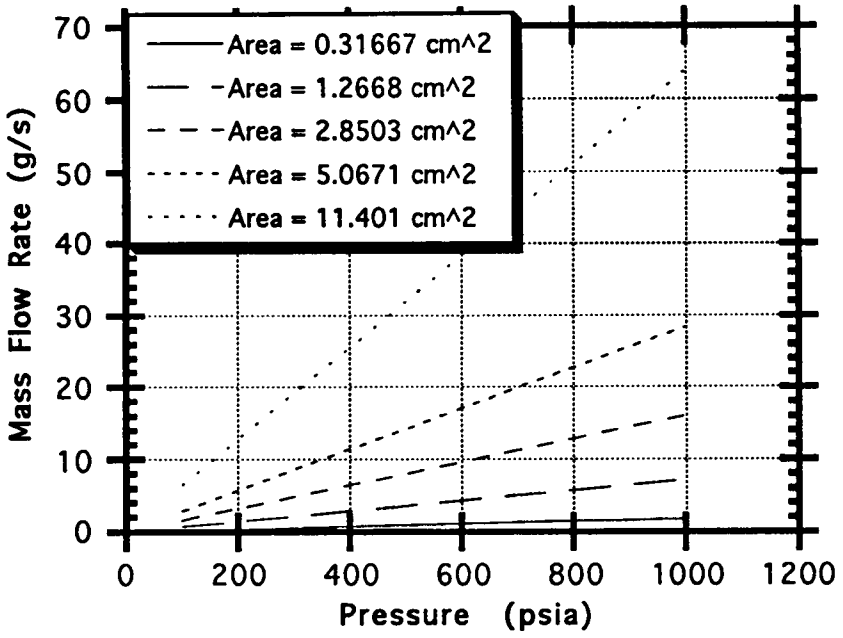


Figure 54: Mass Flow Vs. Pressure
(Gas = Hydrogen, Velocity = 10.0 m/s)

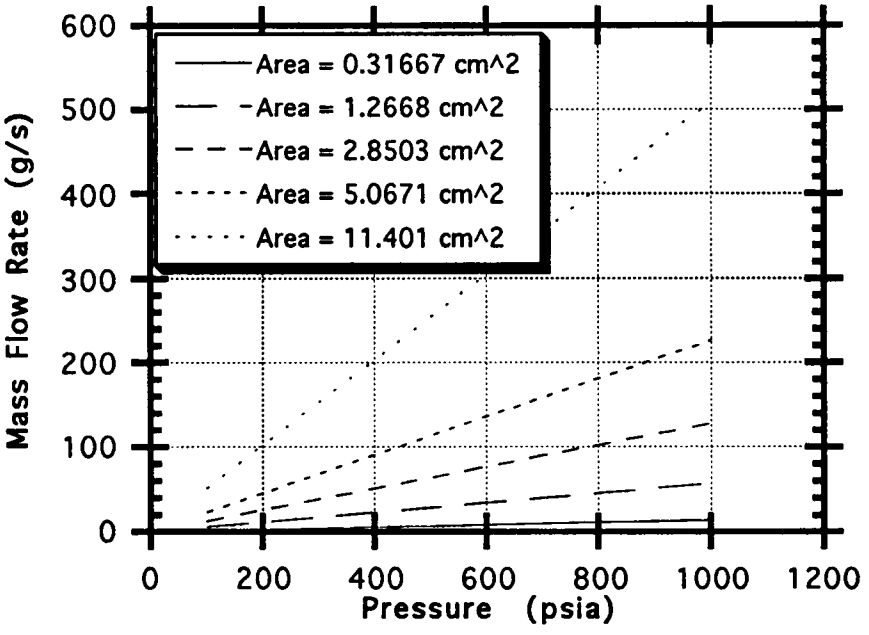


Figure 55: Mass Flow Vs. Pressure
(Gas = Methane, Velocity = 10.0 m/s)

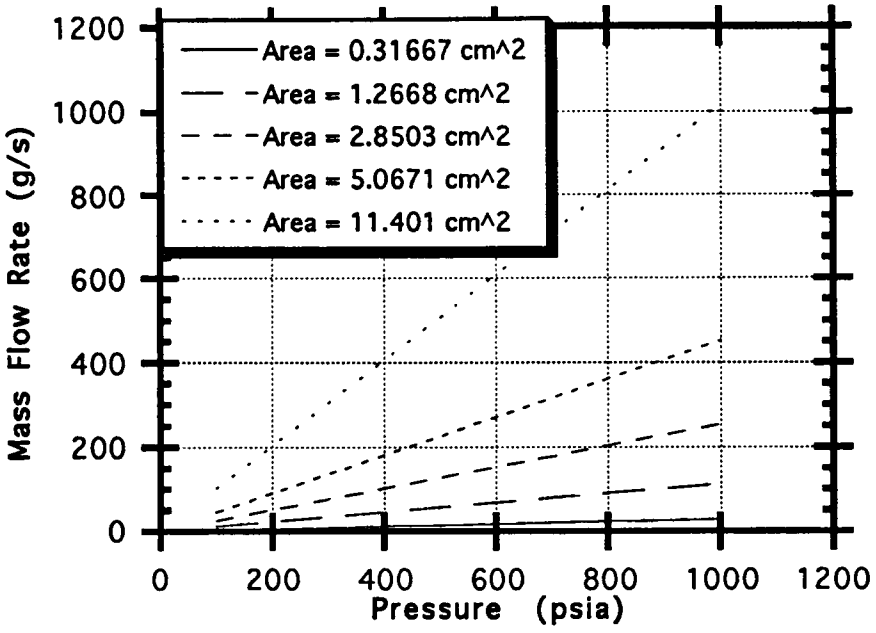


Figure 56: Mass Flow Vs. Pressure
(Gas = Oxygen, Velocity = 10.0 m/s)

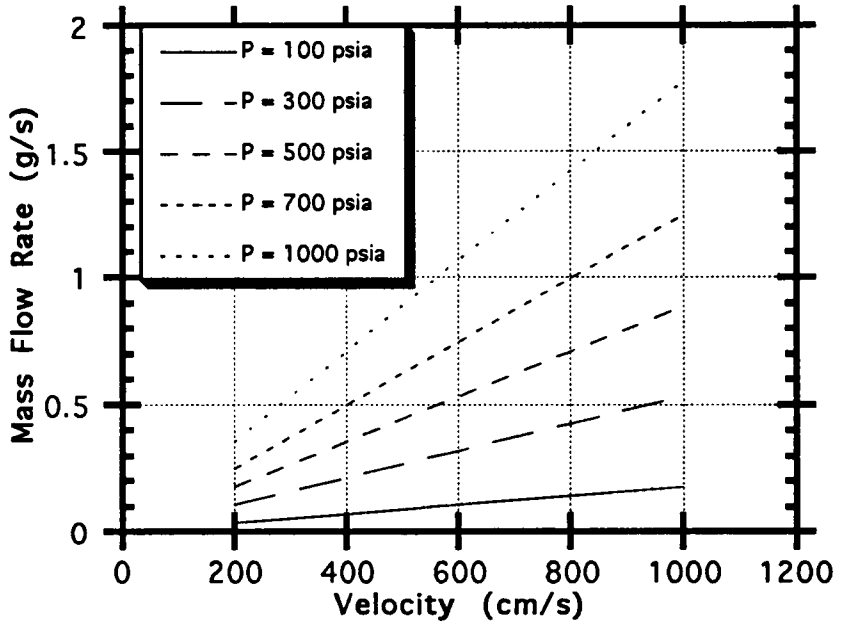


Figure 57: Mass Flow Vs. Velocity
(Gas = Hydrogen, Area =0.31667 cm^2)

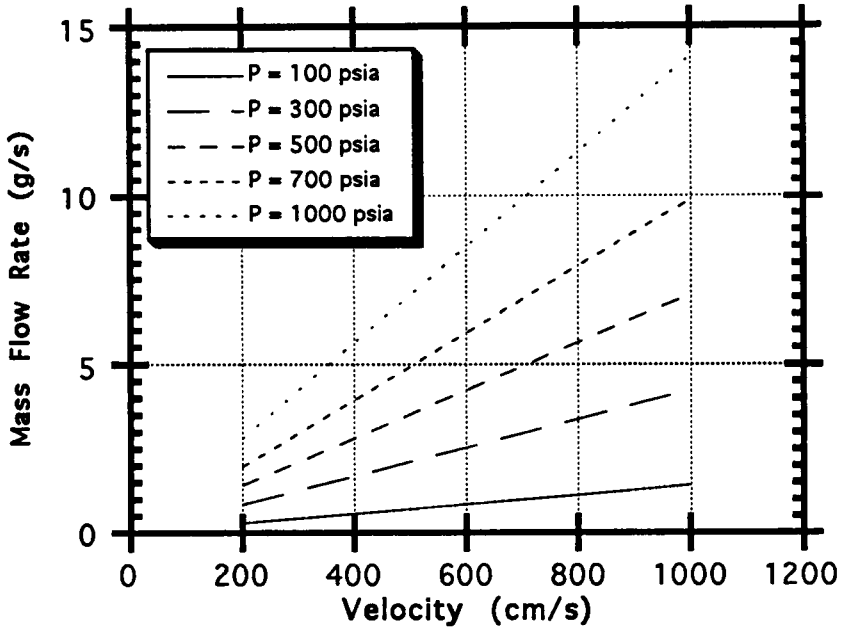


Figure 58: Mass Flow Vs. Velocity
(Gas = Methane, Area = 0.31667 cm^2)

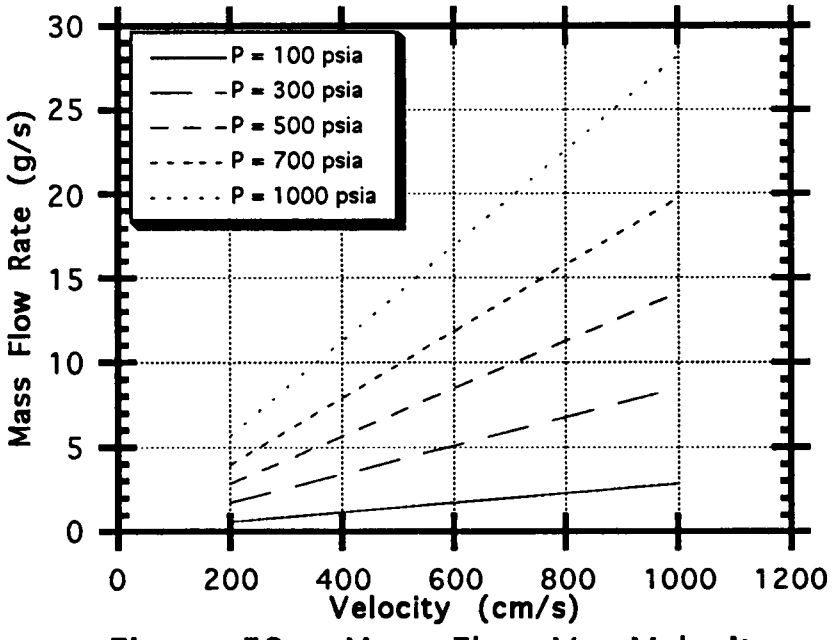


Figure 59: Mass Flow Vs. Velocity
(Gas = Oxygen, Area = 0.31667 cm^2)

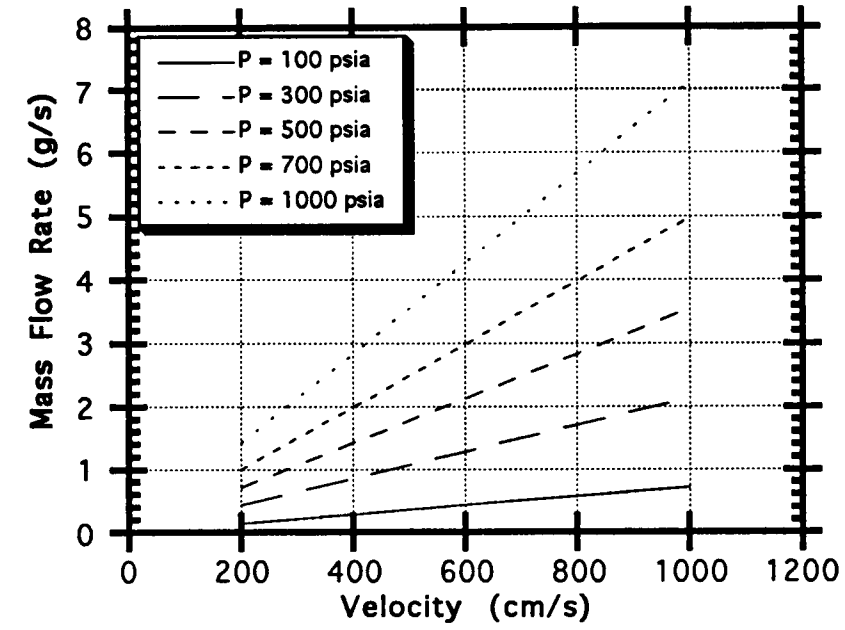


Figure 60: Mass Flow Vs. Velocity
(Gas = Hydrogen, Area = 1.2668 cm^2)

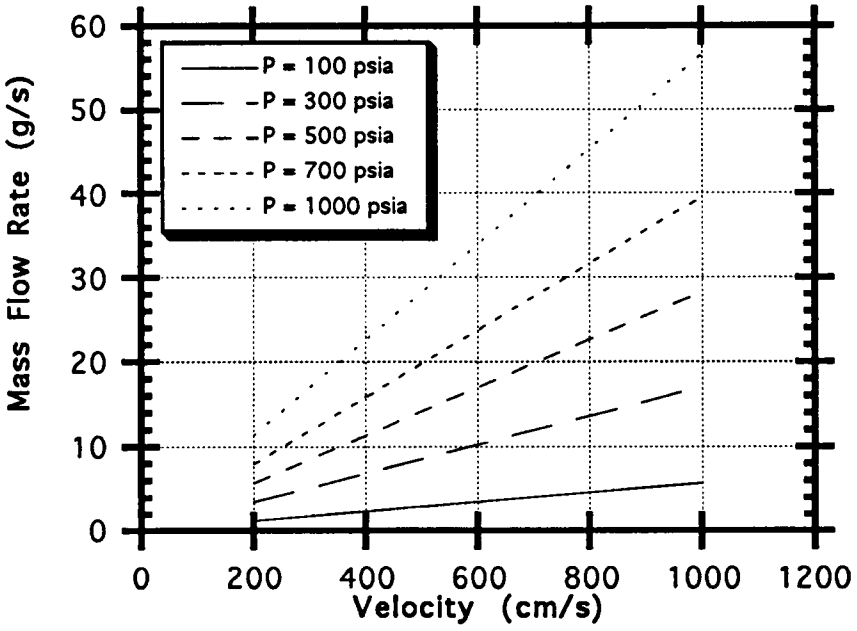


Figure 61: Mass Flow Vs. Velocity
(Gas = Methane, Area = 1.2668 cm^2)

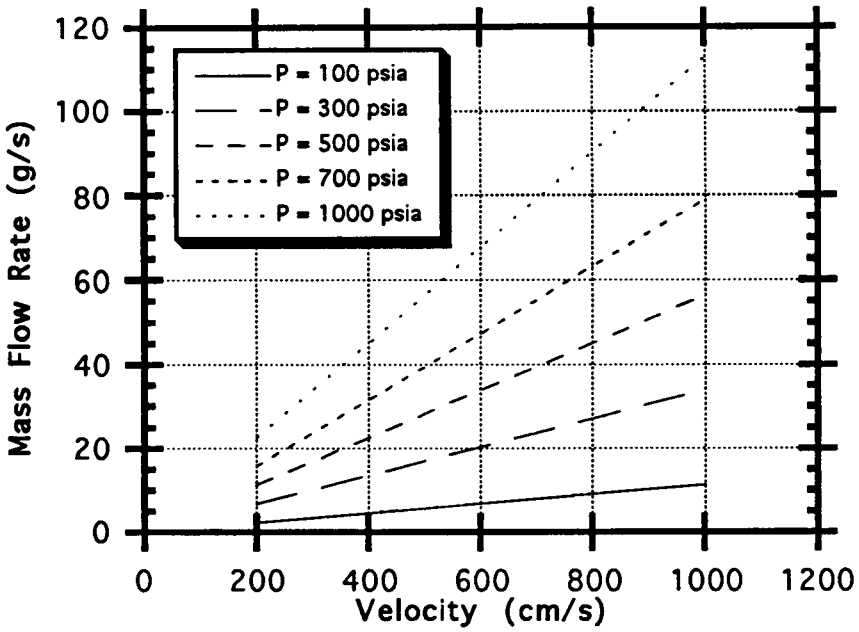


Figure 62: Mass Flow Vs. Velocity
(Gas = Oxygen, Area = 1.2668 cm^2)

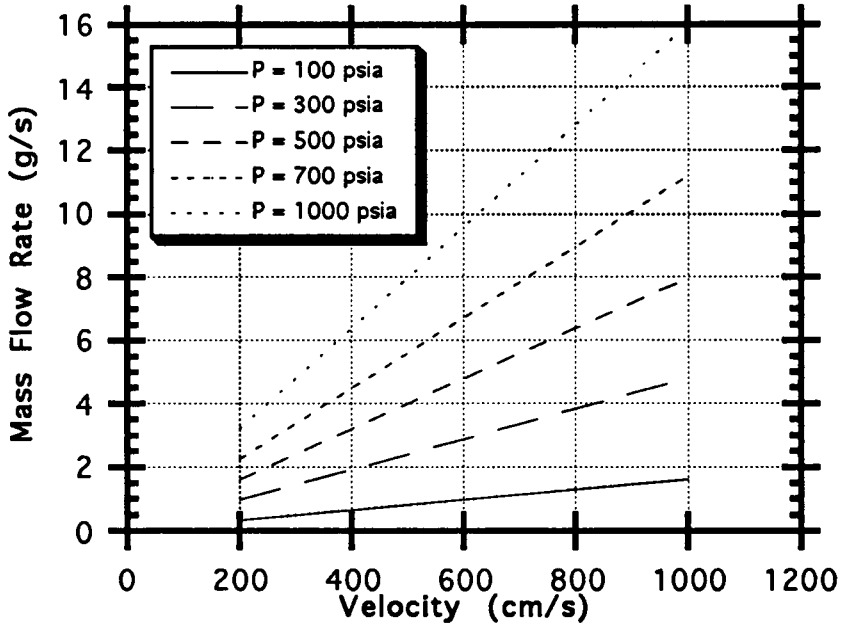


Figure 63: Mass Flow Vs. Velocity
(Gas = Hydrogen, Area = 2.8503 cm^2)

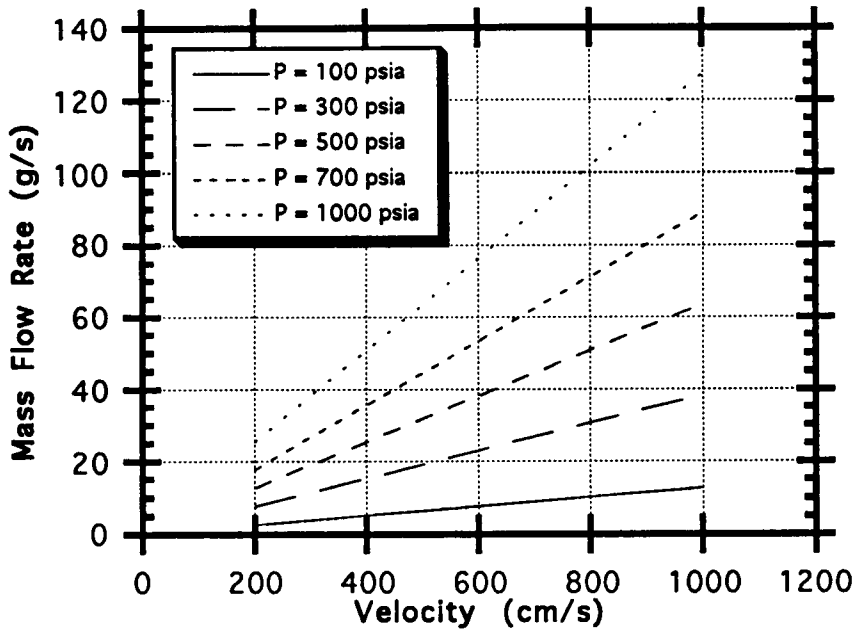


Figure 64: Mass Flow Vs. Velocity
(Gas = Methane, Area = 2.8503 cm^2)

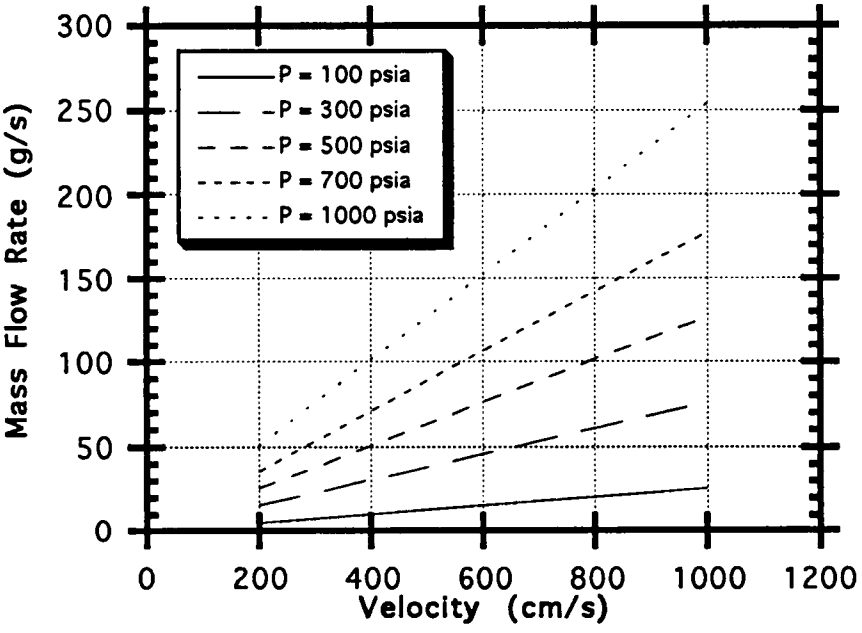


Figure 65: Mass Flow Vs. Velocity
(Gas = Oxygen, Area = 2.8503 cm^2)

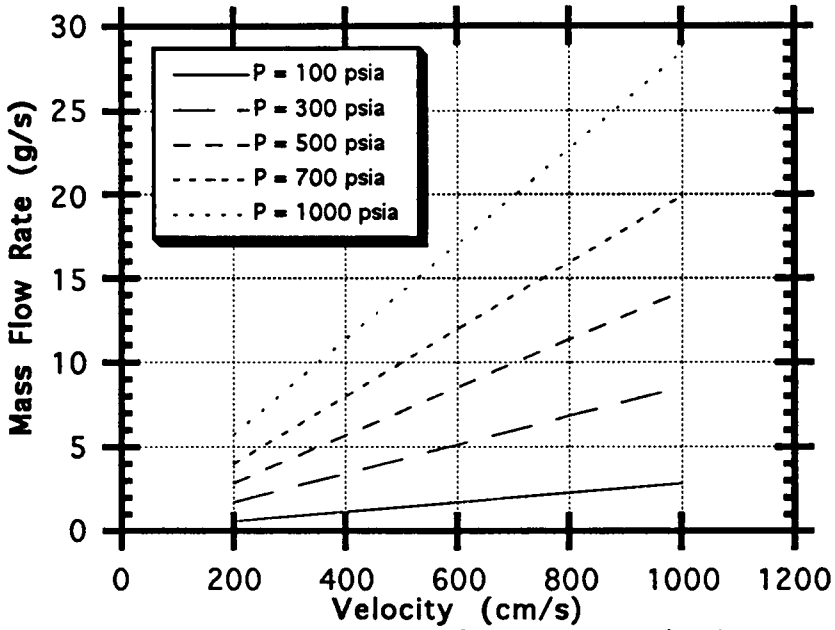


Figure 66: Mass Flow Vs. Velocity
(Gas = Hydrogen, Area = 5.0671 cm^2)

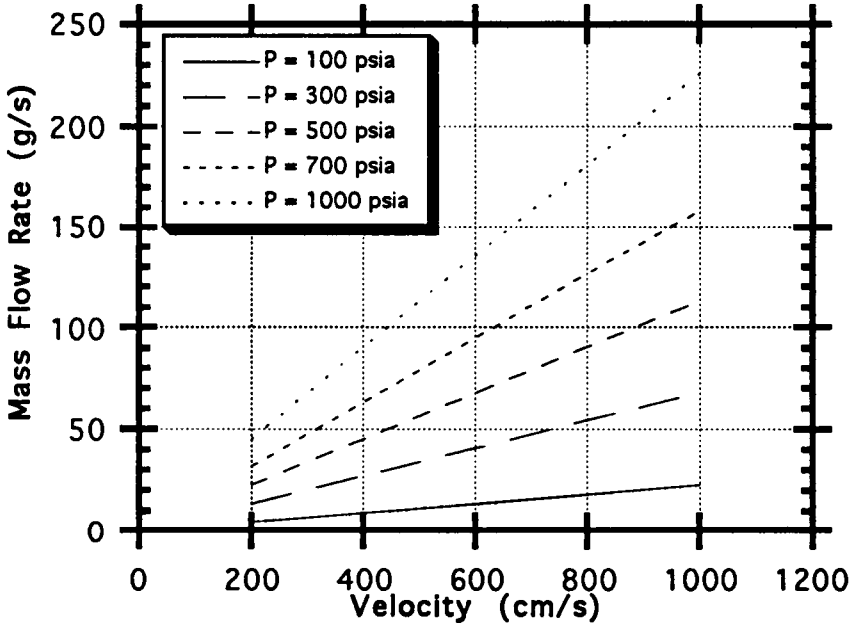


Figure 67: Mass Flow Vs. Velocity
(Gas = Methane, Area = 5.0671 cm^2)

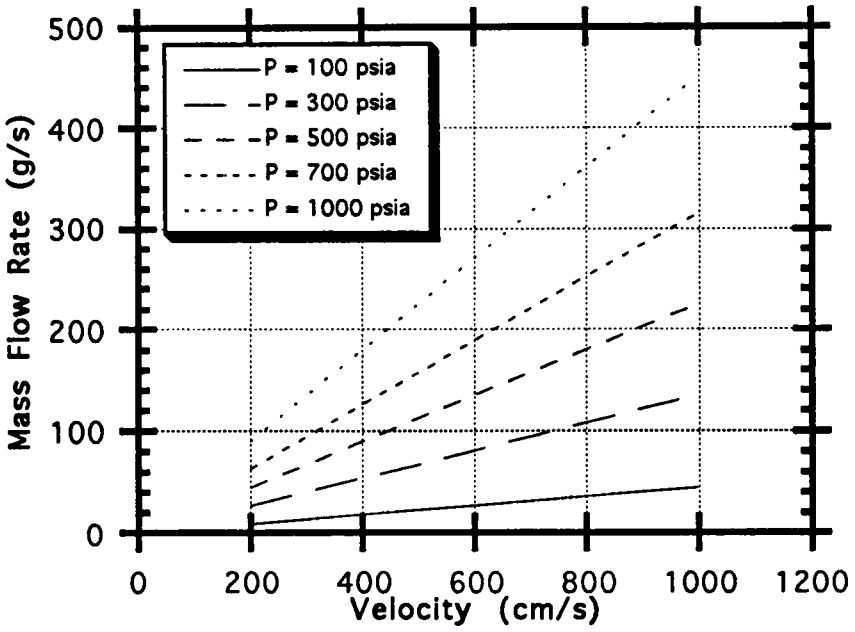


Figure 68: Mass Flow Vs. Velocity
(Gas = Oxygen, Area = 5.0671 cm^2)

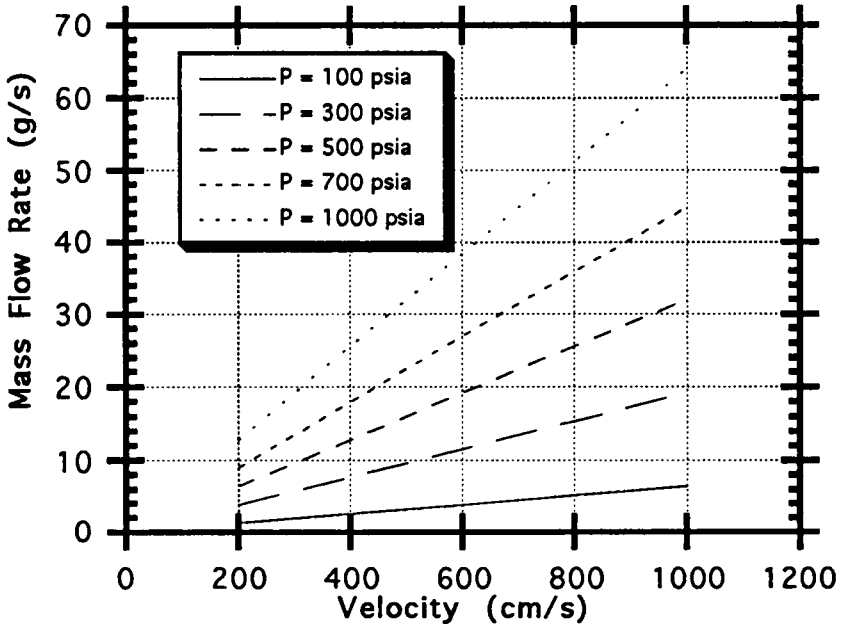


Figure 69: Mass Flow Vs. Velocity
(Gas = Hydrogen, Area = 11.401 cm^2)

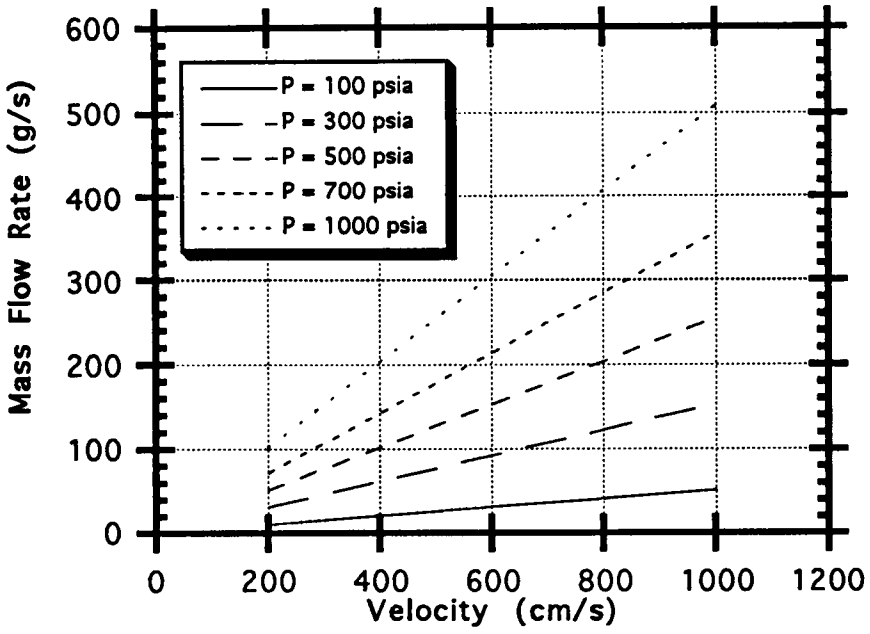


Figure 70: Mass Flow Vs. Velocity
(Gas = Methane, Area = 11.401 cm^2)

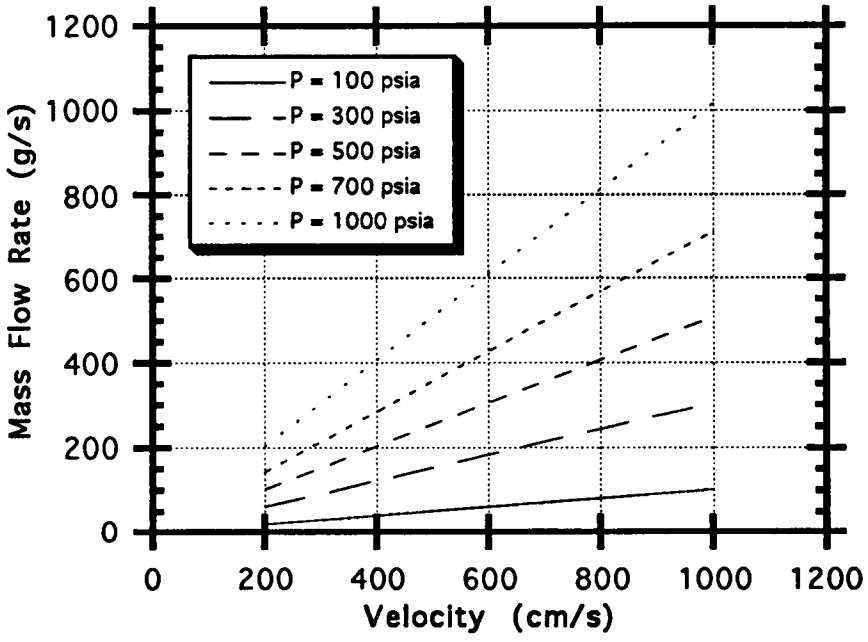


Figure 71: Mass Flow Vs. Velocity
(Gas = Oxygen, Area = 11.401 cm^2)

it should be noted that the densities of the various gaseous species were found at each pressure (and are shown in Figure 72) using the ideal gas equation:

$$\rho = \frac{PM}{\overline{R}T} \tag{19}$$

where P is the pressure at the injector face, M is the species molecular weight, $\overline{R}$ is the universal gas constant, and T is the injection temperature (assumed to be 298.15 K).

Due to the fact that the injector is of a concentric annulus design (Figure 73), it is necessary to use both the inner and outer tube diameters to calculate the flow areas. In other words, the area of annulus n is given by:

$$A_n = \pi\left(R_{i_n}^2 - R_{o_{n-1}}^2\right) \tag{20}$$

where n = 1 for the fuel injector ($R_{o0}$ =0), n = 2 for the oxidizer injector and n = 3 for the nitrogen injector; Ri denotes the inner tube radius, and Ro denotes the outer tube radius of area n.

From chapter 3 it was shown that it is necessary to operate this combustor at O/F ratios which are stoichiometric (or greater) and aluminum mass fractions between 0.5% and 5% (in order for a significant amount of aluminum oxide to be produced). This O/F

| Pressure (psia) | Hydrogen Density (g/cc) | Methane Density (g/cc) | Oxygen Density (g/cc) | Nitrogen Density (g/cc) |
|---|---|---|---|---|
| 100 | 0.000561 | 0.00446 | 0.00891 | 0.00779 |
| 200 | 0.00112 | 0.00892 | 0.0178 | 0.0156 |
| 300 | 0.00168 | 0.0134 | 0.0267 | 0.0234 |
| 400 | 0.00224 | 0.0178 | 0.0356 | 0.0312 |
| 500 | 0.00280 | 0.0223 | 0.0445 | 0.0389 |
| 600 | 0.00336 | 0.0268 | 0.0534 | 0.0467 |
| 700 | 0.00393 | 0.0312 | 0.0623 | 0.0545 |
| 800 | 0.00448 | 0.0357 | 0.0712 | 0.0623 |
| 900 | 0.00505 | 0.0402 | 0.0801 | 0.0701 |
| 1000 | 0.00561 | 0.0446 | 0.0891 | 0.0779 |

**Figure 72: Densities of Species**

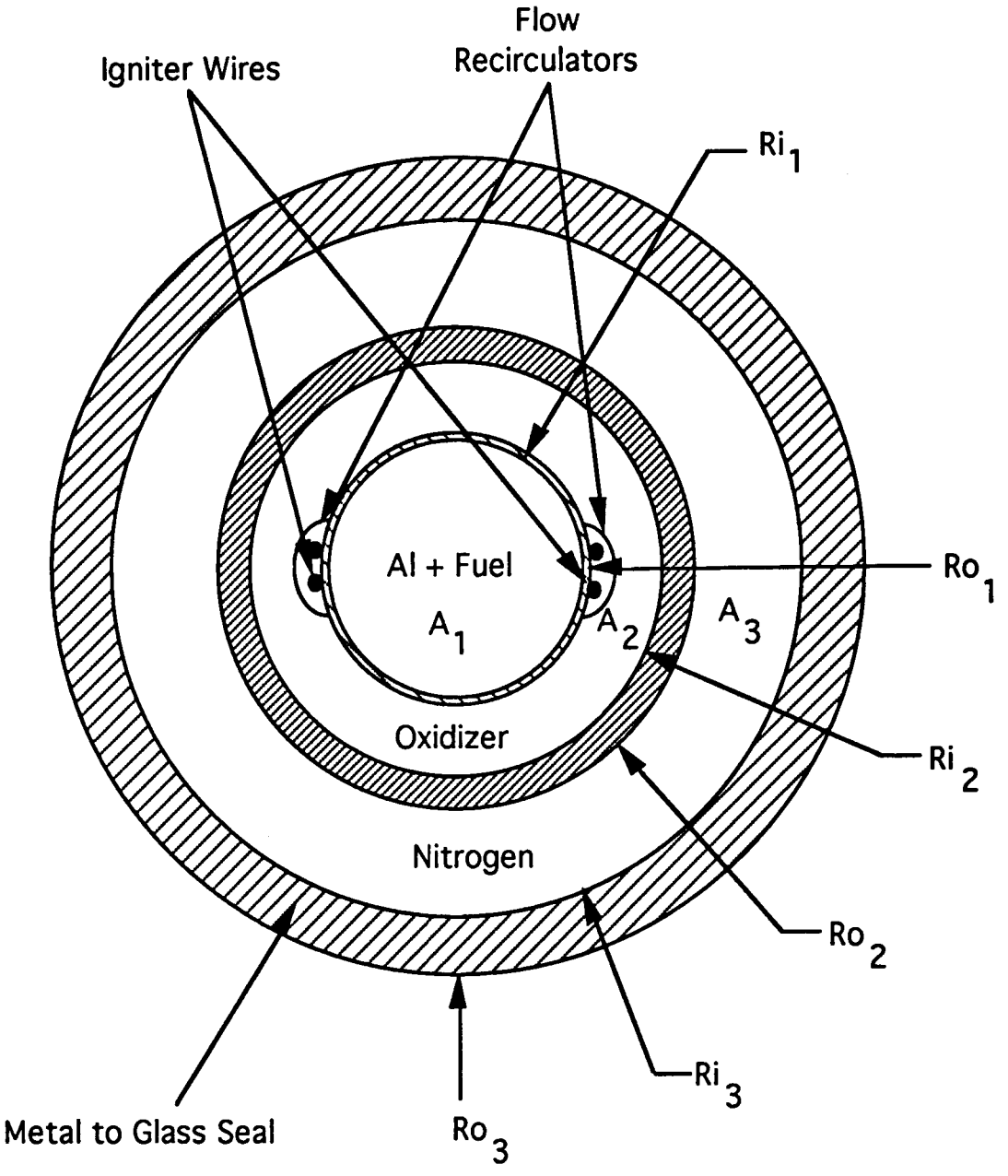


**Figure 73: Injector Dimension Definitions**

ratio equation can also be written as:

$$\frac{O}{F} = \frac{m_o}{m_f} = \frac{(\rho AV)_O}{(\rho AV)_F} \qquad (21)$$

In an effort to improve mixing of the combustion gases, the fuel in this combustor will flow at a faster rate than the oxidizer. Additionally, to simplify the valving required, the initial experiments will vary the fuel velocity (and not the oxygen and nitrogen velocities) to control the O/F ratio. This will also allow the aluminum concentration to be varied.

Since high O/F ratios become dangerous (potential for burning of equipment to occur), it is necessary to run this combustor near the stoichiometric O/F ratio. If the O/F ratio is varied between +/- 20% of stoichiometric, the velocity of the hydrogen fuel would fall into the following ranges:

$$2.6V_{CH_4} \leq V_{H_2} \leq 6.0V_{CH_4} \qquad (22)$$

where $V_{CH_4}$ is the velocity of the methane which would be required for the above mentioned O/F ratios. This range of velocities should easily be accomplished with one injector and a suitable valve system.

For the purpose of this combustor design the diameters of the supply manifolds should be kept to a minimum. By doing so the thickness of the materials will be smaller and therefore usually less costly. Since the center jet will determine the size of the outer annuli, it is necessary to determine its dimensions first. Since the size of the interior injector is mostly arbitrary, it was decided to use a thin-walled 0.25 in. outside diameter (tubing is usually listed according to its outside diameter) stainless steel tube for the fuel injector. Since the center supply injectors are enclosed by the outer nitrogen shroud injector, the pressure requirements will be much lower for the fuel and oxygen injectors than for the nitrogen injector. Even though, theoretically, the fuel and oxygen injectors should experience the same pressures on their inner and outer surfaces, it was determined that a 10% margin of error of the maximum operating pressure should be required of these injectors. In other words, the thickness of the fuel and oxidizer injectors will be designed for 100 psia pressure differential across these injector tube walls.

Using the thin-walled pressure vessel equation [27], the approximate maximum tangential stress is given by:

$$\sigma_{t,max} = \frac{P(d_i + t)}{2t} \qquad (23)$$

where P is the absolute interior pressure, $d_i$ is the inside diameter, and t is the tube thickness. In order to determine the thickness of the tubing, a factor of safety of 2 was used and when the maximum tangential stress equaled the yield point was considered to be the mode of failure. The yield point of AISI 1015 steel, used in these calculations, was found to occur at 30000 psia [28]. Accordingly, the thickness of an inner diameter tube of 0.25 in. is given by :

$$t = \frac{Pd_i}{(\sigma_y - P)} = 0.00084 \text{ in.} \qquad (24)$$

where $\sigma_y$ is the yield strength of the steel. Although this calculation is for an interior diameter of 0.25 in., an outside diameter of this size could also be used (as mentioned previously this diameter is mostly arbitrary). Since the smallest standard thickness is 0.006 in. for a 0.25 in. outside diameter, this size of tube should be more than adequate for the fuel injection nozzle. It should be noted then, however, that the interior area used to calculate mass flow rates is based on the interior diameter of 0.238 in. (0.6045 cm.).

In order to determine the diameters of the outer tubes it was necessary to first determine the maximum flow rate which the oxygen jet would experience. This was done by using the maximum O/F ratio for the hydrogen fuel (9.6). As mentioned earlier, to enhance mixing of the fuel, the fuel was assumed to flow faster than

the oxygen. The ratio of the oxidizer velocity to the fuel velocity was assumed to be a minimum of 0.1. Thus the area ratio of the oxygen supply was calculated using equation 21 and was found to be 6.045. However, as can be seen in Figures 73 and 74, the flow re-circulators and igniter wires obstruct a portion of the area of the oxygen injector. It was assumed that these re-circulators would obstruct 4 times the area of the igniter wires or approximately 0.05 square inches (assuming the diameter of the wires to be 0.125 in.). Thus the area required for this flow rate would require a minimum inside diameter of 0.709 in. and (using equation 24) a thickness of 0.002 in. Therefore, using a standard tubing would require the use of a 0.75 in. outside diameter tube with a thickness of 0.02 in. (or an inside diameter of 0.710 in.). In order for the area ratio to remain constant for an O/F ratio of 6.4, it is necessary to reduce the O/F velocity ratio to 0.067. Thus, the O/F ratio could be decreased by increasing the hydrogen velocity to 15 m/s or by decreasing the oxygen velocity to 0.67 m/s.

Since the stoichiometric O/F ratio is much lower for methane (approximately 4) than for hydrogen (8), the velocity of the methane supply will have to be slower than the velocity of the hydrogen supply. Assuming both fuels will use the same injector, and therefore areas, these velocity ratios can be calculated from equation 21. Thus, the range of velocities for the methane fuel would be between

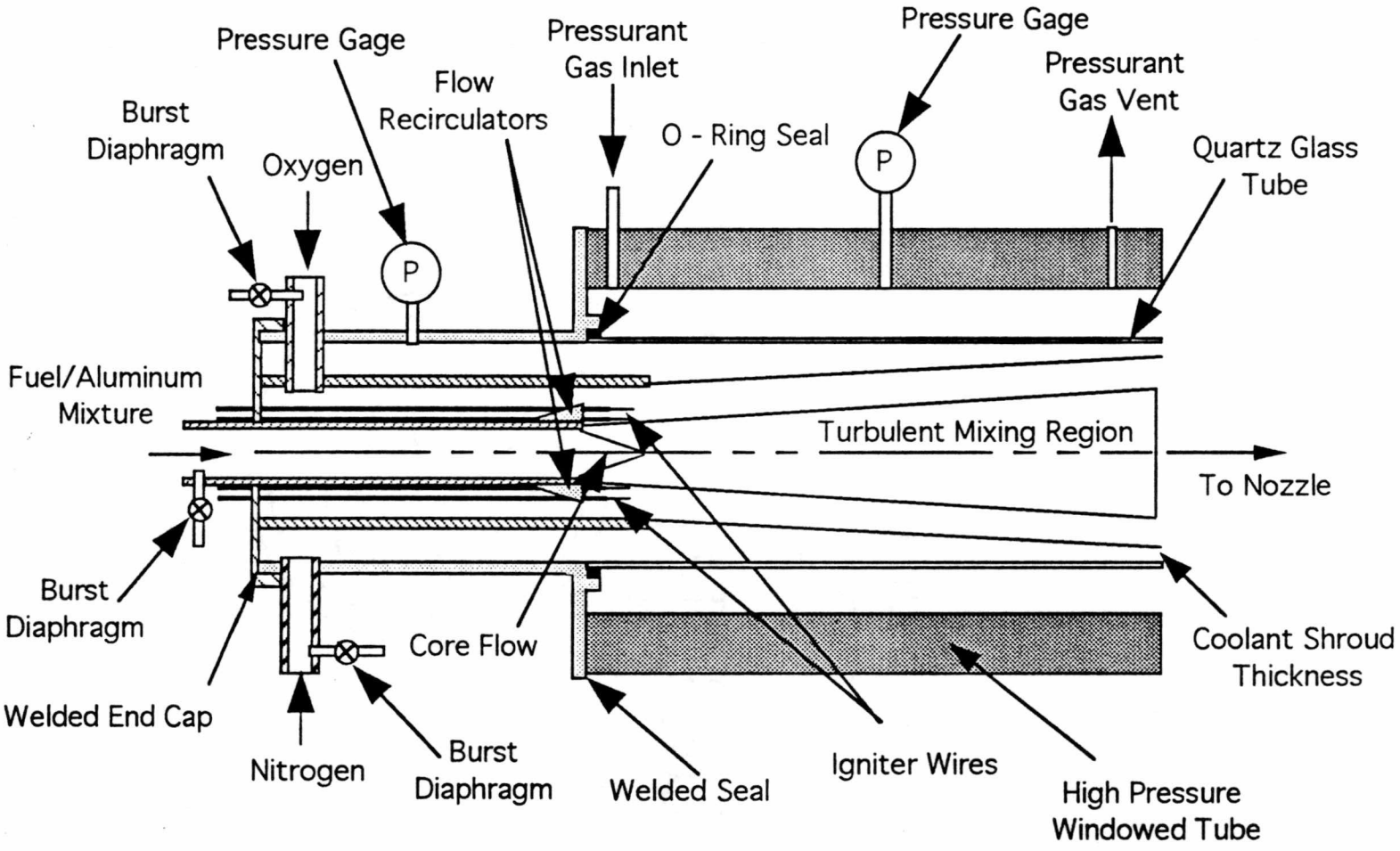


**Figure 74: Injector Manifold Design**

2.5 and 3.8 times the velocity of the oxygen (as opposed to hydrogen where its velocity is up to 15 times that of oxygen).

The final area to be determined is the area of the nitrogen cooling shroud. Since this cooling shroud is designed to protect the quartz glass from conductive and convective heat transfer, it was felt that a flow rate of nitrogen equal to one half of the total mass flow should be sufficient [22]. Therefore, the mass flow rate of the nitrogen would be given by:

$$m_{N_2} = 0.5m_T = 0.5\left[(\rho AV)_{Fuel} + (\rho AV)_{O_2}\right] \tag{25}$$

In order to simplify this equation each side was divided by the mass flow of the oxidizer. In other words:

$$\frac{m_{N_2}}{m_{O_2}} = \frac{(\rho AV)_{N_2}}{(\rho AV)_{O_2}} = 0.5\frac{(\rho AV)_{Fuel}}{(\rho AV)_{O_2}} + 0.5 \tag{26}$$

Since the objective is to eliminate the conductive and convective heat transfer, it is necessary that the velocity of the nitrogen equal the velocity of the oxygen. It is also necessary that the area ratio be largest required. Therefore, the mass flow of the fuel must be its maximum. Since the area ratio of the fuel and oxidizer remains fixed, the maximum mass flow will occur for methane fuel at its

maximum velocity. Therefore, the equation for the area ratio of the nitrogen shroud would simplify to:

$$\frac{A_{N_2}}{A_{O_2}} = 0.752 \qquad (27)$$

Using the same equations as before (20 and 24), it was found that a minimum inside diameter of 0.92 in. and thickness of 0.03 in. was required. It should be noted that this tube was designed to withstand 1000 psia. Since steel tubing does not come in this standard size, it was decided to use a tube of 1 in. outside diameter and 0.035 in. thick (0.930 in. inside diameter).

Since the injector ports should have a uniform circumferential velocity profile (at the face), it is necessary that each injection tube have sufficient length. For this injector, it was felt that a length of 4 to 5 diameters should be sufficient to get a velocity profile which will be constant at each radial location. Therefore the length of the nitrogen injector should be the longest at 4.65 in. However, since this combustor must also be designed for ease of manufacture, it was decided to use a length of 4.75 in. Although the other injection tubes could be much shorter to get fully developed flow, these tubes were designed to be nearly the same length for ease of construction. Thus, the oxygen injection tube will also be 4.75 in. long and the fuel supply tube will be slightly shorter at 4.5

in. long (to enhance mixing). The dimensions of the injection tubes are listed in Figure 75.

### 4.1.2. Nozzle Dimensions

After the diameter of the chamber has been defined, the diameter of the nozzle throat can be calculated. Since this nozzle was designed with a plug to vary the area (see Figure 76), the throat area was designed for the maximum operating conditions. These maximum conditions will occur at a chamber pressure of 1000 psia and the maximum mass flow rates of methane, oxygen, aluminum, and nitrogen. Therefore, the area of the throat was calculated by using [28]:

$$A_t = \frac{m_t\sqrt{\gamma R T_1}}{P_1\gamma\left(\frac{2}{\gamma+1}\right)^{\frac{(\gamma+1)}{2(i\gamma-1)}}} \qquad (28)$$

Since the specific heat ratio ($\gamma$), the gas constant (R), and the chamber temperature ($T_1$) all vary with O/F ratio, it is important to select the correct values when performing this calculation.

The maximum total mass flow is given by:

$$m_{T_{max}} = m_{CH_4} + m_{O_2} + m_{N_2} + m_{Al} = 1.55\left(m_{CH_4} + m_{O_2}\right) = 8.99 m_{CH_4} \qquad (29)$$

| Injection Tube | Inside Diameter (in.) | Outside Diameter (in.) | Tube Length (in.) |
|---|---|---|---|
| Fuel | 0.238 | 0.25 | 4.5 |
| Oxygen | 0.710 | 0.75 | 4.75 |
| Nitrogen | 0.930 | 1.0 | 4.75 |

**Figure 75: Injector Dimensions**

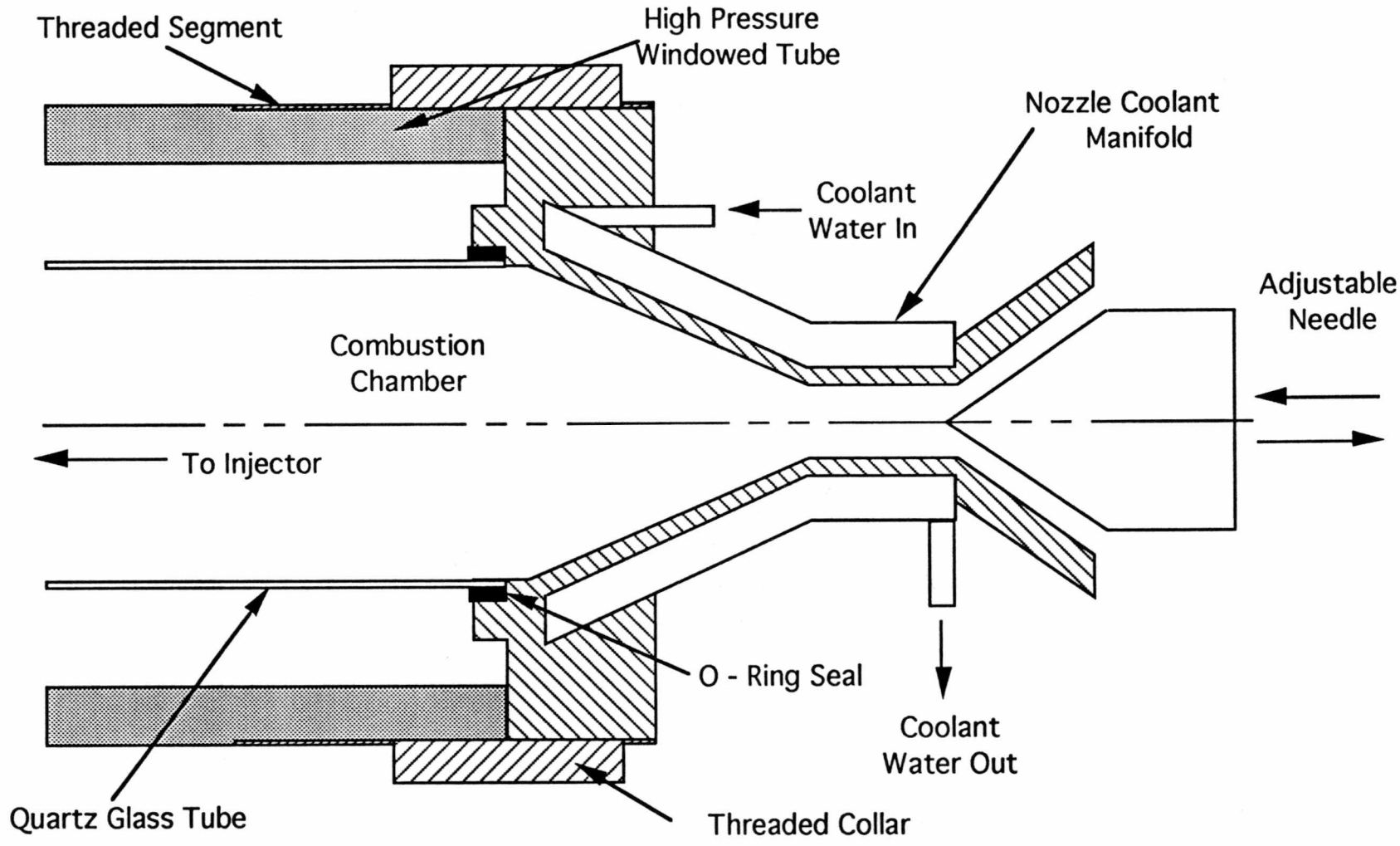


**Figure 76: Nozzle Design Configuration**

where the constants are derived from the maximum O/F ratio and maximum flow rates. Assuming the velocity of the oxygen to be 1 m/s, the maximum velocity of the methane would be 3.8 m/s. Therefore, at 1000 psia, the mass flow of the methane would be 4.86 g/s and the total mass flow would be 43.73 g/s. The values for the temperature, specific heat ratio, and sonic speed of the combustion products were found using Figures 25, 36, and 37, respectively. These values were found to be: temperature - 3800 K; specific heat ratio - 1.135; and sonic speed - 1300 m/s. However, since half of the mass flowing through the nozzle is nitrogen, it is necessary to average these values with the corresponding values for nitrogen at 300 K. The average values used in equation 28 were: sonic speed - 876.4 m/s; and specific heat ratio - 1.266. Using these values it was found that the throat area needed to be 0.0748 square centimeters and the corresponding throat diameter was determined to be 0.12 in.

Using a 40 degree convergent section for the nozzle, the length of the convergent section was found to be:

$$\ell_c = \frac{(d_c - d_t)}{2 \tan \theta} \tag{30}$$

where $d_C$ is the chamber diameter, $d_t$ is the throat diameter, and$\theta$ is the angle of the convergent section. Therefore, the length of the convergent section was found to be 0.48 in.

Since the throat diameter is so small, it is necessary to use a small ceramic needle (instead of a cooled plug) to change the throat area. This needle will have a 20 degree angle at the point which will match the nozzle exit angle. Since the length of this section is not an important design consideration, an arbitrary length of 0.5 in. was chosen for the 30 degree divergent section of the nozzle.

### 4.1.3. Glass Tubing Dimensions

Since the glass tube must contain the flow of the combustion gases and must also eliminate flow recirculation zones at the wall, it is necessary that the interior diameter of the glass tube match the diameter of the largest injector. In other words, it is necessary that the interior diameter of the glass tube be equal to the diameter of the nitrogen injector (0.930 in.). Additionally, due to the fact that quartz glass is much stronger in compression than in tension, this combustor was designed with a pressurized (and windowed) outside chamber (see Figures 75 and 76). This should allow the glass tube to be much thinner and also less expensive to replace in the event of failure. Another factor that will allow this glass tube to be used is that it will only be required to experience small pressure differentials at high temperatures (when the glass becomes weaker). (A more expensive design could incorporate a valve and pressure sensor system which would pressurize the

outside chamber to a slightly higher pressure than the current pressure within the combustion chamber).

Never the less, this glass tube must be capable of withstanding up to 1100 psia compressive load at room temperature. As previously mentioned, quartz glass is outstanding in compression (with a compressive strength of $1.66 \times 10^6$ psia at room temperature [28]). The equation for the tangential stress on a cylinder was used to calculate the thickness of the glass required. Thus, the tangential stress on a cylinder is given by [27]:

$$\sigma_t = \frac{p_i r_i^2 - p_o r_o^2 - r_i^2 r_o^2 \left( \frac{p_o - p_i}{r^2} \right)}{r_o^2 - r_i^2} \qquad (31)$$

where p is the absolute pressure, r is the radius, and the subscripts i and o refer to the inner and outer surfaces, respectively. This equation was solved for the outside radius using the inside pressure as zero, the outside pressure as 1100 psia, and the allowable tangential stress to be 0.1 times the compressive strength (at $r = r_i$). Therefore the required thickness of the glass was found to be 0.0031 in. Even at a factor of safety of 100, the required thickness of the glass would be only 0.034 in. However, since quartz glass tubing is usually sold by a specified outside diameter and thickness, it was decided to use a quartz glass tube of the same dimensions as the steel tubing (used in the nitrogen injector). This means that the

quartz tubing will also have a 1 in. outside diameter and a thickness of 0.035 in. (inside diameter of 0.93 in.).

Unlike the tube diameter, which is mostly defined by the injector diameters, the tube length calculations are complicated by the combustion process occurring in the chamber. The first problem to consider when designing the glass tube length is the fact that the combustion of the aluminum particles must be completed within the combustion chamber. The method used to calculate the burn times used equations 1 through 3. It also assumed the worst case scenario and therefore calculated the longest time required to completely consume 25 $\mu$m aluminum particles in this combustor. The parameters used in equations 1 through 3 are listed in Figure 77. It should be noted that the values of $\lambda_g$ and $T_\infty$ were taken from the figures in Chapter 3.

In order to calculate the length required, the particle velocity was assumed to be the maximum gas velocity of 15 m/s. Thus, the length required to burn the particle was simply calculated by:

$$L_b = V_g t_{tot} = 0.048 \text{ m} \qquad (32)$$

where $V_g$ is the maximum gas velocity. Therefore, the length required to burn a 25 $\mu$m aluminum particle is approximately 1.9 in.

| Parameter | Definition | Value Used |
|---|---|---|
| $\lambda_g$ | gas thermal conductivity | 0.4 cal/m K s |
| $T_\infty$ | gas temperature | 3500 K |
| $T_O$ | initial aluminum temperature | 300 K |
| $\rho_{Al}$ | Aluminum density | 2702 kg/$m^3$ |
| $T_i$ | melting temperature of Aluminum Oxide | 2350 K |
| $T_{mm}$ | melting temperature of Aluminum | 933 K |
| $C_{p_{Al}}$ | heat capacity of Aluminum | 215.67 cal/kg K |
| L | heat of fusion of Aluminum | 95000 cal/kg |
| D | particle diameter | 25 x $10^{-6}$ m |
| k | burn rate constant | 0.5 x $10^{-5}$ s/($\mu$m)(1/n) |
| n | burn rate exponent | 2.0 |
| $t_i$ | ignition time | 0.1 x $10^{-3}$ s |
| $t_b$ | burn time | 3.125 x $10^{-3}$ s |
| $t_{tot}$ | total combustion time required | 3.225 x $10^{-3}$ s |

**Figure 77: Parameters for Burn Time Calculations**

The second consideration for the tube length requirement was the fact that the aluminum particles must first pass through the non reacting core flow (see Figure 78). This potential core length is dependent upon the relative velocities of the fuel and oxidizer. Its length is also dependent upon the diameter of the fuel injector and relative densities. Therefore, an estimate of the length of the core flow was determined from [30]:

$$X_p = d_0\left(4 + 12\frac{(\rho V)_{O_2}}{(\rho V)_{Fuel}}\right) \tag{33}$$

where $d_0$ is the fuel injector diameter. Thus the maximum length of this potential core was found to be 5.5 in. (for $d_0 = 0.238$, $V_{ox} = 1$ m/s, $V_{fuel} = 10$ m/s). However, since the fuel injector is recessed by 0.25 in., the length of the glass required for the potential core region would be only 5.25 in. at its maximum.

An additional consideration which was investigated while calculating the quartz tube length was the consideration of heat transfer effects. As mentioned earlier, the conductive and convective heat transfer effects must be eliminated (or at least limited). Since the nitrogen gas is moving at the same velocity as the oxygen, there should be no turbulent mixing across their interface. However, as the hot fuel/oxidizer mixture burns, it also spreads out towards the quartz tube walls (see Figure 78). Since

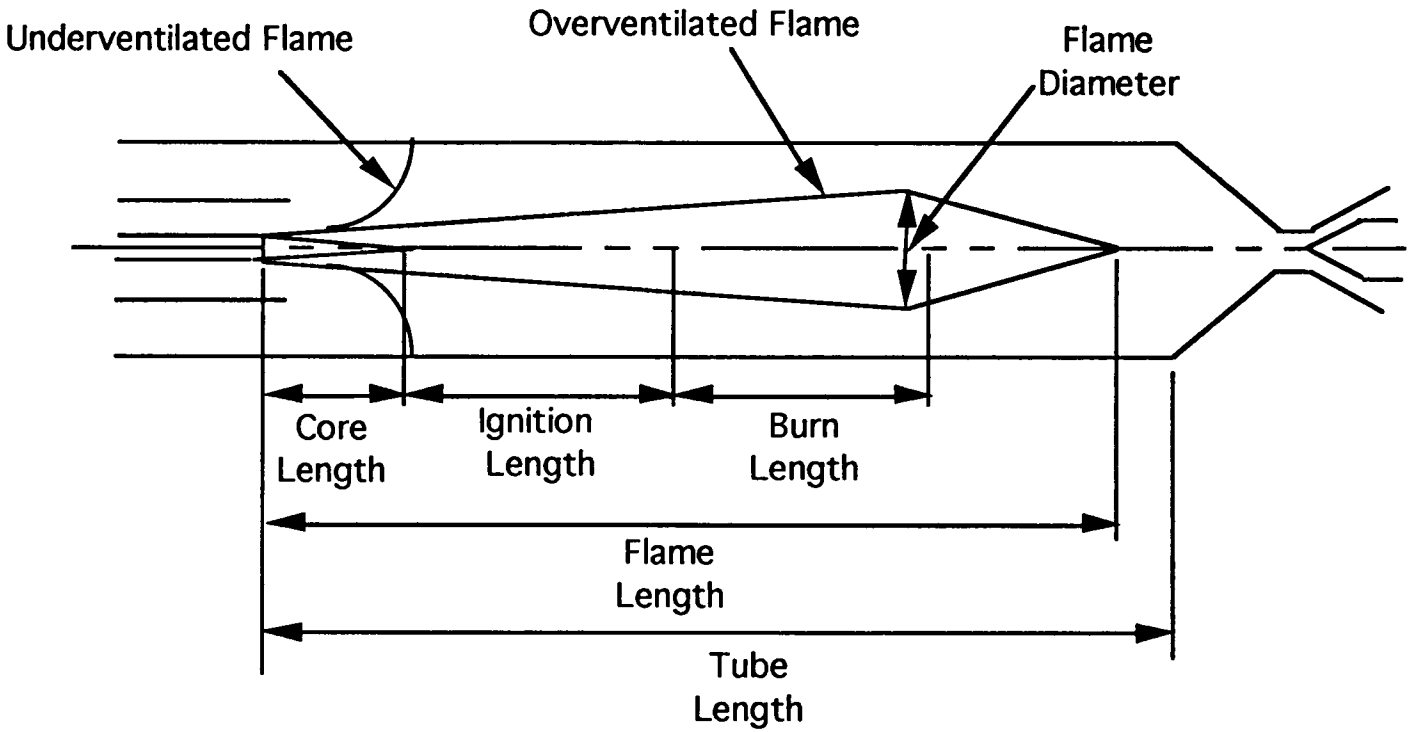


**Figure 78: Simplified Flame Diagram**

this combustor will most likely need to operate in a slightly over ventilated condition (to produce aluminum oxide), it is imperative that the hot flame front does not impinge on the quartz tube walls.

Although the flame envelope does expand from the initial injector face, this combustor assumes that the flame will not expand far into the nitrogen shroud. This assumption is made due to the fact that the oxygen should be mostly consumed by the time the nitrogen shroud is reached. Additionally, since the velocity and density of the nitrogen and oxygen are nearly identical, very little oxygen should diffuse into the nitrogen shroud layer (laminar mixing occurs at the molecular level). Therefore, for the heat transfer calculations in the next section, it is assumed that the flame front will reach a maximum diameter which will only slightly penetrate the coolant shroud. This maximum diameter is arbitrarily assumed to be 0.80 in. As discussed in the next chapter, this assumption will have to be experimentally determined to insure safe operation of this combustor.

Since the main objective of research done when using this combustor is to observe aluminum particles during combustion, it is important to have a glass tube with sufficient length to obtain the required data. In a rocket engine, a large narrow combustion chamber and its associated pressure and temperature drops would be detrimental to engine performance. For this combustor, the opposite

is true. Not only will a long chamber possibly eliminate the need for a cooled nozzle (provided the flame does not expand to the tube walls), but it will also allow for further optical data to be compiled after the aluminum combustion is complete. Even though the nozzle was designed for a constant pressure chamber, it is not necessarily a concern. This is due to the fact that the chamber pressure can be increased by inserting the needle into the nozzle (and decreasing the area).

In order to determine the appropriate length of the tube it is therefore necessary to calculate the flame length and compare it to the sum of the core length and burn length. According to Beer [30] the length of a turbulent diffusion flame is dependent upon the fuel used and the diameter of the jet. The equation used to obtain an estimate of the length of a free turbulent free flame was:

$$L_f = 6d_0(R+1)\left(\frac{\rho_e}{\rho_f}\right)^{0.5} \qquad (34)$$

where R is the stoichiometric air/fuel weight ratio, $\rho_e$ is the fuel gas density, and $\rho_f$ is the average flame density.

Although this equation is fairly accurate for free turbulent flames burning in ambient air, its accuracy would not apply for the high operating pressures of this combustor. Never the less, rough estimates for the longest flames for methane and for hydrogen were

calculated to be 22.6 in. and 15.2 in., respectively. These flame length estimates are grossly exaggerated and would, in reality, be much shorter for this combustor's operational range. Thus, the actual flame length will also have to be experimentally determined. Therefore, it is recommended that a relatively short glass tube and cooled nozzle be used during the initial experiments for this combustor. The length of the quartz tube should be long enough to contain the core length and burn length plus an additional length designated for extra instrumentation. Therefore, the total length of the quartz required will be:

$$L_t = L_b + X_p + L_i \tag{35}$$

where $L_i$ refers to the extra length reserved for additional instrumentation. This additional length will need to be approximately 2.75 in. long for a typical observation window. Thus, the total length of the glass tube required would be 9.9 in. long. Again, for ease of construction, the quartz tube on this combustor will be 10.0 in. long.

## 4.2. Heat Transfer Calculations

The final step in the design of this combustor is to determine the heat transfer rates to the various combustor surfaces. These heat transfer rates determine the transient and steady state

temperatures at various points in the combustor. These temperatures, in turn, determine the operational test times allowable or the necessary coolant which will be required. This section presents the calculations used to determine the heat transfer to the quartz tube and nozzle surfaces.

### 4.2.1. Heat Transfer to the Quartz Tube

The first step in the heat transfer to the quartz tube is to determine what the highest steady state temperature of the interior glass surface would be. Thus, the first portion of the problem would be to set up an energy balance on the glass tube (see Figure 79). That is [31]:

$$E_{in} - E_{out} + E_{gen} = E_{st} \tag{36}$$

where $E_{in}$ is the rate at which radiant energy (since convection and conduction are considered to be negligible) is absorbed by the glass, $E_{out}$ would be the radiant energy emitted and reflected by the glass, $E_{st}$ is the energy stored by the glass, and $E_{gen}$ is the rate at which energy is generated (which would be zero for this case). The $E_{st}$ term would simply be:

$$E_{st} = \frac{d}{dt}(\rho V C_p T) \tag{37}$$

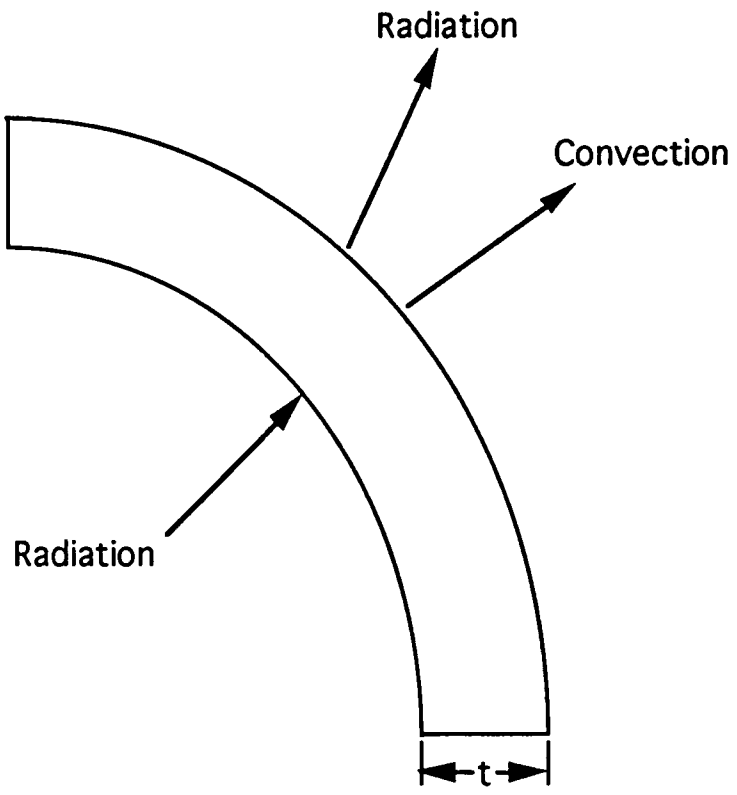


**Figure 79: Simplified Energy Diagram of Quartz Glass Section**

where $\rho$ is the density of the glass, V is the volume of the glass, $C_p$ is the specific heat of the glass, T is the temperature, and d/dt represents the time derivative of the quantity.

Since the glass tube is so thin, it is likely that the conduction effects within the quartz will be negligible. In order to verify this assumption it was necessary to verify that the Biot number was sufficiently small. If this is true, the temperature of the quartz can be assumed to be uniform. Thus, the criteria for which the glass canbe assumed to be of uniform temperature is given by [31]:

$$B_i = \frac{hL_c}{k} \leq 0.1 \qquad (38)$$

where $B_i$ is the Biot number, h is the convection coefficient at the exterior surface of the glass, $L_C$ is the characteristic length, and k is the thermal conductivity of the glass. Since the value of the convection coefficient on the outside of the glass will be somewhere between that of forced convection and that of free convection, a borderline value of 25 $W/m^2K$ was assumed [31].

It should be noted that the characteristic length in this equation is given by the volume of the object divided by its exposed surface area. Thus, the characteristic length for the quartz tube would be

given by:

$$L_c = \frac{V}{A_s} = \frac{\pi\left(r_o^2 - r_i^2\right)L}{2\pi\left(r_o + r_i\right)L} = \frac{\left(r_o - r_i\right)}{2} \tag{39}$$

Therefore, the Biot number for the quartz tube is only 0.004 (far less than 0.1) and the temperature can be assumed uniform.

As mentioned earlier, the energy into the glass is the radiation from the flame. Assuming the flame to be an infinite cylinder enclosed by an infinite cylinder (the glass tube), the net heat transfer to the glass would be given by [31]:

$$q_{fg} = \frac{\sigma A_f\left(T_f^4 - T_q^4\right)}{\frac{1}{\varepsilon_f} + \frac{1-\varepsilon_q}{\varepsilon_q}\left(\frac{r_f}{r_{q_i}}\right)} \tag{40}$$

where $\sigma$ is the Stefan - Boltzmann constant ($5.67 \times 10^{-8}$ $W/m^2K^4$), $A_f$ is the surface area of the cylindrical flame, $T_f$ is the predicted flame temperature, $T_q$ is the temperature of the quartz glass, $r_f$ is the maximum radius of the flame, and $r_{q_i}$ is the inside radius of the quartz tube.

Since hydrogen will be the first fuel to be tested in this combustor, it was decided to use the hydrogen flame temperature of approximately 3700 K for these heat transfer calculations.

However, quartz glass has very poor transmittance properties in the water vapor wavelengths (see Figure 80). Since hydrogen fuel produces mostly water vapor, it was assumed that the quartz glass would absorb all of the radiation between 2.5 and 3 $\mu$m. It was also assumed that the quartz glass would absorb all of the radiation above 3.5 $\mu$m. The simplified transmittance plot for the quartz glass is shown in Figure 81. Since the sum of the transmissivity, reflectivity, and absorptivity are equal to one, it was assumed that the transmissivity would be one at places where the actual transmissivity was greater than 0.9. In other words, since the sum of the reflectivity and absorptivity would be less than 0.1 in these regions, it was assumed that the absorptivity would be negligible. Therefore, this assumption should only slightly underestimate the heat transfer rate to the quartz glass.

Since quartz glass does not absorb all of the radiation in all of the wavelengths, it is necessary to calculate the fraction of blackbody radiation which will be absorbed. This is done by obtaining the plot of the blackbody spectral emissive power at the assumed flame temperature (see Figure 82). Due to the transmittance properties of quartz glass it is necessary to calculate the fraction of the blackbody emissive power at the wavelengths between 2.5 and 3 $\mu$m and greater than 3.5 $\mu$m. This was accomplished by first computing the fraction of the blackbody

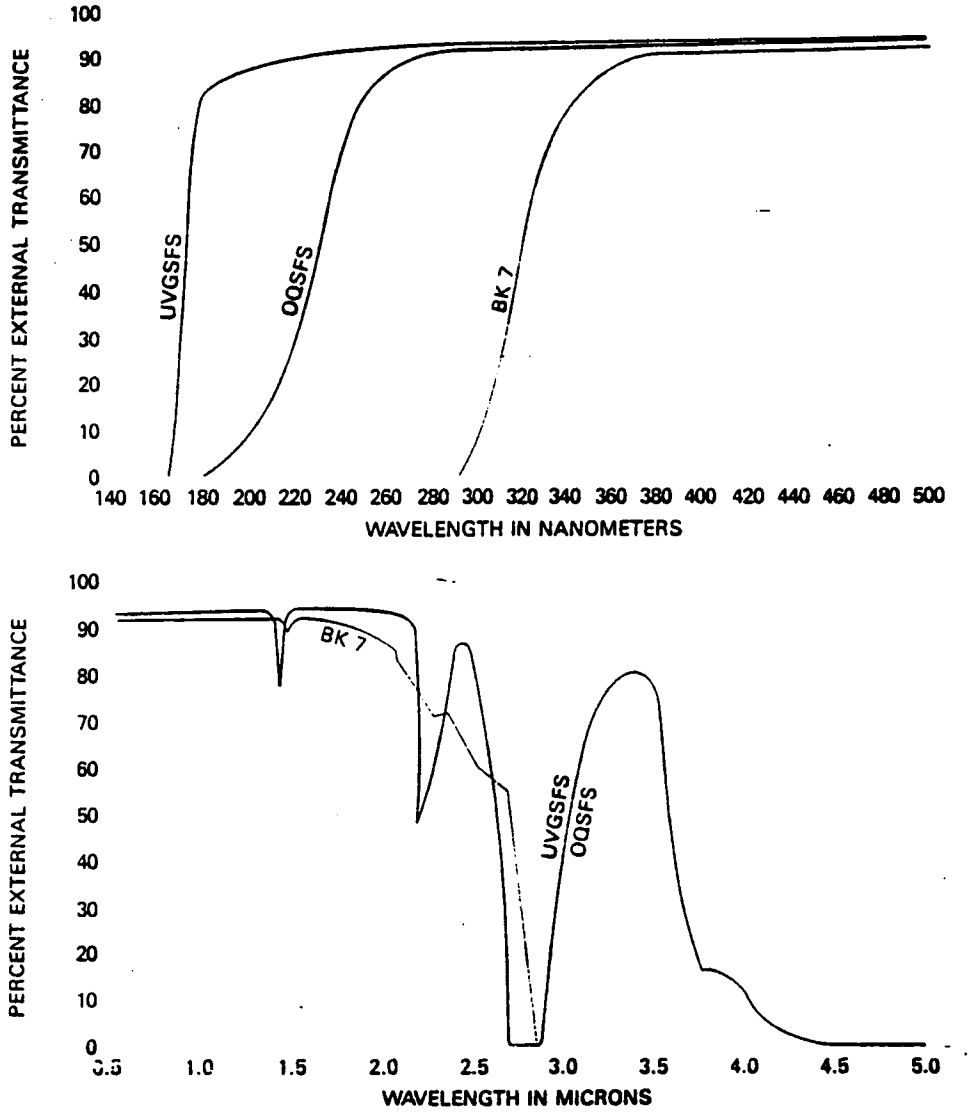


**Figure 80: Actual Transmissibility Curve For Quartz Glass** [Copied from: 32. Melles Griot, "Optics Guide 4", (Optics Catalog), pp. 3-4.]

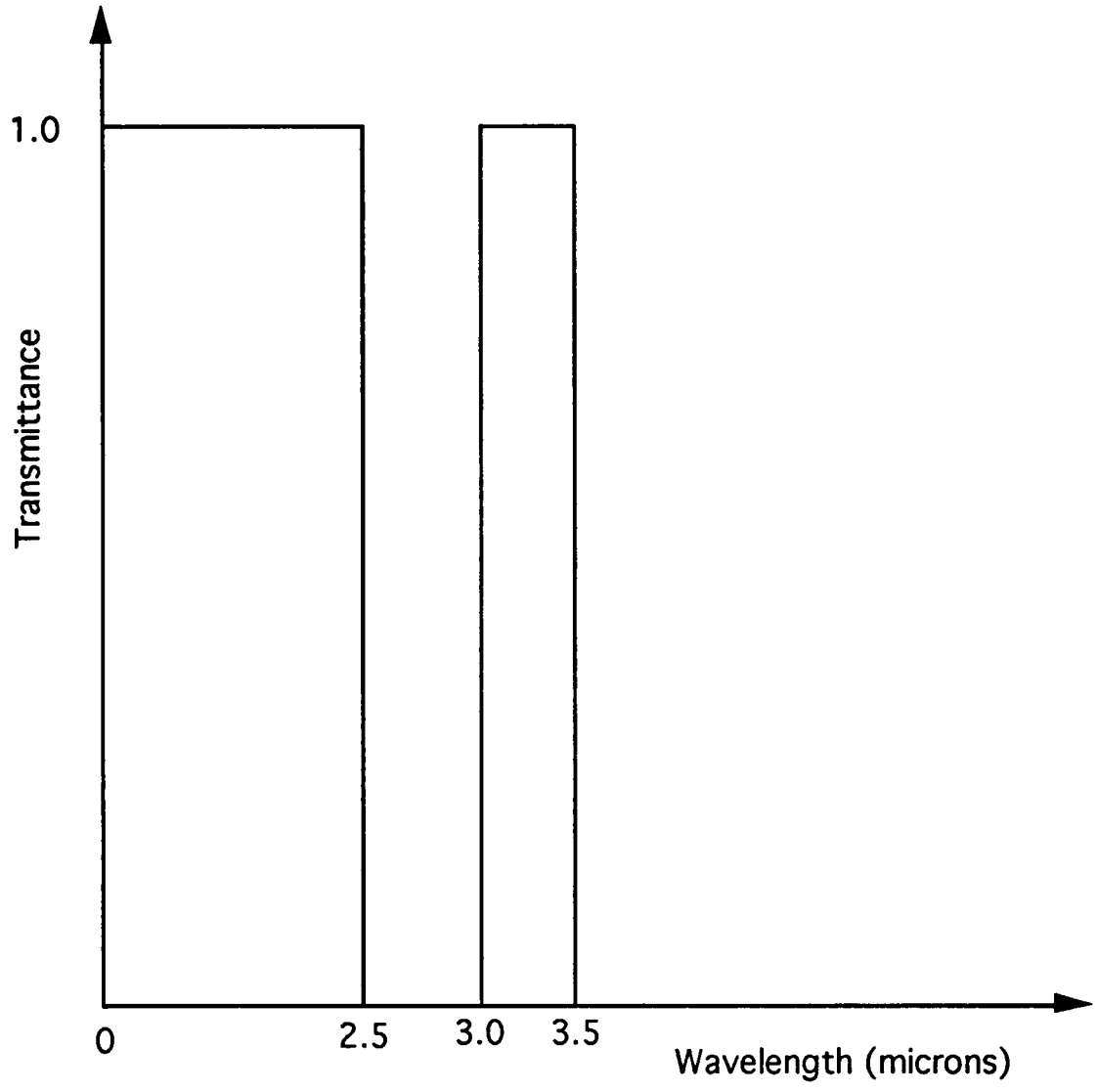


**Figure 81: Simplified Quartz Transmittance Properties**

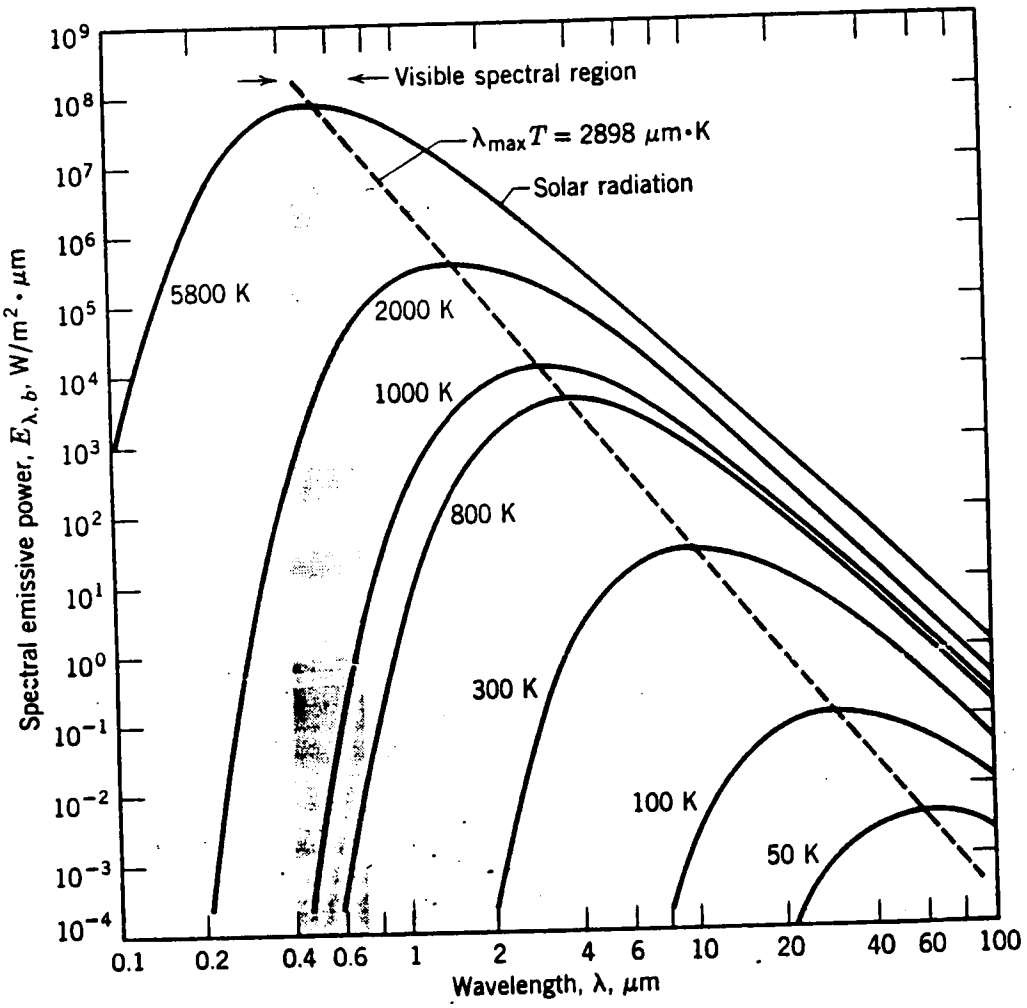


**Figure 82: Black Body Radiation Emissive Power Vs. Wavelength**

[Copied from: 31. Incopera, F. P. and DeWitt, D. P., "Fundamentals of Heat and Mass Transfer", John Wiley & Sons, Inc., 1985.]

radiation emitted from zero to the desired wavelength. This fraction is given by [31]:

$$F_{0\to\lambda} = \frac{\int_0^{\lambda} E_{\lambda B} d\lambda}{\sigma T^4} = \int_0^{\lambda T} \frac{E_{\lambda B} d(\lambda T)}{\sigma T^5} \qquad (41)$$

Thus the fraction of blackbody radiation emitted up to a given wavelength is a function of the product of $\lambda$ and T. The value of $F_{0\to\lambda}$ is tabulated in most heat transfer textbooks.

In order to find the fraction of blackbody radiation emitted between two wavelengths it is necessary to subtract the fraction emitted up to the lower wavelength from the fraction emitted up to the higher wavelength. Thus, the fraction emitted between two wavelengths is given by:

$$F_{\lambda_1\to\lambda_2} = F_{0\to\lambda_2} - F_{0\to\lambda_1} \qquad (42)$$

For the design of this combustor, it was necessary to determine the fraction of blackbody radiation emitted by the flame between 2.5 and 3 $\mu$m and for wavelengths greater than 3.5 $\mu$m. The fractions for these two bands were found to be 0.0369 and 0.0665, respectively. Since water vapor emits between 2.5 and 3 $\mu$m, it is likely that this portion of the emission will behave as a blackbody. However, beyond 3.5 $\mu$m, few of the products would behave as a

blackbody. It was therefore deemed acceptable to scale the larger band widths by a graybody emissivity of 0.5. Thus, the total fraction of the blackbody emission, or the flame emissivity, in these desired wavelengths was found to be:

$$F_T = \varepsilon_f = \left(F_{0\to 3} - F_{0\to 2.5}\right) + 0.5\left(1 - F_{0\to 3.5}\right) = 0.07015 \qquad (43)$$

This value was used in equation 40 for the flame emissivity.

Since the conduction of the quartz tube is negligible, the outflow of energy can only occur by convection and radiation. The convection heat transfer from the quartz tube to the surroundings is:

$$q_{qs(conv)} = hA_{s_2}\left(T_q - T_\infty\right) \qquad (44)$$

where h is the convective heat transfer coefficient, and subscript $S_2$ denotes the outside surface of the glass. Since the pressurizing gas on the outside of the quartz glass tube would most likely be between forced and free convection, it was decided that a value of 25 $W/m^2K$ would be appropriate for the convective heat transfer coefficient [31].

Due to the fact that some of the radiation can escape through the high pressure vessel window(s) (and the fact that the outer pressure vessel will be substantially larger than the quartz tube), it was

deemed appropriate to treat the surroundings as a blackbody at $T_\infty$ (instead of using the infinite cylinder equation). Thus, the radiation from the quartz tube to the surroundings would simply be:

$$q_{qs(rad)} = A_{s_2}\varepsilon_q\sigma\left(T_q^4 - T_\infty^4\right) \tag{45}$$

Assuming the term $\rho VC_p$ is constant, equation 36 would become:

$$\frac{\sigma A_f\left(T_f^4 - T_q^4\right)}{\frac{1}{\varepsilon_f} + \frac{1-\varepsilon_q}{\varepsilon_q}\left(\frac{r_f}{r_{q_i}}\right)} - A_{s_2}\left[h\left(T_q - T_\infty\right) + \varepsilon_q\sigma\left(T_q^4 - T_\infty^4\right)\right] = \rho VC_p\frac{dT}{dt} \tag{46}$$

expanding the area terms and cancelling, this equation would become:

$$\frac{2r_f\sigma\left(T_f^4 - T_q^4\right)}{\frac{1}{\varepsilon_f} + \frac{1-\varepsilon_q}{\varepsilon_q}\left(\frac{r_f}{r_{q_i}}\right)} - 2r_{q_2}\left[h\left(T_q - T_\infty\right) + \varepsilon_q\sigma\left(T_q^4 - T_\infty^4\right)\right] = \rho C_p\left(r_{q_2}^2 - r_{q_i}^2\right)\frac{dT}{dt} \tag{47}$$

In order to obtain the steady state solution it is necessary to set the right side of the equation equal to zero and iterate the temperature of the quartz glass for a given emissivity. Since the emissivity of quartz glass ranges from 0.41 to 0.9, the steady state temperature was found to occur between 1800 K and 2250 K. However, this temperature as expected, is well above the maximum temperature (for continuous life) of quartz glass (1273 K).

Since the time dependent equation is nonlinear, it was necessary to use a numerical procedure in order to obtain a solution. Since this equation is already in terms of dT/dt, a fourth order Runge Kutta solution was obtained [33]. Using this computer program and the range of emissivities of quartz glass and the specific heat of quartz glass (0.25 cal/g K (1047 J/kg K)), the temperature of the quartz tube was found as a function of time (see Figure 83). As can be seen from Figure 83, both curves reach 1273 K after only four seconds. If one wished to operate a fused quartz tube at its limited life temperature of 1573 K, the operating time limit would increase to approximately eight seconds. Depending upon the duration of the experiment, the failure criteria of the glass could be changed to the annealing point (1453 K) or the softening point (2003 K). An alternative to this dangerous approach would be to choose a glass with similar optical properties yet higher operational temperature capabilities (see Figure 84). One such glass is sapphire. Although sapphire is capable of significantly higher operating temperatures, it is also much more expensive. Therefore, it is recommended that this combustor initially run for very short times (two to three seconds) witha fused quartz or fused silica tube. Obviously the flame temperature in the actual combustor will be less due to losses in the chamber and mixing with nitrogen. Never the less, these computed combustion times provide for worst case conditions and suggested run times should not be exceeded until after this heat

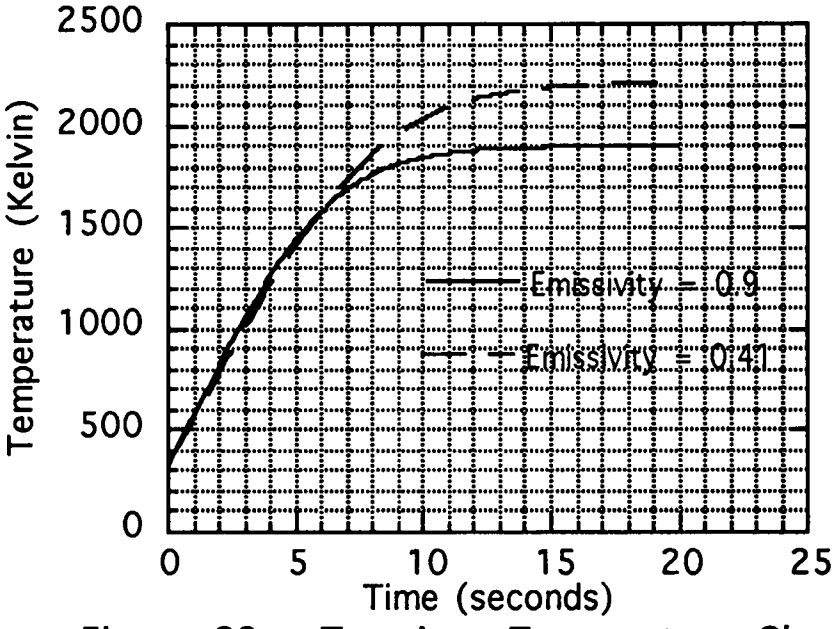


**Figure 83: Transient Temperature Change for Quartz Tube with Various Emissivities**

| | Fused Quartz | Fused Silica | Pyrex | Sapphire |
|---|---|---|---|---|
| Softening Point (K) | 2003 | 1873 | 1093 | 2313 |
| Anealing Point (K) | 1453 | 1393 | 838 | |
| Strain Point (K) | 1348 | 1298 | 788 | |
| Max. Temp. continuous (K) | 1273 | 1223 | 503 | 1373 |
| Max. Temp. limited life (K) | 1573 | 1473 | 763 | |

**Figure 84: Physical Properties of Optical Materials**
Adapted from: 34. ESCO Products, Inc., "Optical Materials and Components Handbook", Oak Ridge, New Jersey, pp. 6.

transfer analysis has been adequately investigated with experimental data.

### 4.2.2. Heat Transfer to the Nozzle

Unlike the quartz tube heat transfer problem, the nozzle of this combustor is expected to operate at steady state conditions (or at least significantly longer than the quartz tube). Additionally, the nozzle, unlike the quartz tube or the injector, will experience both high temperature and high pressure operating conditions. Since the strength of most materials decreases dramatically at high temperatures, it is necessary to first define what the maximum operating temperatures of the nozzle will be. Also, the nozzle throat will experience large convective heat transfer rates.

Since the nozzle throat will experience the largest convective heat transfer rate, the convective heat transfer coefficient, for this area, must be calculated. The convective heat transfer coefficient for the nozzle throat was calculated from [30]:

$$h_g = \frac{0.026}{D^{0.2}}\left(\frac{C_p \mu^{0.2}}{Pr^{0.6}}\right)(\rho v)^{0.8}\left(\frac{\rho_{am}}{\rho_\infty}\right)\left(\frac{\mu_{am}}{\mu_o}\right) \qquad (48)$$

where $\mu$ is the viscosity, Pr is the Prandtl number, v is the local velocity, and the subscripts am and o refer to the arithmatic mean and stagnation properties, respectively. The term $\rho_\infty$ is the free stream value of the local gas density which was assumed to be equal

to the arithmetic mean density. Since the nozzle was designed for the maximum flow rate of methane fuel, the average values of the physical properties for methane combustion products and nitrogen were used in this calculation. From equation 48, it was found that the convective heat transfer coefficient at the nozzle throat was 12700 $W/m^2K$.

To calculate the heat transfer rate to the nozzle wall, the following equation was used:

$$q_{ft} = h_g A_t (T_g - T_s) \tag{49}$$

where $T_g$ is the average gas stagnation temperature (2050 K), $T_s$ is the temperature of the inner surface (1033 K (assumed to be 0.66 times the melting temperature of stainless steel)), and $A_t$ is the surface area of the entire nozzle (including the convergent (0.000668 $m^2$), throat (0.0000606 $m^2$), and divergent (0.000479 $m^2$) sections of the nozzle). Certainly, in reality, the convective heat transfer coefficient would not be as large as the one calculated, in equation 48, along the entire nozzle area. However, by assuming this coefficient is constant, a worst case heat transfer rate of 16000 W was calculated. Since radiation heat transfer is less than three percent of the convective heat transfer, it can be ignored in this heat transfer calculation.

After the convection heat transfer to the nozzle area was calculated, the dimensions of the various nozzle components were determined. Since the temperature of the inner nozzle surface is 1033 K or less, the thickness calculations must use the strength of the nozzle material at this temperature. For stainless steel at this temperature, the yield strength drops to approximately 15000 psia. Therefore, the thickness of each section of the nozzle must be significantly greater than the other sections. Again using a factor of safety of two and equation 24, the thickness at each section was calculated and the dimensions of the nozzle are shown in Figure 85. Note, these dimensions also correspond to standard tubing dimensions.

In order to determine the temperature distribution in the stainless steel nozzle, it was again necessary to calculate the Biot number. Since the nozzle convection coefficient will most likely be maximum at the interior of the nozzle throat, the value from equation 48 was use to determine the Biot number. Additionally, the volume of steel and interior and exterior surface areas of the throat region were used to calculate the characteristic length. Thus, the Biot number was found to be 0.102. This value was sufficiently

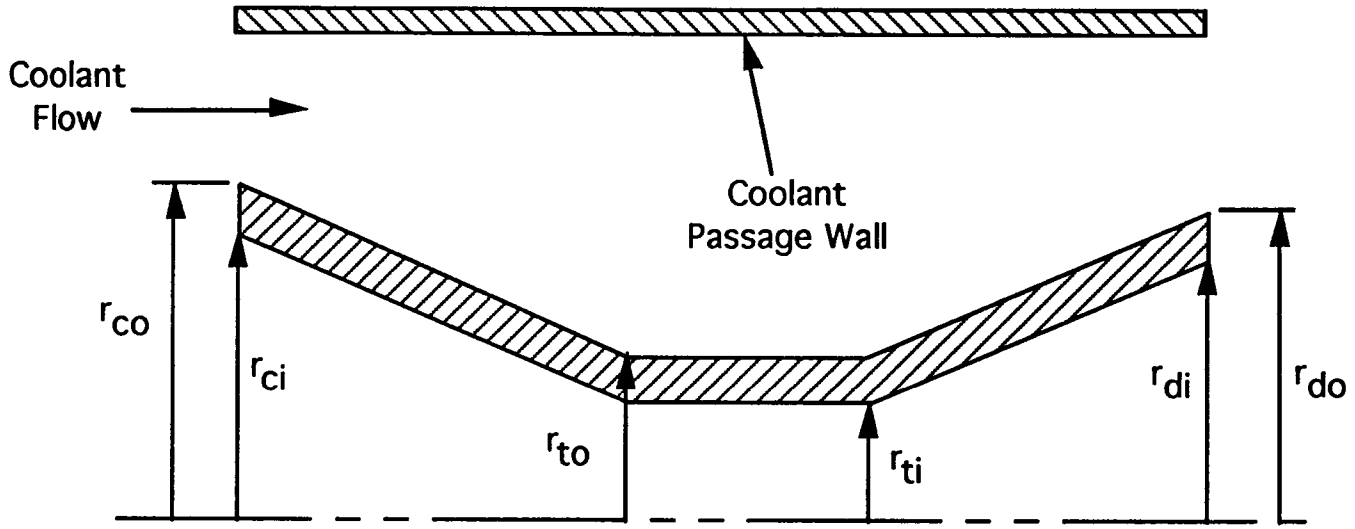


Note: Dimensions are in inches

| rco | rci | rto | rti | rdo | rdi |
|---|---|---|---|---|---|
| 0.5625 | 0.4675 | 0.078125 | 0.062 | 0.444 | 0.349 |

**Figure 85: Nozzle Dimensions**

close enough to 0.1 for the uniform temperature assumption to be valid.

Since the Biot number is sufficiently small, the only heat transfer outflow is due to convection of the coolant water (radiation can also be neglected here). The energy balance on the nozzle section therefore simplifies to:

$$h_g A_i (T_g - T_s) = h_l A_o (T_s - T_\infty) \tag{50}$$

where $A_i$ is the inner surface area and $A_o$ is the outer surface area. In order for the water coolant to be effective, it must not be heated above its boiling point. It was assumed that the water would enter the coolant passage at 300 K and be heated to no more than 368 K. Thus, $T_\infty$ was assumed to be the average value of 334 K. Therefore, it follows that $h_l$ must have a value of approximately 13873 $W/m^2K$.

In order to achieve this coolant coefficient, it is necessary that the water flow rate be sufficient. In order to determine the water flow rate, the following equation was used [30]:

$$h_l = 0.023 C_p (\rho v)^{0.8} \left(\frac{\mu}{D_h}\right)^{0.2} (Pr)^{\frac{-2}{3}} \tag{51}$$

Substituting the constants and simplifying, equation 51 becomes:

$$v = 8.414 D_h^{0.25} \tag{52}$$

where $D_h$ is the hydraulic radius (4 times the cross-sectional area divided by the wetted perimeter). For the worst case, the wetted perimeter would be that of an annulus with the inner radius equal to the outer radius of the nozzle throat. Thus, the hydraulic radius for this case is:

$$D_h = \frac{4\pi\left(r_o^2 - r_{to}^2\right)}{2\pi\left(r_o + r_{to}\right)} = 2\left(r_o - r_{to}\right) \tag{53}$$

where $r_o$ is the inner radius of the coolant jacket, and $r_{to}$ is the outer radius of the nozzle throat.

Thus, for a coolant passage of 1.25 in. inside diameter, a volume flow rate of 42.4 gallons per minute (with the mean velocity of the water equal to 3.43 m/s) is required to produce the necessary convection coefficient at the throat region. This would correspond to a flow rate 2.63 kg/s. These flow rates should easily be obtainable with standard pumps.

Additionally, it must be verified that the water will enter and exit the coolant tube at the desired temperatures. This can be easily

accomplished by using [30]:

$$q = mC_p\left(T_{m_o} - T_{m_i}\right) = 749KW \tag{54}$$

where $T_{m_o}$ and $T_{m_i}$ are the coolant fluid outlet and inlet mean temperatures, respectively. Since this heat transfer rate is much larger than the required heat transfer rate, the temperature change of the coolant water will not be as large as anticipated. Never the less, the predicted flow rate should be sufficient to provide adequate nozzle cooling, especially for the short run times of this combustor.

# CHAPTER V - Safety and Operational Requirements

Once this combustor has been constructed there are several important tests which must be conducted before actual testing of the apparatus may begin. These tests are designed to ensure the safe and stable operation of this combustor. This chapter divides these test requirements into four sections. The first section deals with the verification of flame stability. The second section describes the procedure to be used to ensure an adequate supply of aluminum particles. The third section discusses the necessary tests required to guarantee that the operating pressures and temperatures can safely be achieved. The fourth section of this chapter describes the safety procedures and devices to be used on this combustor.

## 5.1. Flame Stability

The first, and most important, topic discussed in this chapter is the issue of flame stability. These tests are divided into two categories: cold flow tests and combustion analysis.

The first step in determining the flame stability of this combustor is to conduct cold flow experiments. In this portion of the combustor development process, it is necessary to verify that the velocities discussed in chapter 4 are achievable by setting the defined O/F ratios and pressures specified. This will be accomplished by installing the necessary valving and measuring the velocity profiles at atmospheric pressure (no nozzle) to ensure a uniform flow at the injector face. The gases used in these cold flow experiments will be inert gases (or merely non-reacting) which will have similar physical properties as the corresponding fuels and oxidizers (nitrogen will still be used). Additionally, glass beads may be used to simulate the aluminum particulates in the fuel flows. After the flow fields and particle flows have been verified, the non combustible gases will be fed in at operational pressure ranges (500-1000 psia), and the average velocities will be calculated (by equation 18) from the flow rates into the chamber. By observing the flow meters, the velocities of the gases may be calibrated to the valve positions. Next, the gases may be injected with smoke to establish the flow fields which will be important for the combustion analysis. From these flow fields it should be possible to determine the length of the core flow and an adequate location for the ignition source. Alternatively, liquids could be used with dyes as long as Reynolds similarity was maintained. Additionally, a good approximation of the diameter of the flame may be obtained by observing the distance which the simulated oxygen diffuses into the

nitrogen. From this distance the heat transfer problem in chapter 4 will be reexamined, and verified.

The next step in ensuring flame stability is to verify that the actual fuels to be used will burn in a predictable and safe manner. From observing the cold flow experiments (and making the necessary design changes), the igniter wires should be placed in their proper position. It should be verified (before actually trying to ignite the mixture) that there is an adequate voltage supply to permit a continuous spark at the desired flow rates. After the wires are in position, the voltage source is turned on, then the gas (no particles) is started. Hopefully, this will result in a stable flame which does not impinge on the glass tube walls. If the flame hits the tube-wall, the combustor is immediately shut down and a larger quartz tube and nitrogen injector will be made. However, if the flame does not impinge on the glass, temperatures at various locations along the outside of the glass tube will be recorded in order to verify the heat transfer analysis. If this step is successful the process is ready to be repeated with the aluminum particles.

## 5.2. Aluminum Particle Feed System

This section describes the method which will be used to inject the particles into the flow of the combustor. The particle injection mechanism will consist of a tube (capable of withstanding up to

2000 psia) filled with aluminum particles (see Figure 86). The gaseous fuel will be injected into one end of the tube and leave through a small orifice at the other end. It has been found in a similar experiment that the diameter of this orifice should be approximately 3 times the diameter of the particles to be injected [35]. Therefore this feed system should be calibrated for each fuel used and each particle size used. The pressure drop across the tube should also be recorded.

From the heat transfer analysis the operational time limits were determined. Using these time limits and the maximum flow rate of particles, the mass of aluminum in kg to be contained in the tube can be found from:

$$m_{Al} = 1.5 m_{max} t_{op} \tag{55}$$

where1.5 is used to ensure that particle supply does not run out during the test, $m_{max}$ is the maximum flow rate of particles in kg/s, and $t_{op}$ is the operational time specified in the heat transfer process. From this equation the tube volume can easily be estimated by:

$$V = \frac{m_{Al}}{C_1 \rho_{Al}} \tag{56}$$

where $C_1$ is a constant for the packing fraction which can be obtained (which should be near unity for these small particles).

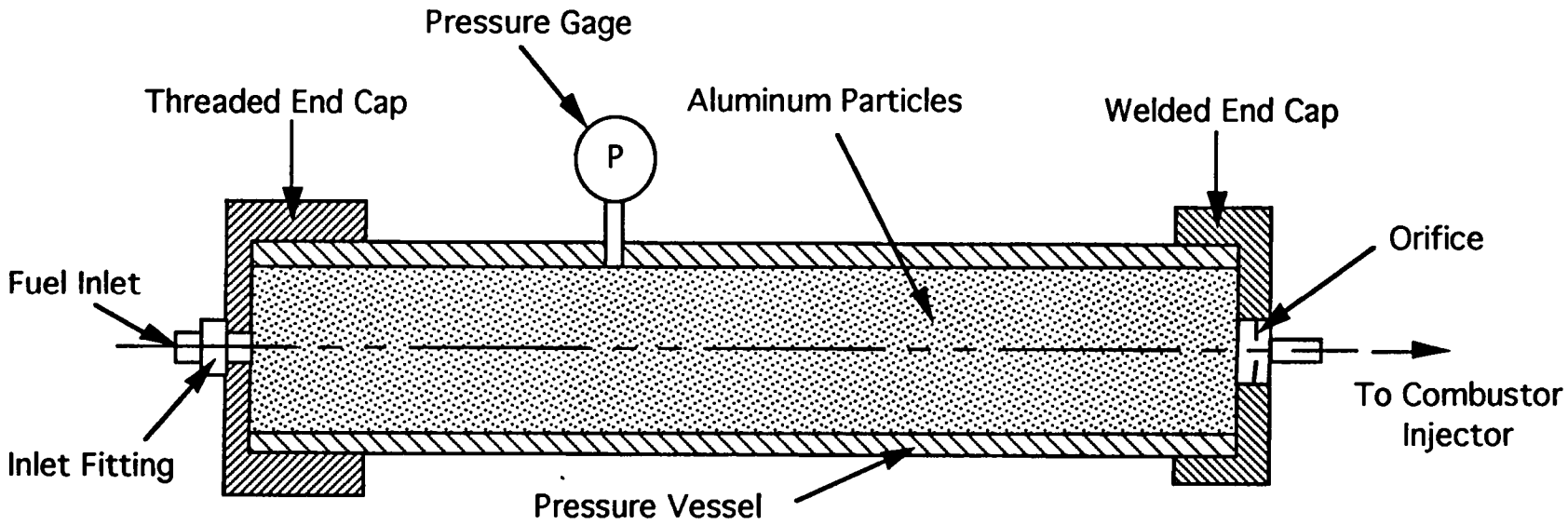


**Figure 86: Aluminum Particle Supply System**

## 4.3. Operational Temperature and Pressure Requirements

Since this device operates at extreme temperatures and pressures it is important to guarantee that the design of this combustor is sound before operational tests can begin. One of the first design assumptions which should be verified is the heat transfer and temperature calculations. More importantly, it is necessary to find the time required for quartz tube to reach its maximum operating temperature. Before the actual combustor is built, a (very) rough estimate of this time could easily be obtained by heating a small quartz tube sample with a torch (in roughly the same orientation as the flame will be inside the combustor) and recording the temperature of the glass surfaces. The parameters of the torch should be used in the heat transfer equations in chapter 4 and the experimental data compared with the theoretical data. If there are any major discrepancies the heat transfer assumptions may have to be re-evaluated and a new design obtained. Likewise, before the nozzle has been constructed the same type of experiment may be conducted to verify its heat transfer analysis. Alternatively, the combustor could be built and transient temperatures of critical components could be measured with thermocouples.

After the temperature ranges have been verified, the pressure ranges of the combustion apparatus must be verified. This can easily be done by assembling the combustor and plugging the ends.

The chambers can then be filled with liquids and pressurized at the desired pressure (see Figure 87). In this way the seals can be checked by coloring one of the liquids. Thus, a leak could easily be detected and corrected before operational tests.

## 5.4. Safety Devices and Procedures

Obviously, due to the high pressures and temperatures involved the primary concern of operating this combustor should be the safety of the test personnel. Of secondary importance should be the safety of the equipment and instrumentation. This section discusses the considerations which were made to ensure the safety of both the personnel and equipment.

The first, and easiest step, in personnel safety is to separate the test crew from the combustor during test operations. This can be accomplished by placing the combustor in a test bay (similar to the one in UTSI's propulsion lab) and observing the overall operation with a real-time camera. Both the observation point of the crew and the camera should be adequately protected in the event of failure. The crew protection may come from sufficient separation distance and the camera protection could be provided by a Plexiglas shield. Since some of the gases used in this combustor may become detonable or poisonous, it is also necessary to provide for leak

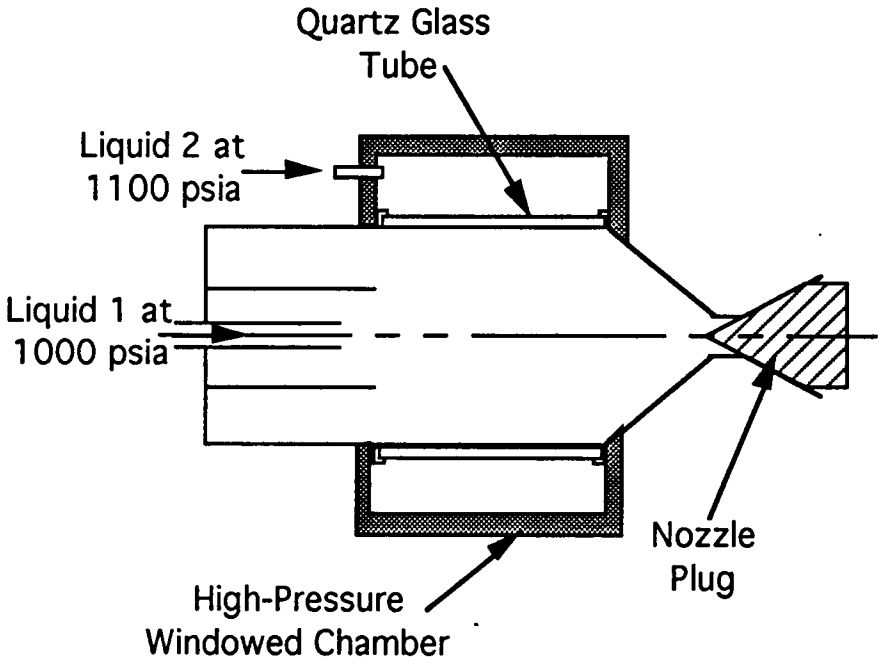


**Figure 87: Pressure Test Diagram**

detection devices within the test cell to ensure crew safety (especially between operational tests).

Besides the safety of the personnel, the integrity of the combustor and instrumentation is also important. In order to protect the instrumentation, it is necessary to shield all detection devices from debris formed in the event of a failure. This is usually accomplished by using Plexiglas shields. In addition, the combustor can be designed so that if failure does occur, it does so in a predictable manner. One way to accomplish this is to place burst disks on the gas feed lines which do not face the instrumentation. The burst disk on the interior chamber protects the integrity of the combustor in the event the nozzle becomes plugged while the outside burst disk should protect the instrumentation. It should also be incorporated into the combustor operation that all valves will shut once one of these burst disks is compromised.

As mentioned earlier in this thesis, this combustor development program will start with the simpler experiments and then work towards more complicated experiments. This is also done to ensure the safe operation of this combustor. It makes it safer to allow the operators to observe the characteristics of this combustor under various conditions and recording the data for future personnel to use.

# CHAPTER VI - Instrumentation Requirements

This chapter describes briefly the instrumentation required for the operation of this combustor. The instrumentation necessary can be divided into two groups: -l) those which are necessary to insure the safe operation of the combustor and -2) those which are necessary to collect the desired data pertinent to the aluminum combustion. As mentioned earlier, these instruments are only mentioned briefly and the exact specifications are not listed. Never the less, the two aforementioned instrumentation divisions are discussed below.

## 6.l. Instruments Used for Safety Purposes

The first safety instruments to be discussed are the pressure sensors. These sensors should be capable of determining the pressure in the combustion chamber and within the outer chamber. If the pressure reaches over 1100 psia in the combustion chamber or over 1200 psia in the outer chamber, the fuel and oxidant feed systems of the combustor should be automatically and immediately shut down. Since these sensors must be capable of determining the pressures nearly instantaneously, these pressure sensors must be

capable of high speed response. This is due to the fact that any catastrophic failure would most likely result in a rapid pressure increase. Therefore, it is necessary that these pressure sensors have fast response times.

The second type of safety instruments for this combustor is the temperature sensors. One thermocouple should be on the outside of the quartz glass tube. Once the maximum temperature, as specified by the heat transfer analysis in chapter 3, of this outside surface is reached, the device should immediately and automatically stop. Similarly, a thermocouple should be placed on the outside of the nozzle throat with its own criteria for emergency shutdown. Since these thermocouples also require nearly instantaneous data acquisition, they should also have response times on the order of 1 millisecond.

The third, and final, safety instrument to be used is an ordinary video camera. This camera should be capable of providing real-time video output. It should have a wide angle view of the experimental apparatus so in the event of any malfunction the operator can manually implement emergency shut down procedures. Additionally, in order to protect the camera, the camera should be placed in a Plexiglas compartment (shield) and/or the camera should be at a far enough distance to remain out of harm's way.

## 6.2. Data Acquisition Instrumentation

Since one of the main objectives of this project is to obtain accurate optical data on aluminum/aluminum oxide particles, it is necessary to have several optical sensors. These optical sensors must be capable of determining the spectral radiation emitted from the flame/particles. The observed spectral reaction should show the relative intensity of the radiation verses the wavelength for that intensity. The device recommended for this data acquisition is the Optical Multi-Channel Analyzer. This device is capable of acquiring and recording the required data.

Another optical sensor, which is necessary for data acquisition during the operation of this combustor, is the mass spectrometer. This device is capable of identifying individual species by their emitted wavelengths. It is also capable of determining the mass fractions of each of these individual species.

The third instrument required for data acquisition is a high speed motion camera. This camera should be capable of observing the combustion of individual aluminum particles. It is therefore necessary that the camera also have adequate magnification capabilities. This device will be extremely useful to determine the best location for the other optical devices. This will be done by running trial experiments with the camera at various axial

positions. By viewing the camera data, the optimum placement for the other optical sensors will be determined.

The fourth, and final, instruments necessary are the flow meters in the gas supply lines. These flow meter readings will be necessary to determine the exact operating conditions (i.e., O/F ratio, etc.) which the combustor was operating. Since this data will be necessary for later analysis, it is recommended that the output of the flow meters be recorded.

# CHAPTER VII - Conclusions and Recommendations

As stated throughout this thesis, the design of this combustor was intended as a simple-as-possible initial design, with the need to gradually work towards more complex designs that would more accurately simulate the combustion of aluminum in a solid rocket motor environment. Therefore, this design work was mainly based upon simplified pressure vessel equations, equilibrium chemistry calculations, and a simplified heat transfer analysis. (Each of these design criterion are discussed below.)

Although the simplified pressure vessel equations are by no means a finite element analysis, they should be sufficiently accurate for the intended operations of this combustor. However, the dimension of the central injector was arbitrarily chosen. In reality, the area and flow rate of each injection tube could drastically change the stability of the flame and the combustion products which are formed. In addition, this design assumed that the nitrogen and oxygen would not intermix. In reality, this is not the case. This is due to the fact that there will be some vorticity produced between the oxygen and nitrogen interface. Any substantial mixing between these two gases could cause the flame

to expand to the quartz tube wall resulting in excessive heat transfer rates. For these reasons, it is imperative that the flow rates and flame stability be verified and all necessary redesign work be completed before the initial test operations begin. These redesigns may include changing the dimensions of the injectors, the flow re-circulator locations, and the flow rates of the gases.

The use of equilibrium chemistry for this combustor should provide a fairly accurate overview of the species, transport properties, and temperatures which will be produced in this combustor. The accuracy of the NASA equilibrium chemistry code has been confirmed in numerous tests. However, since these chemistry calculations assume infinite reaction rates and reactions which continue until completion, the actual species produced in this combustor will probably be slightly different from those which were predicted. In reality, the rate of reaction will be mainly controlled by the turbulent mixing of the species at the injector face. Also, the reaction of the aluminum particles (with oxygen) may be difficult due to the (possible) lack of oxygen along the center of the combustor. Further complications which may affect the aluminum particle combustion include the formation of a protective oxide on the particles and the collision of molten aluminum particles which may form large agglomerates (and therefore, substantially longer burn times). All of these factors must also be experimentally

verified and any necessary design changes must be incorporated into the combustor before actual tests can begin.

Another problem which may occur during the operation of this combustor is the erosion of the nozzle throat. Although the heat transfer calculations should insure that the nozzle will be maintained below its melting temperature, it does not necessarily guarantee that the nozzle throat will not erode. The high flow velocities of the reactive and corrosive combustion gases can still erode (and possibly react) with the stainless steel nozzle. Since the velocities should be their maximum at the nozzle throat, it is recommended that the nozzle design be incorporated with graphite inserts in the nozzle throat. Although the graphite insert will still probably erode, it should not threaten the integrity of the nozzle itself. This should, in the long run, decrease the cost and increase the safety of the nozzle design. Additionally, since the ceramic needle may cause the nozzle to plug with aluminum slag (resulting in catastrophic over pressures), it is recommended that the variable throat area design be carefully evaluated in testing, and, if it proves unsatisfactory, it should be discarded in favor of alternative nozzle designs. Each of these nozzles would have graphite inserts with the throat area corresponding to choked flow for the flow rate of the particular experiment. Although this may be more expensive, it may necessary to insure the safe operation of this device.

As mentioned in chapter 4, due to the high heat transfer rates it was necessary to use a two wall construction for the quartz observation windows (Figure 74). This was also necessary due to the poor strength of quartz in tension (especially at high temperatures). If a single glass tube were used for this combustor, it would require a tube which would be approximately 0.5 in. thick for a 1.0 in. inside diameter tube. This thick tube would act as a (powerful) lens which would make data acquisition difficult. Alternatively, the combustor could use a single chamber with a thick recessed quartz window. In order to cool this recessed window, it would be necessary to purge this window with a coolant gas. This may make it difficult to observe the combustion process along the entire length of the combustor. Also, this alternative design may result in the formation of recirculation zones of hot combustion gases near the combustor walls (unlike the two wall design) resulting in catastrophic heat transfer rates. Not only may this alternative design be more dangerous, but it could also be more expensive to develop the purge system for the recessed window design. For these reasons, it is recommended to develop the two wall design configuration.

Obviously, the combustion of aluminum particles in a flame may not accurately simulate the heterogeneous reactions which occur within an actual solid rocket motor. However, this combustor concept is designed to be capable of observing the effects of the

individual species on the aluminum combustion process. This design should also be able to observe the effects of individual species on the optical properties of aluminum and its oxides. In order to accurately simulate the solid rocket motor species, it is necessary to operate this combustor in the fuel rich regime for the first two suggested fuels (hydrogen and methane). (The two main species produced in a typical rocket motor are free hydrogen and carbon monoxide.) Fuels which will be used in later experiments should produce hydrochloric acid and free nitrogen (two other species produced in solid rocket motors). It is recommended that each of these species and their effects on aluminum be studied individually (if possible). Eventually, after numerous limited specie tests, this combustor may be able to provide observations of aluminum combustion in an environment which contains all of the prevalent species found in a solid rocket motor.

Once this combustor is built (after all of the necessary design verifications and/or have been incorporated), it should provide a versatile research tool. Not only should this combustor provide insight into the aluminum combustion process, but it could also be a valuable tool for the observation and measurement of coaxial jet mixing and combustion. This combustor may be used to study the combustion characteristics of new fuels and additives for solid rocket motors. In conclusion, this combustor (or its derivatives) should be a valuable research tool for years to come.

# LIST OF REFERENCES

## List of References

1. Mitani, T. and Izumikawa, M., "Combustion Efficiencies of Aluminum and Boron in Solid Propellants", Journal of Spacecraft and Rockets, Vol. 28, No. 1, 1991, pp. 79-84.

2. Sauerwein, H. P., Lampert, A. and Schmucker, R. H., "Erosive and Transient Burning Effects on Performance Prediction Accuracy of Tactical Rockets", AGARD Propulsion and Energetics Symposium on Solid Rocket Motor Technology, 1979.

3. Wood, W. A., "Metal Combustion in Deflagrating Propellant", Solid Propellant Rocket Research, Progress in Astronautics and Rocketry, Vol. 1, 1960, pp. 287-291.

4. Nir, E. C., "Combustion of Powdered Metals in Contact with a Solid Oxidizer (Ammonium Perchlorate)", Thirteenth Symposium (International) on Combustion, 1971, pp. 1019-1029.

5. Price, E. W., "Combustion of Aluminum in Solid Propellant Flames", AGARD Propulsion and Energetics Symposium on Solid Rocket Motor Technology, 1979, pp. 14-1 - 14-15.

6. Belyaev, A. F., et. al., "Combustion Characteristics of Powdered Aluminum", Translated from Fizika Goreniya i Vzrya, Vol. 5, No. 2, 1969, pp. 207-217.

7. Povinelli, L. A. and Rosenstein, R. A., "Alumina Size Distributions from High-Pressure Composite Solid-Propellant Combustion", AIAA Journal, Vol. 2, No. 10, 1964, pp. 1754-1760.

8. Gany, A. and Caveny, L. H., "Agglomeration and Ignition Mechanism of Aluminum Particles in Solid Propellants", Seventeenth Symposium (International) on Combustion, 1978, pp. 1453-1461.

9. Caveny, L. H. and Gany, A., "Aluminum Combustion Under Rocket Motor Conditions", AGARD Propulsion and Energetics Symposium on Solid Rocket Motor Technology, 1979.

10. Brennan, W. D., Hovland, D. L. and Netzer, D. W., "Measured Particulate Behavior in a Subscale Solid Propellant Rocket Motor", Journal of Propulsion and Power, Vol. 8, No. 5, 1992, pp. 954-960.

11. Drew, C. M., Gordon, A. S. and Knipe, R. H., "Study of Quenched Aluminum Particle Combustion", Heterogeneous Combustion, Progress in Astronautics and Aeronautics, Vol. 15, 1964, pp. 17-39. See also: AIAA Preprint Paper No. 63-487.

12. Fassell, W. M., et. al., "The Experimental Nature of the Combustion of Metallic Powders", Solid Propellant Rocket Research, Progress in Astronautics and Rocketry, Vol. 1, 1960, pp. 259-269.

13. Friedman, R. and Macek, A., "Ignition and Combustion of Aluminum Particles in Hot Ambient Gases", Combustion and Flame, Vol. 6, 1962, pp. 9- 19.

14. Macek, A., "Fundamentals of Combustion of Single Aluminum and Beryllium Particles", Eleventh Symposium (International) on Combustion, 1967, pp. 203-217.

15. Prentice, J. L., Drew, C. M. and Christensen, H. C., "High-Speed Photography of Aluminum Combustion in Flames", Presented at the Meeting of the Western States Section of the Combustion Institute, 1964, Salt Lake City, Utah.

16. Gordon and McBride, "Computer Program for Calculation of Complex Equilibrium Compositions, Rocket Performance, Incident and Reflected Shocks and Chapman - Jouquet Detonations", NASA SP-273, February, 1973.

17. Brzustowski, T. A. and Glassman, I., "Vapor-Phase Diffusion Flames in the Combustion of Magnesium and Aluminum: II. Experimental Observations in Oxygen Atmospheres", Heterogeneous Combustion, Progress in Astronautics and Aeronautics, Vol. 15, 1964, pp. 117-158.

18. Mellor, A. M. and Glassman, I., "Vapor-Phase Diffusion Flames in the Combustion of Magnesium and Aluminum: III. Experimental Observations in Carbon Dioxide Atmospheres", Heterogeneous Combustion, Progress in Astronautics and Aeronautics, Vol. 15, 1964, pp. 159-175.

19. Razdobreev, A. A., Skorik, A. I. and Frolov, Yu. V., "Ignition and Combustion Mechanism in Aluminum Particles", Tomsk State University, Translated from Fizika Goreniya i Vzryva, 1976, Vol. 12, No. 2, pp. 203-208.

20. Lifschitz, A. and Bauer, S. H., "Studies with a Single Pulse Shock Tube", Journal of Chemical Physics, Vol. 38, No. 9, 1963, pp. 2056-2060.

21. Driscoll, J. F., et. al., "Aluminum Combustion at 40 Atmospheres Using a Reflected Shock Wave", AIAA Journal, Vol. 24, No. 5, 1986, pp. 856-858.

22. Reed, R. A., Personal Communications, May, 1993.

23. Lee, S. C. and Tien, C. L., "Optical Constants of Soot in Hydrocarbon Flames", Proceedings of the Eighteenth Symposium (International) on Combustion, 1981, pp. 1159-1166.

24. Konopka, W. L., Reed, R. A. and Calia, V. S., "Measurements of Infrared Optical Properties of Al2O3 Rocket Exhaust Particles", AIAA Paper No. 83-1568, AIAA Thermophysics Conference, June 1-3, 1983, Montreal, Canada.

25. Nordine, P. C., et. al., "Optical Properties of Liquid Aluminum Oxide", AIAA Paper No. 85-0320, AIAA Twenty-Eighth Thermophysics Conference, July 6-9, 1993, Orlando, Florida.

26. Crawford, R. A., Personal Communications, June, 1993.

27. Shigley, J. E. and Mischke, C. R., "Mechanical Engineering Design", Fifth Edition, McGraw-Hill Publishing Company, 1989.

28. Eshbach, O. W. and Souders, M., "Handbook of Engineering Fundamentals", Third Edition, John Wiley & Sons, Inc., 1975.

29. Sutton, G. P., "Rocket Propulsion Elements: An Introduction to the Engineering of Rockets", Sixth Edition, John Wiley & Sons, Inc., 1992.

30. Bee'r, J. M. and Chigier, N. A., "Combustion Aerodynamics", John Wiley & Sons, Inc., 1972.

31. Incopera, F. P. and DeWitt, D. P., "Fundamentals of Heat and Mass Transfer", Second Edition, John Wiley & Sons, Inc., 1985.

32. Melles Griot, "Optics Guide 4", (Optics Catalog), pp. 3-4.

33. Maddock, R. W., Personal Communications, July, 1993

34. ESCO Products, Inc., "Optical Materials and Components Handbook", Oak Ridge, New Jersey, pp. 6.

35. Thompson, K., Personal Communications, June, 1993.

# APPENDICES

# Appendix A

## CETPC Output Data for Hydrogen Fuel Combustion Products and 0.01 Aluminum Mass Fraction

| Species | O/F=6.0 | O/F=7.3 (Stoich.) | O/F=8.0 | O/F=10 | O/F=15 | O/F=20 |
|---|---|---|---|---|---|---|
| Al | 0.00003 | 0.00001 | 0.00001 | 0 | 0 | 0 |
| AlO | 0.00029 | 0.00027 | 0.00023 | 0.00011 | 0.00001 | 0 |
| AlOH | 0.00029 | 0.00020 | 0.00015 | 0.00007 | 0.00001 | 0 |
| AlO2 | 0.00002 | 0.00003 | 0.00003 | 0.00002 | 0.00001 | 0 |
| AlO2H | 0.00249 | 0.00282 | 0.00272 | 0.00208 | 0.00076 | 0.00024 |
| H | 0.05283 | 0.04437 | 0.03894 | 0.02458 | 0.00750 | 0.00232 |
| HO2 | 0.00007 | 0.00019 | 0.00025 | 0.00040 | 0.00050 | 0.00042 |
| H2 | 0.21482 | 0.13238 | 0.10651 | 0.05857 | 0.01757 | 0.00623 |
| H2O | 0.62902 | 0.64951 | 0.64914 | 0.62898 | 0.55055 | 0.48030 |
| H2O2 | 0.00001 | 0.00003 | 0.00003 | 0.00004 | 0.00004 | 0.00003 |
| O | 0.01069 | 0.02080 | 0.02463 | 0.03038 | 0.02426 | 0.01403 |
| OH | 0.07565 | 0.10825 | 0.11740 | 0.12547 | 0.09654 | 0.06244 |
| O2 | 0.01225 | 0.03988 | 0.05868 | 0.12785 | 0.30053 | 0.43233 |
| Al2O3 | 0.00153 | 0.00126 | 0.00127 | 0.00146 | 0.00172 | 0.00165 |

**Figure 88: Mole Fractions of Hydrogen Combustion Product Species Vs. O/F Ratios**
(Pressure = 500 psia, Aluminum Mass Fraction = 0.01)

# Appendix B

CETPC Output Data for Methane Fuel Combustion Products and 0.01 Aluminum Mass Fraction

| Species | O/F=2.0 | O/F=3.0 | O/F=3.8 (Stoich.) | O/F=5.0 | O/F=10 | O/F=15 |
|---|---|---|---|---|---|---|
| Al | 0.00014 | 0.00009 | 0.00004 | 0.00001 | 0.00001 | 0 |
| AlH | 0.00002 | 0.00001 | 0 | 0 | 0 | 0 |
| AlO | 0.00046 | 0.00099 | 0.00068 | 0.00031 | 0 | 0 |
| AlOH | 0.00060 | 0.00048 | 0.00026 | 0.00011 | 0 | 0 |
| AlO2 | 0.00001 | 0.00007 | 0.00009 | 0.00006 | 0.00001 | 0 |
| AlO2H | 0.00153 | 0.00369 | 0.00353 | 0.00261 | 0.00043 | 0.00004 |
| Al2O | 0.00004 | 0.00002 | 0.00001 | 0 | 0 | 0 |
| Al2O2 | 0.00001 | 0.00001 | 0.00001 | 0 | 0 | 0 |
| CO | 0.28514 | 0.21687 | 0.16620 | 0.11432 | 0.02216 | 0.00345 |
| CO2 | 0.03078 | 0.07066 | 0.09652 | 0.11840 | 0.12998 | 0.10752 |
| H | 0.06076 | 0.06376 | 0.04645 | 0.02856 | 0.00384 | 0.00043 |
| HCO RAD | 0.00003 | 0.00002 | 0.00001 | 0 | 0 | 0 |
| HO2 | 0.00001 | 0.00013 | 0.00029 | 0.00045 | 0.00046 | 0.00024 |
| H2 | 0.31328 | 0.13241 | 0.07506 | 0.04044 | 0.00583 | 0.00097 |
| H2O | 0.27429 | 0.36133 | 0.36432 | 0.34601 | 0.26163 | 0.20720 |
| H2O2 | 0 | 0.00001 | 0.00002 | 0.00003 | 0.00002 | 0.00001 |
| O | 0.00287 | 0.02581 | 0.04268 | 0.05085 | 0.02686 | 0.00745 |
| OH | 0.02571 | 0.09460 | 0.12160 | 0.12620 | 0.06888 | 0.02680 |
| O2 | 0.00098 | 0.02738 | 0.08057 | 0.16965 | 0.47780 | 0.64423 |
| Al2O3 | 0.00335 | 0.00165 | 0.00167 | 0.00196 | 0.00208 | 0.00166 |

**Figure 89: Mole Fractions of Methane Combustion Product Species Vs. O/F Ratios**
(Pressure = 500 psia, Aluminum Mass Fraction=0.01)

# VITA

Robert John Geierman was born in Saline, Michigan on August 17, 1967. He moved to Hillman, Michigan in 1972 and attended Montmorency Elementary School. He graduated from Hillman High School in June 1985. The following September, he attended Alpena Community College in Alpena, Michigan, and received his associate of Science Degree in May 1987. He continued his education at Michigan Technological University in Houghton, Michigan and received his Bachelor of Science Degree in Mechanical Engineering in May, 1991. Also during his education at Michigan Technological University, Robert participated in the cooperative education program and spent three terms working at General Electric Aircraft Engines in Evendale, Ohio. In September of 1991, he enrolled in the University of Tennessee Space Institute in Tullahoma, Tennessee and will receive a Master of Science Degree in Mechanical Engineering in December, 1993.